HYDRODYNAMIC ANALYSIS OF FLOATING OFFSHORE WIND TURBINE CONCEPTS: A CASE STUDY IN BLACK SEA

A THESIS SUBMITTED TO
THE GRADUATE SCHOOL OF NATURAL AND APPLIED SCIENCES
OF
MIDDLE EAST TECHNICAL UNIVERSITY

BY

BÜŞRA YILDIRIM

IN PARTIAL FULFILLMENT OF THE REQUIREMENTS
FOR
THE DEGREE OF MASTER OF SCIENCE
IN
CIVIL ENGINEERING

OCTOBER 2022

Approval of the thesis:

HYDRODYNAMIC ANALYSIS OF FLOATING OFFSHORE WIND TURBINE CONCEPTS: A CASE STUDY IN BLACK SEA

submitted by **BÜŞRA YILDIRIM** in partial fulfillment of the requirements for the degree of **Master of Science** i**n Civil Engineering, Middle East Technical University** by,

Prof. Dr. Halil Kalıpçılar
Dean, Graduate School of **Natural and Applied Sciences** _____

Prof. Dr. Erdem Canbay
Head of the Department, **Civil Engineering** _____

Assoc. Prof. Dr. Elif Oğuz
Supervisor, **Civil Engineering, METU** _____

Examining Committee Members:

Prof. Dr. Ayşe Burcu Altan-Sakarya
Civil Engineering, METU _____

Assoc. Prof. Dr. Elif Oğuz
Civil Engineering, METU _____

Assoc. Prof. Dr. Nejan Huvaj-Sarıhan
Civil Engineering, METU _____

Assoc. Prof. Dr. Nilay Sezer-Uzol
Aerospace Engineering, METU _____

Asst. Prof. Dr. Mehmet Adil Akgül
Civil Engineering, Yeditepe University _____

Date: 19.10.2022

I hereby declare that all information in this document has been obtained and presented in accordance with academic rules and ethical conduct. I also declare that, as required by these rules and conduct, I have fully cited and referenced all material and results that are not original to this work.

Name Last name : Büşra Yıldırım

Signature :

ABSTRACT

HYDRODYNAMIC ANALYSIS OF FLOATING OFFSHORE WIND TURBINE CONCEPTS: A CASE STUDY IN BLACK SEA

Yıldırım, Büşra
Master of Science, Civil Engineering
Supervisor : Assoc. Prof. Dr. Elif Oğuz

October 2022, 143 pages

In the literature, well-validated hydrodynamic programs such as WAMIT are used to analyze the hydrodynamics of floating offshore wind turbines (FOWTs). In this thesis, potential use of an opensource hydrodynamic solver for the hydrodynamic modeling of FOWTs is investigated using HAMS. For this purpose, hydrodynamic coefficients obtained from HAMS are compared to the first-order hydrodynamic solution of AQWA and WAMIT. The hydrodynamic model of three FOWT concepts, such as OO-Star, Nautilus, and CENTEC TLP, is compared in terms of the added mass, radiation damping, and wave excitation forces. The result of this objective presents that HAMS provides an accurate solution compared to WAMIT and AQWA models. In the case of CENTEC TLP, the hydrodynamic coefficients are almost the same, especially for smaller frequencies (smaller than 2 rad/s).

Verified hydrodynamic coefficients are used as input to OpenFAST and coupled analysis of FOWTs is carried out for the benchmark load cases. The effects of the hydrodynamic modeling program on the system behavior are investigated such as power generation, system motion and mooring tension.

The final objective of this thesis is to examine whether a previously designed FOWT concept can be applied to a different site without requiring any further optimization. For this purpose, the environmental conditions of the potential site in the Black Sea were computed, and numerical analyses were carried out to evaluate whether the three FOWT concepts can be applied or not. Although the numerical results showed that the three systems were operable in the selected area, further detailed analyses are required for a precise application.

Keywords: Offshore Wind Energy, Renewable Energy, Hydrodynamics, Floating Platforms

ÖZ

AÇIK DENİZ YÜZER RÜZGAR TÜRBİN KONSEPTLERİNİN HİDRODİNAMİK ANALİZİ: KARADENİZ'DE BİR VAKA ÇALIŞMASI

Yıldırım, Büşra
Yüksek Lisans, İnşaat Mühendisliği
Tez Yöneticisi: Doç. Dr. Elif Oğuz

Ekim 2022, 143 sayfa

Literatürde, açık deniz yüzer rüzgar türbinlerinin hidrodinamik analizini için WAMIT gibi iyi çalışılmış hidrodinamik programlar kullanılmaktadır. Bu tezde ise açık kaynaklı bir hidrodinamik program olan HAMS'ın, açık deniz yüzer rüzgar türbinlerinin hidrodinamik modellemesi için kullanılabilirliği araştırılmıştır. Bu amaçla, HAMS'den elde edilen hidrodinamik katsayılar, AQWA ve WAMIT'in hidrodinamik model sonuçları ile karşılaştırılmıştır. OO-Star, Nautilus ve CENTEC TLP gibi üç açık deniz yüzer rüzgar türbini konseptinin hidrodinamik modeli, katma kütle, radyasyon sönümleme ve dalga uyarma kuvvetleri karşılaştırılmıştır. Bu modellemenin sonucu, HAMS'ın WAMIT ve AQWA modelleriyle yakın bir çözüm sağladığını göstermektedir. CENTEC TLP modelinde ise, hidrodinamik katsayılar, özellikle daha küçük frekanslar için (2 rad/s'den küçük) yaklaşık olarak aynıdır.

OpenFAST'a girdi olarak önceki adımda doğrulanmış hidrodinamik katsayılar kullanılmış ve kıyaslama farklı yük durumları için açık deniz yüzer rüzgar türbinlerinin birleştirilmiş analizi ile yapılmıştır. Sistem davranışları, farklı hidrodinamik modelleme programlarıyla belirlenmiş, elektrik üretimleri, sistemin hareketleri ve bağlama halatlarına gelen gerilmeler araştırılmıştır.

Bu tezin en son amacı, önceden tasarlanmış bir açık deniz yüzer rüzgar türbini konseptinin daha fazla optimizasyon olmaksızın farklı bir potansiyel bölgeye uygulanıp uygulanamayacağını incelemektir. Bu amaçla, Karadeniz'deki potansiyel sahanın çevresel koşulları hesaplanmış ve üç açık deniz yüzer rüzgar türbini konseptinin uygulanıp uygulanamayacağını değerlendirmek için sayısal analizler yapılmıştır. Sayısal analiz sonuçlar, üç sistemin bölgede çalışabilir olduğunu gösterse de, kesin bir uygulama için daha detaylı analiz gereklidir.

Anahtar Kelimeler: Açıkdeniz Rüzgar Enerjisi, Yenilenebilir Enerji, Hidrodinamik, Yüzer Platformlar

To my family and loved ones

ACKNOWLEDGMENTS

I would like to express my sincere gratitude to my thesis advisor Assoc. Prof. Dr. Elif Oğuz. Without her support, knowledge and experience this thesis could not be concluded and I could not meet this exciting area of floating offshore wind turbines which became my passion. She is a great advisor; mentor and I am grateful to be her master student.

I would like to thank Dr. Emre Uzunoğlu for providing the WAMIT output and the mesh of operational CENTEC TLP. This ensured a better comparison of the hydrodynamic solvers and the methodology. Additionally, his comments were very valuable for the development of this thesis.

I would like to thank Dr. Hasan Gökhan Güler for answering my questions about wave statistics and even though I was not officially enrolled to the Wave Hydrodynamics course, it widened my perspective of wave nonlinearity and statistics which is an important base for theory behind this thesis.

Although it has been long time, I would like to thank Dr. Talia Ekin Tokyay for guiding me my first footsteps in the academy. This was very important to me as an individual who will be a first generation academic in her family. The undergraduate research that I conducted with her was a breakthrough for me for my academic and personal development. She was a very valuable person for METU family.

I would also like to thank Prof. Dr. Erhan Karaesmen and Prof. Dr. Engin Karaesmen. Their guidance was very important to me when I was feeling lost during my bachelor. They always encouraged me to continue my music passion, playing cello and motivated me to be an engineer with an international mindset and creativity.

Especially I would like to thank my parents Sündüs Yıldırım, Mehmet Yıldırım and my brother Burak Yıldırım. I am very lucky to have such a family. They always

supported me for my decisions and believed in me. I am very grateful for their support, and I will continue making them proud.

The publicly available FAST V8 models are used for the OO-STAR (Pegalajar-Jurado et al., 2018) and NAUTILUS platforms (Galván et al., 2018) from the Lifes50+ project (Yu, 2018) in this thesis. The OO-Star platform concept is developed by Dr.techn.Olav Olsen AS and owned by Floating Wind Solution AS.

The extreme value analysis in this thesis has been conducted using the wave parameters from E.U. Copernicus Marine Service Information (Link) and wind parameters used are retrieved from ERA5 dataset (Link) (Hersbach et al., 2018). For preparation of figure of the selected area, the bathymetric data has been retrieved from EMODnet Bathymetry portal (Link) and the seabed properties are also retrieved from EMODnet Seabed Habitats Map (Link).

TABLE OF CONTENTS

ABSTRACT v

ÖZ vii

ACKNOWLEDGMENTS x

TABLE OF CONTENTS xii

LIST OF TABLES xv

LIST OF FIGURES xvii

LIST OF ABBREVIATIONS xxi

LIST OF SYMBOLS xxiii

CHAPTERS

1 INTRODUCTION 1

1.1 Objectives 5

2 LITERATURE REVIEW 9

2.1 Applications of Offshore Renewables 9

2.2 Design Spesifications 11

2.3 Experimental Studies on FOWTs 12

2.4 Numerical Modeling of FOWTs 20

3 THEORETICAL BACKGROUND 27

3.1 Fundamentals of Wave Theory 27

3.1.1 Small Amplitude Wave Theory (Regular Waves) 27

3.1.2 Irregular Waves 28

3.1.3 Potential Flow Theory 29

3.1.4 Second Order Stokes Waves 32

3.2 Hydrodynamics of Floating Body 32
3.2.1 Equation of Motion 32
3.3 Load Description 33
3.3.1 Hydrodynamic Loads 34
3.3.2 Aerodynamic Loads 35
3.3.3 Other Loads 35
4 NUMERICAL MODELLING AND METHODOLOGY 37
4.1 DTU 10 MW Reference Wind Turbine (RWT) 39
4.2 Platform Types 40
4.2.1 Nautilus DTU-10 Floating Wind Turbine 40
4.2.2 OO-Star DTU-10 Floating Wind Turbine 42
4.2.3 CENTEC TLP DTU-10 Floating Wind Turbine 44
4.3 Numerical Modelling Tools 47
4.3.2 OpenFAST 51
4.4 Project Location 53
4.4.1 Extreme Value Analysis 57
4.5 Model Comparison Tests 61
4.5.1 Free Oscillation (Free Decay) Tests 61
4.5.2 Regular Wave Test 63
5 RESULTS AND DISCUSSION 69
5.1 Numerical Model Verification 70
5.1.1 OO-STAR 73
5.1.2 NAUTILUS 87
5.1.3 CENTEC TLP DTU-10 99

5.2 Comparison of Platform Concepts 109
6 CONCLUSION 117
REFERENCES 121
APPENDICES 139
A. Mesh Sensitivity Analysis for the HAMS (OO-Star Platform) 139
B. Input File for CENTEC TLP 141

LIST OF TABLES

TABLES

Table 1 Comparison of the BEM-based hydrodynamic solvers available. Taken from (Penalba, Kelly, &Ringwood, 2017), modified 6
Table 2 Technology Readiness Levels for OWTs. Prepared from (ITTC Proceedings, 2021b)..... 13
Table 3 Previous experimental studies for FOWTs. 19
Table 4 Overall design parameters of DTU 10MW RWT. (Borg, Manuel, Collu, &Liu, 2015)..... 39
Table 5 Nautilus platform properties with fully loaded ballast, including DTU 10 MW RWT (Yu, 2018)..... 42
Table 6 Properties of LIFES50+ OOS-Star platform properties with ballast (Yu, 2018) 44
Table 7 Mass data for the CENTEC TLP (Uzunoglu & Guedes Soares, 2020)..... 46
Table 8 Installed properties of the CENTEC TLP (Uzunoglu & Guedes Soares, 2020). 47
Table 9 Results of the extreme value analysis for significant wave height using Gumbel distribution 57
Table 10 Results of the extreme value analysis for wind speed at 10 m using Gumbel distribution 58
Table 11 Scatter Table H_s vs T_p for Kıyıköy region 58
Table 12 Scatter table for Kıyıköy region for wind speed at hub height..... 59
Table 13 Load cases used in the analysis..... 61
Table 14 Cell numbers and % volume for Cases of mesh sensitivity analysis with y symmetric geometry..... 70
Table 15 Benchmark load cases modeled..... 74
Table 16 Natural frequencies of OO-Star platform. 76
Table 17 Maximum and minimum responses of OO-Star system in operational sea states with a comparison of three potential flow solvers 78

Table 18 Maximum and minimum responses of ultimate sea states of OO-Star DTU 10 system with a three potential flow solvers comparison.....82
Table 19 Natural frequencies of the Nautilus platform.....88
Table 20 Maximum and minimum values of the operational sea states of Nautilus DTU 10 system with three potential flow solvers comparison.....90
Table 21 Maximum and minimum responses of the ultimate sea states of Nautilus DTU 10 system with three potential flow solvers comparison.....93
Table 22 Maximum and minimum responses of the extreme sea states of Nautilus DTU 10 system with a three potential flow solvers comparison.....96
Table 23 Comparison of the natural frequencies of CENTEC TLP.....100
Table 24 Maximum and minimum responses of the rated conditions of CENTEC TLP.....103
Table 25 Maximum and minimum responses of the above-rated conditions of CENTEC TLP.....106
Table 26 Maximum and minimum responses to the extreme conditions of CENTEC TLP.....108
Table 27 Natural frequencies of the modeled three platform concepts computed by the (HAMS+OpenFAST) model.....109
Table 28 Environmental conditions of platform concepts and selected region in Turkey.....110
Table 29 The load cases (LCs) selected for Kıyıköy.....111
Table 30 Input files for the CENTEC TLP rated operational condition.....141

LIST OF FIGURES

FIGURES

Figure 1 Stability triangle presenting well-known FOWT concepts (Borg & Collu, 2014) 3
Figure 2 Technical offshore wind potential in Turkey. Taken from (ESMAP, 2019) 5
Figure 3 On the left, 6 DOF HIL experimental setup (Bayati, Bernini, et al., 2018), and on the right, hexafloat robot (Bayati, Facchinetti, Fontanella, Giberti, et al., 2018) representing the platform motions. (modified) 15
Figure 4 HIL approach for a hybrid FOWT experimental test (Bayati et al., 2018) 16
Figure 5 Experimental campaigns for the floating platforms in the literature: a) DeepCWind (Koo et al., 2014), b) Tension Leg Platform (TLP) (Oguz et al., 2018), c) WindFloat platform (Roddier et al., 2010), d) SATH 10 MW InWind (Vittori et al., 2021), e) HYWIND Spar (Nielsen et al., 2006) 17
Figure 6 Experimental tests for the OO-Star (Thys et al., 2018) on the left, Nautilus (Madsen et al., 2018) in the middle, and CENTEC TLP (Mas-Soler et al., 2021) on the right 18
Figure 7 Coordinate system and definition of a vertical cylinder system (Sumer & Fredsøe, 2006) 30
Figure 8 Overall flowchart of the thesis presenting the methodology and tools 38
Figure 9 Nautilus DTU-10 FOWT concept (Galván, Sanchez-Lara, et al., 2018) . 41
Figure 10 OO-Star FOWT concept (Dr.techn. Olav Olsen AS, 2018) 43
Figure 11 CENTEC TLP model with DTU 10 MT RWT in its installed draft (Uzunoglu & Guedes Soares, 2020) 45
Figure 12 Flowchart of the numerical part of this thesis for hydrodynamic solution 48
Figure 13 Submodules of FAST (Matha, 2010) 51

Figure 14 The global coordinate system for the Hydrodyn Module for a FOWT (Jonkman, Robertson, &Hayman, 2016) 52
Figure 15 Detailed bathymetry and selected location for the FOWT modeling 55
Figure 16 Annual mean wind speed values at 100 m for the potential site in Kıyıköy 56
Figure 17 Free oscillation (decay) tests for the Nautilus platform with three different hydrodynamic models 63
Figure 18 Regular wave responses of the Nautilus system modeled with three hydrodynamic solvers coupled with OpenFAST 64
Figure 19 RAOs for Nautilus platform without wind excitation 65
Figure 20 RAOs for OO-Star platform without wind excitation 66
Figure 21 RAOs for CENTEC TLP without wind excitation 67
Figure 22 Percent volume and computational time for mesh sensitivity analysis .. 72
Figure 23 Case 1 mesh with 2.5 m average cell length on the left and on the right Case 5 mesh with 1.5 m average cell length on the right for OO-Star platform 73
Figure 24 Natural frequencies of OO-Star computed with OpenFAST using input from different hydrodynamic models 75
Figure 25 Hydrodynamic coefficients of OO-STAR computed by three potential flow solvers 77
Figure 26 Mooring line configuration of OO-Star system 79
Figure 27 Maximum and minimum values of the OO-Star system in operational sea states 80
Figure 28 Dynamic response of OO-Star in operational condition 81
Figure 29 Maximum and minimum values of OO-Star system in ultimate sea states 83
Figure 30 Ultimate response of OO-Star system 84
Figure 31 Maximum and minimum OO-Star system response in extreme sea states 85
Figure 32 Responses of the OO-Star system in extreme load case 86

Figure 33 Natural frequencies of Nautilus computed with OpenFAST using input from different hydrodynamic models 87
Figure 34 Hydrodynamic coefficients of the Nautilus platform 89
Figure 35 Mooring configuration of the Nautilus platform where wave direction is zero (head wave) 90
Figure 36 Maximum and minimum responses of Nautilus system in operational sea states 91
Figure 37 Operational response of Nautilus system 92
Figure 38 Maximum and minimum responses of Nautilus system in ultimate sea states 94
Figure 39 Response of the Nautilus platform in ultimate conditions 95
Figure 40 Maximum and minimum values of Nautilus system in extreme sea states 97
Figure 41 Extreme response of the Nautilus platform 98
Figure 42 Natural Period of the CENTEC TLP 99
Figure 43 Hydrodynamic coefficients for CENTEC TLP 101
Figure 44 Normalized maximum and minimum responses for rated wind conditions 102
Figure 45 Top view and mooring configuration of CENTEC TLP 103
Figure 46 Dynamic responses of the rated operational case of CENTEC TLP 104
Figure 47 Normalized nondimensional maximum and minimum values for above-rated wind conditions 105
Figure 48 Above rated operational condition of CENTEC TLP 107
Figure 49 Dimensions of the selected concepts: a) OO-Star concept (Dr.techn. Olav Olsen AS, 2018)(Modified), b) Nautilus concept (Galván et al., 2018) (Modified), c) CENTEC TLP (Uzunoglu & Guedes Soares, 2020) 111
Figure 50 System behavior of the selected platforms in Kıyıköy for LC1 112
Figure 51 System behavior of the selected platforms in Kıyıköy for LC2 113
Figure 52 System behavior of the selected platforms in Kıyıköy for LC3 114
Figure 53 System behavior of the selected platforms in Kıyıköy for LC4 115

Figure 54 Added Mass for the OO-Star computed using HAMS 139
Figure 55 Radiation damping for the OO-Star computed using HAMS 140

LIST OF ABBREVIATIONS

ABBREVIATIONS	
BEM	Boundary Element Method
BEMT	Blade Element Momentum Theory
CENTEC	Centre for Marine Technology and Ocean Engineering
CFD	Computational Fluid Dynamics
DLC	Design Load Case
DOF	Degree of Freedom
DTU	Danmarks Tekniske Universitet
EDF	Electric Ducted Fan
FOWT	Floating Offshore Wind Turbine
HAMS	Hydrodynamic Analysis of Marine Structures
HAWC	Horizontal Axis Wind Turbine Simulation Code
HAWT	Horizontal Axis Wind Turbine
IEC	International Electrotechnical Commission
IWRC	Independent Wire Rope Core
LC	Load Case
NREL	National Renewable Energy Laboratory
OWT	Offshore Wind Turbine
O&M	Operation and Maintenance
PSD	Power Spectral Density

RAO	Response Amplitude Operator
RWT	Reference Wind Turbine
R&D	Research and Development
QTF	Quadratic Transfer Function
SIL	Software in the Loop
TLB	Tension Leg Buoy
TLP	Tension Leg Platform
WEC	Wave Energy Converter

LIST OF SYMBOLS

SYMBOLS

a_i	Incident Wave Amplitude [m]
A	Added Mass [kg or kgm^2]
C_D	Drag Coefficient [-]
C_M	Inertia Coefficient [-]
f_i	Phase of Incident Wave [radian]
g	Gravitational Acceleration [m/s^2]
H	Above Sea Level Height [m]
H_s	Significant Wave Height [m]
k	Wave Number [-]
KC	Keulegan Carpenter Number [-]
L	Wavelength [m]
m	Mass [kg]
N	Number of Wave Frequencies [-]
Re	Reynolds Number [-]
T	Averaging Period for Wind Dataset [hour]
T_p	Peak Wave Period [s]
U_0	Hourly Averaged Wind Speed [m/s]
$U_{50\text{-years}}$	50 Year Wind Speed Value [m/s]
X	Displacement of the System [m or degree]

ω	Angular Wave Frequency [rad/s]
ω_n	Natural Frequency of the System [Hz]
ρ	Density [kg/m^3]
Φ	Velocity Potential [m^2/s]

CHAPTER 1

INTRODUCTION

The deadline for 2030 approaches to keep the 1.5 degrees Celcius global warming limit from the Paris agreement (United Nations [UN], 2015), which is the highest revocable temperature change. The last few years on earth have shown us the importance of energy resilience and security. The operational dynamics in the world have changed significantly due to the pandemic and regional conflicts, including war. The negative impacts of war and the pandemic on the global energy system have threatened fossil fuel security, higher prices for fossil fuels, and increased investment risk (Climate Action Tracker, 2022). The negative effects on the global energy system have brought doubts about energy resilience and security, which slow down efforts to decrease carbonization and fossil fuel usage. The imbalance in the energy system may lead governments to reverse their sustainable solutions to fossil fuel investments. Hence to further accelerate the sustainable transition, alternative renewable energy sources and cost-effective solutions should be pursued and prioritized. To further accomplish this goal, renewables might offer a solution.

Before the pandemic, there was already a goal of decreasing the effects of climate change and net zero targets, which have accelerated the green energy transition using various energy harvesting types. Wind energy is one of those energy harvesting types with one of the highest percentages, with 94 GW installations globally and 837 GW of total wind power capacity only in 2021 (Lee & Zhao, 2022).

As the second highest renewable energy type, wind energy consists of two primary harvesting types: offshore and onshore. Wind energy technology started with onshore installations. The need for greater energy production then carried the onshore turbines into the water, where larger turbines were allowed, and a massive wind source was available. Although the onshore installations are still ongoing and

the onshore wind industry is maturing, limited space for onshore causes the onshore wind to slow down. Hence offshore wind might promise an acceleration of the renewable energy transition, specifically for countries with limited space, including less opposition from local authorities and residents due to their distance from the shoreline (Hopstad & Pollicino, 2020).

The shift from onshore wind started with the fixed bottom offshore wind turbines, which could be installed up to 50 m water depth. However, to yield greater electricity from offshore wind and to reduce the negative effects of turbines, such as noise and visual pollution, floating offshore wind turbines (FOWTs) started to design for waters greater than 50 m in depth. Initially shaped from the platform designs of the oil&gas industry, current Offshore Wind Turbine (OWT) platforms have evolved considering the distinctive offshore wind features such as aerodynamic loads, loads due to turbine control, and coupled effects. Floating platforms can be divided into three main groups based on their stability principle (Butterfield, Musial, Jonkman, & Sclavounos, 2005).

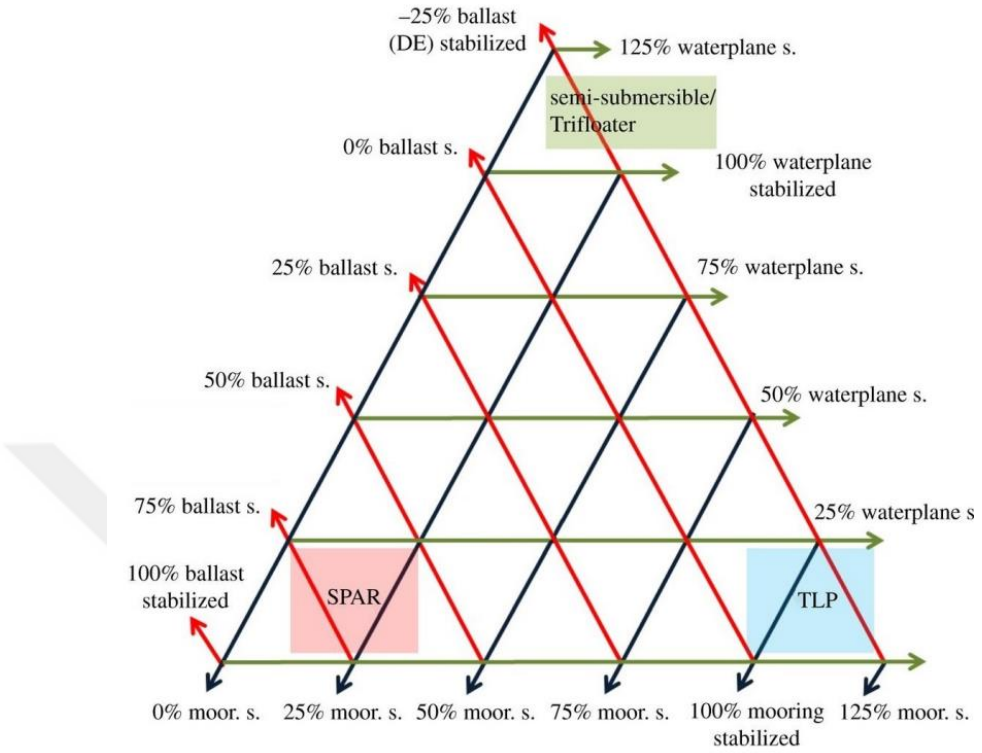


Figure 1 Stability triangle presenting well-known FOWT concepts (Borg & Collu, 2014)

As seen in Figure 1, floating platforms could be classified considering their stability methods, into three main groups: ballast stabilized, mooring stabilized, and buoyancy stabilized. The platform types can have multiple stability types. For instance, the stability of semisubmersible is a combination of buoyancy and ballast stabilization where the buoyancy has a higher percentage, and the body has a strong motional response to the sea states (Müller, Faerron-Guzmán, Manjock, &Borg, 2018). Tension Leg Platform (TLP) is a platform design with a fully submerged substructure in its installed condition. TLP provides a stiffer behavior, particularly in heave, pitch, and roll degrees of freedom (DOFs). Its stability is mainly mooring dependent with contribution from buoyancy. Newer generations of the TLPs might combine two approaches. For instance, the Centre for Marine Technology and Ocean Engineering (CENTEC) TLP floats freely during its transportation phase as a barge,

and when installed, it is mooring stabilized (Uzunoglu & Guedes Soares, 2020). Barges are fully buoyancy-stabilized structures, and their station-keeping systems are similar to the semisubmersibles. Greater platform motions due to sea states result in barges' higher pitch and roll motions. Single Point Anchor Reservoirs (Spars or Spar Buoys) are highly ballast-stabilized substructure types with a ballast located at the bottom of the structure (Müller et al., 2018).

Having a 74% dependency on foreign resources for energy production using mainly fossil fuels highlights Turkey's significant need for harnessing renewable energy sources to decrease energy dependency. The current energy balance of Turkey at the end of June 2022 includes 45.7% fossil fuel and renewables, including 31.1 % hydropower, 10.8% wind, 8.4% solar, 1.7% geothermal energy, and 2.3% other sources (Republic of Turkey Ministry of Energy and Natural Resources, 2022). Wind is one of the promising energy resources, especially for the western part of Turkey. Similar to the global development of wind turbines (from onshore to offshore), wind industry development started with onshore installations in Turkey. According to the Wind Europe 2021 statistics, the installed onshore capacity is over 10 GW and is mainly located in the Aegean region (Wind Europe, 2021). Currently, there are no offshore wind installations in Turkey. However, it is one of the attractive regions due to its high technical offshore wind potential of 75 GW, where 12 GW is suitable for fixed bottom foundations, and 63 GW is ideal for floating foundations (Energy Sector Management Assistance Program [ESMAP], 2019). Convenient locations for offshore wind farms and annual wind speeds can be seen in Figure 2, where offshore wind might contribute to sustainable development as an efficient solution (Lee & Zhao, 2022). Currently, the technology is in its development stage, and the cost reduction strategies are still being investigated to ensure the commercialized process.

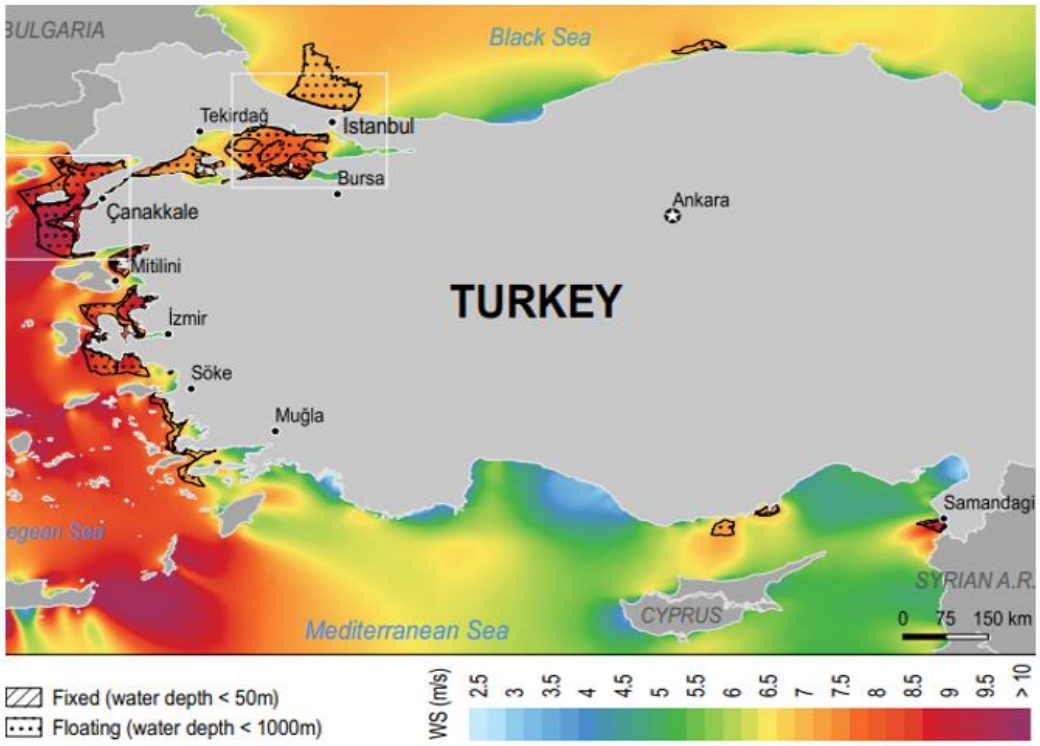


Figure 2 Technical offshore wind potential in Turkey. Taken from (ESMAP, 2019)

1.1 Objectives

The overall design of FOWTs might be divided into three subsections: platform design, turbine design, and mooring design. As FOWTs are designed for the areas with more excellent wind sources, which results from coexistent greater waves, the hydrodynamics of the structure requires further attention, which makes the investigation of the hydrodynamic characteristics of the platform and moorings crucial during the lifespan of the system.

The potential flow approach is widely used in the hydrodynamic analysis of FOWTs since it provides a precise solution. WAMIT (Lee, 1995) is a verified, widely used commercial potential flow solver for the computation of wave load and floating body motions. As commercial software, the code behind the software is not accessible to the public, limiting possible modifications to encounter different problems. As can

be seen from Table 1, most of the Boundary Element Method (BEM) based hydrodynamic solvers are commercial.

Table 1 Comparison of the BEM-based hydrodynamic solvers available. Taken from (Penalba, Kelly, &Ringwood, 2017), modified

BEM Solver	Frequency Domain	Time Domain	Opensource
ACHILD3D	✗	✓	✗
AQWA	✓	✗	✗
Aquaplus	✓	✗	✗
HAMS	✓	✗	✓
NEMOH	✓	✗	✓
WADAM	✓	✗	✗
WAMIT	✓	✗	✗

To clarify the issue of not having access to the code and provide an alternative for the numerical modeling of FOWTs, an open-source potential flow solver Hydrodynamic Analysis of Marine Structures (HAMS) (Liu, 2019), was selected. Open source software has the properties of free distribution, source code access aiming for transparency, and availability for modifications (O'Neill, 2012). Hence, the applicability of HAMS as an alternative to WAMIT might eliminate the disadvantages of using commercial software and contribute to further developments in the potential flow solver.

In this scope for model verification, three FOWT concepts, including OO-STAR (Pegalajar-Jurado et al., 2018), Nautilus (Galván, Sánchez-Lara, et al., 2018), and CENTEC TLP (Uzunoglu & Guedes Soares, 2020) are selected and modeled with two hydrodynamic solvers as AQWA (Aqwa Theory Manual, 2013) and HAMS (Liu, 2019) in this thesis. The hydrodynamic coefficients from these models are compared to WAMIT (Lee, 1995) outputs from previous studies. The coupled numerical model is then compared using OpenFAST and a hydrodynamic solver. The publicly available FAST v8 models are used for OO-Star (Pegalajar-Jurado et

al., 2018) and Nautilus platforms (Galván, Sánchez-Lara, et al., 2018) and converted to OpenFAST v3.0 for compatibility. For those models, the hydrodynamic coefficients are previously computed with WAMIT(Lee, 1995). The relevant WAMIT outputs are publicly available in the Lifes50+ Project (Galván et al., 2018; Pegalajar-Jurado et al., 2018). OpenFAST v3.0 input files are prepared for CENTEC TLP. For the comparison of hydrodynamic coefficients WAMIT outputs for the operational condition are provided by Dr. Emre Uzunoğlu.

As mentioned earlier, Turkey has no offshore wind turbine installed, although the technical offshore wind potential is very high. Hence, after verifying the hydrodynamic and coupled models, metocean parameters of a previously selected site in the Southwestern Black Sea region in Turkey are computed. Load cases are chosen considering the metocean parameters. Finally, the three platform concepts are modeled to assess the dynamic behavior of the platforms for the selected region, and the results are compared to select a platform type for the area.

This thesis has multiple objectives. The initial motivation is to provide an alternative for commercial hydrodynamic codes for the coupled analysis of FOWTs. The comparison is carried out for three hydrodynamic solvers and OpenFAST coupled simulation outputs. Models are created using AQWA and opensource HAMS. The hydrodynamic code outputs are compared to WAMIT results from the benchmark studies. The secondary objective is the application of three platform concepts with DTU 10MW RWTs in Kıyıköy, Black Sea.

To sum up, this thesis aims to provide answers to the following research questions:

1. How does coupling of OpenFAST with an open source hydrodynamic solver HAMS and commercial hydrodynamic codes AQWA and WAMIT compare in first-order hydrodynamic modeling of different platform concepts?
2. How does the hydrodynamic modeling tool affect the system's power generation and global response?
3. Can the previously designed FOWT concept be applied to a different site without further optimization?

In the next chapter, a literature review for the basis of this study can be found. Firstly, the current status of the offshore renewable types is given. The design specifications used in the modeling and certification of FOWTs are reviewed. The laboratory experiments and their methodology for FOWTs are explained. Finally, the numerical modeling studies of FOWTs and studies using two primary coupled numerical tools are reviewed.

The third chapter discusses the theoretical background behind the numerical tools used. First-order wave theory is given initially. The linear potential flow theory equations are explained briefly. Lastly, the environmental load that a FOWT is exposed to during its lifetime is discussed in detail.

The fourth chapter presents the turbine (DTU 10 MW RWT) and modeled platform concepts (e.g., OO-STAR, Nautilus, and CENTEC TLP) together with their properties. The hydrodynamic solvers (HAMS and AQWA) and their theoretical backgrounds are discussed. The last part of this section explains the project location and the details of the extreme value analysis for the computation of environmental parameters. Finally, the model tests (numerical tests) are presented.

In Chapter 5, numerical results are given and compared. Initially, the hydrodynamic coefficients computed by HAMS and AQWA are compared to the WAMIT results from relevant studies. For OO-Star and Nautilus platforms, the hydrodynamic coefficients are compared to outputs of the Lifes50+ project (Galván et al., 2018; Pegalajar-Jurado et al., 2018), and for the CENTEC TLP compared to Uzunoglu & Guedes Soares (2020). Additionally, the relevant load cases from those studies are modeled with (HAMS+OpenFAST) and (AQWA+OpenFAST). The results are compared to modeled (WAMIT+OpenFAST) simulations. The dynamic response of the three platform concepts for the Kıyıköy region is compared.

In the last chapter, the outcomes of this thesis and numerical simulations are given. Recommendations for further studies and improvements are also given briefly.

CHAPTER 2

LITERATURE REVIEW

This chapter presents previous offshore renewable energy research focusing on FOWTs and fixed-bottom offshore wind turbines. Also, a brief review of offshore marine renewables and the energy islands are given. Previous concepts are discussed, and the numerical modeling of FOWTs is discussed in detail.

2.1 Applications of Offshore Renewables

According to Jonkman (2009), immense wind energy potential in deeper water promotes the increased use of offshore wind turbines. Roddier (et al., 2010) stated that the limit to placing fixed bottom offshore wind turbines is 30 to 50 m in depth. Although most offshore wind farms have fixed-bottom foundations, the limit for placing fixed-bottom offshore wind turbines prevents greater energy production. Therefore, FOWTs might provide an alternative to harness greater wind potential further offshore. Surprisingly, floating offshore wind turbines have become commercialized recently (Aird, Gaertner, &Lackner, 2019). The main reason for this delay is the presence of 6 platform DOFs to consider where there are more significant structural motions on the rotor due to the platform motion.

Regardless of the difficulties in design and construction, FOWTs have additional advantages over fixed-bottom offshore wind turbines (Roddier et al., 2010). The location of the wind farms may be flexible. FOWTs could be located according to wind efficiency. The floating offshore turbines might be placed on a limited shallow continental shelf, and the visual impact of the turbines can be eliminated by locating the turbines further offshore.

Efforts to decrease the cost of renewable energy shift the development and improvements of future trends through sustainable energy systems. The progress in renewables concentrates on combined offshore renewable energies due to the greater energy potential and less environmental impact. Offshore wind farms and combined wave-wind energy systems are promising research areas of marine renewable energy systems. The combined systems could be classified as co-located wave-wind farms, hybrid energy converters, and energy islands (Pérez-Collazo, Jakobsen, Buckland, & Fernández-Chozas, 2013):

i) Co-located wave wind farms help to reduce the grid connection costs and the farm's operation and maintenance (O&M) costs while increasing the produced energy. Floating solar energy plants are a promising research area that might be combined with co-located wave wind farms.

ii) Hybrid energy converters reduce costs by combining different energy harvesting types into a single structure. Muliawan et al. (2013) modeled a combination of spar-type FOWT and Torus-shaped wave energy converter (WEC) and compared the coupled analysis results to a Spar FOWT. Perez-Collazo (2018) proposed two systems as a combination of water column WEC, monopile, and jacket-type fixed structure.

iii) Energy islands or multipurpose platforms could be an efficient solution for harnessing marine and maritime resources. Multipurpose platforms have different functions, combining leisure facilities, offshore renewables, and aquaculture. A sustainable service hub for O&M of offshore renewables and offshore terminal as an energy and transportation center might be additional usage for the multipurpose platform concepts (TROPOS, 2015). Further research is conducted with European Union-funded projects such as the MARINA platform (MARINA Platform, 2014), ORECCA (ORECCA, 2011), H2OCEAN (H2OCEAN, 2014), and MERMAID (MERMAID, 2015).

Having discussed future trends in offshore renewables, Section 2.2 briefly summarizes the design specifications used in the offshore wind industry. Section 2.3 provides detailed information on the experimental studies on FOWTs, and Section 2.4 presents information on the numerical modeling of FOWTs. The rest of this thesis will focus on the single FOWT systems and modeling approach.

2.2 Design Spesifications

As a relatively new concept, the design guidelines for offshore wind turbines evolved considering the industrial challenges and needs. Initially, the submerged body's design standards for the oil and gas industry were adopted. For the offshore turbine, the onshore wind energy guidelines were considered. For hydrodynamics, ISO (The International Organization for Standardization [ISO], 2007), DNV (Det Norske Veritas [DNV], 2010), and NORSOK (Standards Norway, 2007) standards were prepared for the fixed bottom steel offshore structures, and standards for oil platforms were used in some studies (see (Fevåg, 2012)). Due to the different environmental and operational conditions that OWTs encounter, including hydrodynamics, aero-hydro coupling, sea ice, aerodynamic loads, and more significant shallow water effects (Uzunoglu, 2019), OWTs differed from oil and gas platforms, fixed bottom offshore structures, and onshore turbines. Hence, there was a need for specific standards to design OWTs. The design guidelines evolved through the offshore wind industry following industrial developments.

Although the standards generally applied to fixed bottom and floating types, relevant design guidelines were prepared for the specific parts of floating concepts, such as the floating platform and the station-keeping system for the FOWTs (see. (Kyokai, 2012; ABS, 2015; Veritas, 2015; DNV GL, 2018; International Electrotechnical Commission [IEC], 2019) One should keep in mind that those standards did not apply to turbines. Hence the design specifications for onshore wind turbines should be employed considering the necessary changes to integrate the turbine offshore,

including modifications in the control model and the tower (Hopstad & Pollicino, 2020).

Another significant point of the design guidelines was location dependency. As Freedman et al. (2010) mentioned, there are substantial differences between the metocean conditions of Europe and the United States, including the extreme events in the United States due to severe storms, which result in different design considerations and certifications. Since most offshore wind projects have been installed in European waters, current offshore wind guidelines might not align with the United States region. The stakeholders should ensure that the applied design codes are relevant to the project area (Sirnivas, Musial, Bailey, &Filipelli, 2014). Hence as an emerging market, there is a significant need for an applicable guideline/certification for the United States region.

2.3 Experimental Studies on FOWTs

As mentioned in Section 2.1, the 6 DOF motion of the support structure alters the orientation of the turbine. It affects its aerodynamic performance and forces on the structure, where the additional mooring system increases the complexity (Liu, Xiao, Incecik, Peyrard, & Wan, 2017). The Technology Readiness Level (TRL) demonstrates a structured progress monitoring approach for renewable energy technology, including FOWTs. TRL is a convenient concept to determine the development stage of a specific technology, with levels from one to nine representing its maturity level (Tzinis, 2015). From the initial Research and Development (R&D) stage to the commercialization, the development of FOWTs requires numerical models and experimental tests simultaneously. Even though this thesis follows a numerical approach, to better present the idea behind the FOWTs, the background of experimental setups is also given in this thesis.

The experiments start at TRL 1-3 with small-scale model and component tests in the wave basin for validation and optimization of power. After the initial small-scale

tests, the prototype stage (TRL 4-6) takes place, where validation of the design is considered, better performance is aimed at, and the mooring system is validated with medium-scale tests (International Towing Tank Conference [ITTC] Proceedings, 2021). For later stages of development, full-scale tests are conducted in an open environment and finally at the sea/ocean (Table 2).

Table 2 Technology Readiness Levels for OWTs. Prepared from (ITTC Proceedings, 2021b)

Development Stage	**TRL**	**Objectives**
Validation	1-3	◦ Validate the OWT Concept ◦ Investigation of system variables and physical properties ◦ Small-scale models for power production optimization
Development	4-6	◦ Validate OWT Design ◦ Development of control models ◦ Medium-scale models for mooring system verification ◦ Using Site specific wind/wave spectra
Demonstration	7-8	◦ Near-full/full-scale tests in an open environment ◦ Deployed in relevant sea conditions
Commercial/System Development	9	◦ Full-scale tests at sea/ocean

Several experimental campaigns have been conducted as scaled models to investigate the assumptions made during the design phase, validate the numerical design codes, and verify the model performance in relevant environmental conditions (ITTC Proceedings, 2021a). FOWT experiments might be purely hydrodynamic or coupled with aerodynamics, including a rotor or actuator disk

approach, limited by the experimental facilities (Stewart & Muskulus, 2016). Experimental models of FOWTs have differences from the offshore wind turbines (OWTs) considering the effects of blade rotation and the elasticity of the structure components, which creates challenges to the FOWT model tests in the following areas: scaling, blade pitch control, calibration methods, and the experimental facilities (Chen, Chen, &Hu, 2020). A fully scaled rotor and wind generated by fans might be selected to model the aerodynamics in model experiments. However, this might be challenging considering the issue of Froude scaling for the hydrodynamics and Reynolds scaling for the aerodynamics. For some experiments, a predefined constant thrust force might be applied to the turbine, as in Utsunomiya et al. (2009). Although a constant thrust force might represent the coupled nature of FOWTs for a single load case, there might be a need for a more sophisticated approach to understanding FOWTs behavior fully.

Hybrid experimental testing methods are developed with increased computational power and the development of tools. Those hybrid methods might include software in the loop (SIL) and hardware in the loop (HIL) methodology. The SIL approach consists of an active control system where the fan simulates the instantaneous aerodynamics using a numerical tool (e.g., OpenFAST) using the displacement/position of the floating body. The SIL method could be carried out without wind generation in the wave basin eliminating the need for a scaled rotor construction. Without a scaled rotor, the model set up could be constructed for hydrodynamics using Froude scaling only. Since the aerodynamic effects are modeled with a numerical model, different wind directions could be tested. Finally, extreme cases with parked turbines and emergency stop tests can be simulated accurately in full-scale behavior (Oguz et al., 2018).

Unlike the SIL approach, in the HIL methodology, aerodynamic loads are obtained from a scaled wind turbine in a wind tunnel where the global body response and the hydrodynamic part are computed using a numerical model (Bayati, Facchinetti, Fontanella, & Belloli, 2018). Examples of the SIL method can be found in Azcona

et al. (2014); Day et al. (2017); Oguz et al. (2018); Vittori et al. (2021), and the examples of the HIL method can be found in Bayati, Bernini, et al. (2018).



Figure 3 On the left, 6 DOF HIL experimental setup (Bayati, Bernini, et al., 2018), and on the right, hexafloat robot (Bayati, Facchinetti, Fontanella, Giberti, et al., 2018) representing the platform motions. (modified)

The procedure of the HIL can be seen in Figure 4, where the hydrodynamics are computed with a numerical code (e.g., OpenFAST). Related platform displacements are transmitted to the turbine base with the hexafloat robot, and the aerodynamics are tested simultaneously in the wind tunnel (Bayati et al., 2018). This hybrid experimental approach might test various platform concepts with the same experimental setup for the platform. The details of the experimental setup with the DTU 10 MW RWT turbine and the hexafloat robot can be seen in Figure 3. Although two-hybrid testing methods have similar approaches, no study compares the two in the literature. Looking from the hydrodynamics modeling side of this issue, with the hydrodynamic experiments, the limitations of the numerical techniques in hydrodynamic modeling, such as inviscid flow assumption, might be investigated better with the hydrodynamic experiments with the SIL approach. On the other hand, for the cases where the aerodynamic performance validation is crucial HIL approach might provide a better approximation.

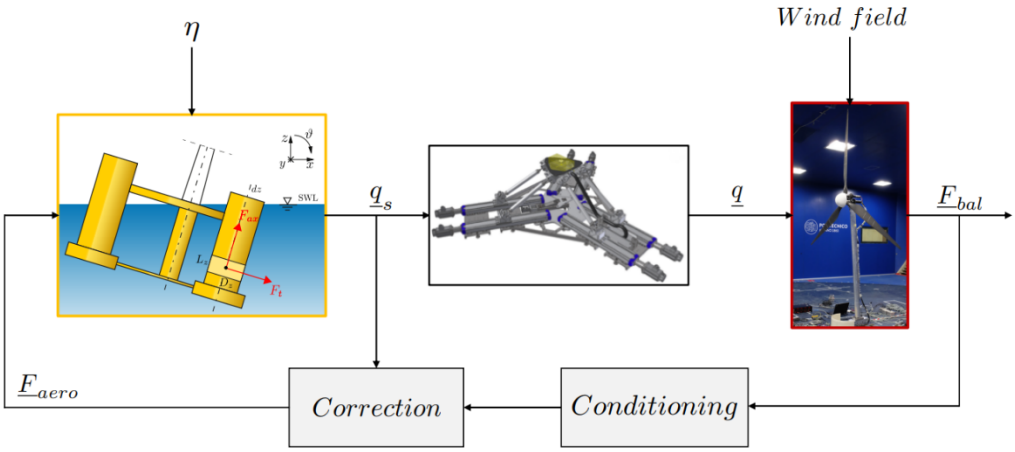


Figure 4 HIL approach for a hybrid FOWT experimental test (Bayati et al., 2018)

Previous experimental studies for the platform types discussed can be seen in Figure 5 and Figure 6. As seen in Figure 5, experiments for the DeepCWind semisubmersible and Hywind Spar have scaled rotors and wind generated in the wave basin for aerodynamics. In DeepCWind experimental campaign, three floater concepts are tested and compared with coupled tests. This campaign emphasizes that the tower's natural frequency depends heavily on the floater type. A stiffer platform, TLP resulted in lower bending frequency than other tested concepts such as spar and semisubmersible (Koo et al., 2014).

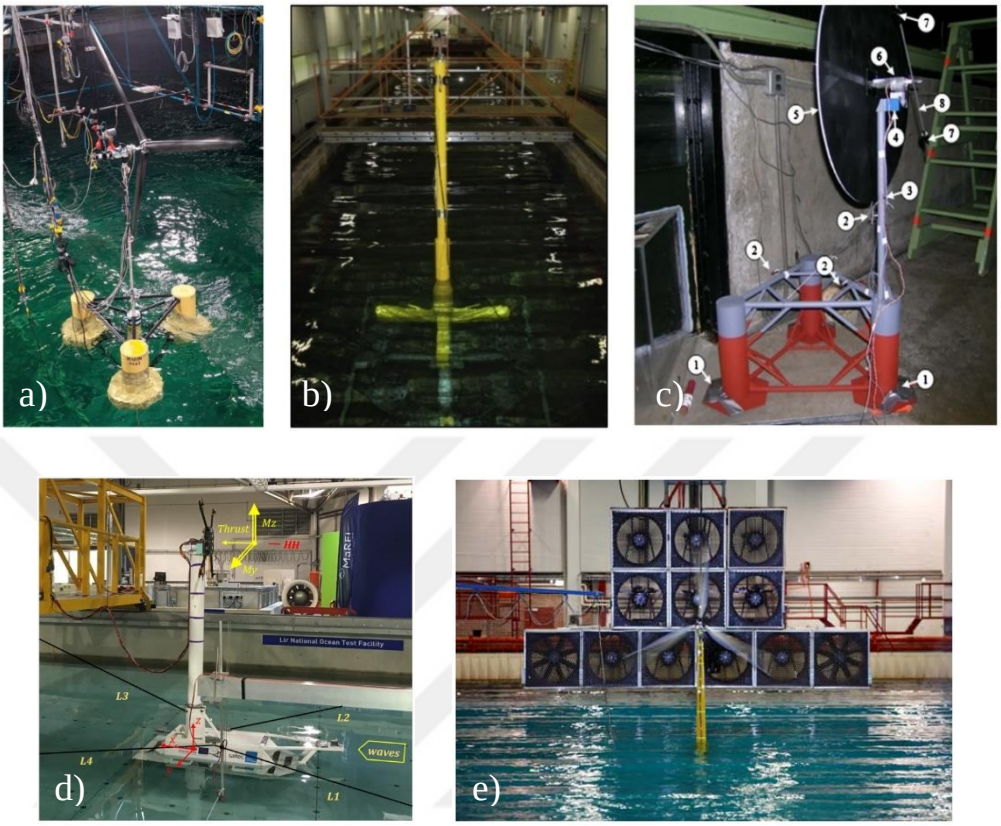


Figure 5 Experimental campaigns for the floating platforms in the literature: a) DeepCWind (Koo et al., 2014), b) Tension Leg Platform (TLP) (Oguz et al., 2018), c) WindFloat platform (Roddier et al., 2010), d) SATH 10 MW InWind (Vittori et al., 2021), e) HYWIND Spar (Nielsen et al., 2006)

In 2017 and 2018, model experimental tests were also conducted in Sintef Ocean Basin (https://www.sintef.no/en/ocean/) for OO-Star and Nautilus platforms within the Lifes50+ Project scope to verify the design performance, to obtain data for numerical model calibration and to develop hybrid testing methods (Thys et al., 2018). OO-Star and Nautilus concepts are scaled to 1/36 size, and hardware in the loop methodology is selected for the aerodynamic loads where the instantaneous aerodynamic loads are computed numerically and applied to the system at the tower top (Madsen et al., 2018).



Figure 6 Experimental tests for the OO-Star (Thys et al., 2018) on the left, Nautilus (Madsen et al., 2018) in the middle, and CENTEC TLP (Mas-Soler et al., 2021) on the right

The experimental test results with a 1/60 scale for the CENTEC TLP are published for its transportation stage, only representing its free-floating behavior where it is stabilized due to its large waterplane area. The regular and irregular wave tests are conducted in sea states suitable for FOWT installation in calm water and waves, considering its motion and resistance during towing (Mas-Soler et al., 2021). It should be noted that in this thesis, CENTEC TLP is only investigated in its installed operational condition. The overall properties of the experimental studies of FOWTs in the literature can be seen in Table 3.

Table 3 Previous experimental studies for FOWTs.

Reference	Laboratory	Platform	Scale	Aerodynamics
(Nielsen et al., 2006)	Marintek	HYWIND Spar	1/47	Full Rotor
(Utsunomiya et al., 2009)	NMRI (National Maritime Research Institute)	Spar	1/22.5	Steady Force application
(Roddier et al., 2010)	UC Berkeley	WindFloat Semisubmersible	1/105	Actuator Disk / Rotating mass
(Nihei & Fujioka, 2010)	University of Tokyo	TLP	1/100	Full rotor
(Gueydon & Weller, 2013)	MARIN (2011)	DeepCWind Spar, TLP, Semisubmersible	1/50	Full rotor
(Myhr et al., 2011)	MARINTEK	HYWIND Spar, Tension Leg Buoy (TLB)	1/100	None
(Naqvi, 2012)	Alden Research Laboratories	TLP, Spar Buoy	1/100	Rotor / Aerodynamic Disk
(Azcona et al., 2014)	Ecole Centrale Nantes (ECN)	Concrete Star Semisubmersible	1/40	SIL / Ducted fan
(Myhr & Nygaard, 2014)	IFREMER	TLB	1/40	None
(Myhr & Nygaard, 2015)	IFREMER	MARINET 3 TLBs	1/40	None
(Azcona et al., 2016)	ECN & DHI	Semisubmersible	1/60	Ducted fan / Rotor
(Madsen et al., 2018)	SINTEF Ocean (Lifes50+)	Nautilus, OO-Star Semisubmersible	1/36	SIL / Numerical Model

Table 3 (continued)

(Bayati et al., 2018)	Politecnico di Milano (Lifes50+)	Nautilus, OO-Star Semisubmersible	1/225 RE Scale	HIL / Hexafloat
(Oguz et al., 2018)	University of Strathclyde	TLP	1/36.67	SIL / Electric Ducted Fan (EDF)
(Vittori et al., 2021)	Lir National Ocean TF	SATH 10 MW InnWind	1/49	SIL / Propeller Actuator
(Mas-Soler et al., 2021)	CENTEC	CENTEC TLP	1/60	None

Experimental data is crucial to understanding the physical phenomena behind the complex dynamic behavior of FOWTs and validating numerical models. On the other hand, considering the cost of the experiments, the capabilities of the physical facilities, the time-consuming process, and the uncertainties in the data measurements, numerical modeling might provide an efficient approach to understand the dynamic response of FOWTs in more complex environments.

2.4 Numerical Modeling of FOWTs

Different approaches are present for the numerical modeling of FOWTs, considering the purpose of the model. For instance, high-resolution computational fluid dynamics (CFD) models might be required to capture the flow dynamics for applications where the aim is a high accuracy, especially in the order of boundary layer height. On the contrary, if computational time has higher importance than high-fidelity CFD models, potential flow solvers can be selected for the platform hydrodynamics.

Various specialties should be included in the numerical modeling of FOWTs to represent their strongly coupled dynamic response to hydrodynamics and aerodynamics, including moorings, control, and structural mechanics. Widely used and well-validated coupled analysis tools for FOWT modeling can be given as i)

HAWC2 (Larsen & Hansen, 2007) and ii) OpenFAST (previously known as FAST) (Jonkman, 2013).

HAWC2 is the second generation of HAWC, and the code was developed by Danmarks Tekniske Universitet (DTU) Department of Wind Energy between 2003-2007. The code is capable of time domain analysis of onshore horizontal axis wind turbines (HAWTs), vertical axis wind turbines (VAWTs), and offshore turbines, including fixed bottom and floating platforms with moorings. Hydrodynamics can be solved using Morison Equation-based external interface or coupling with well-known hydrodynamic solvers (Bischoff Kristiansen, 2022).

Skaare et al. (2007) investigated the fatigue life of an HYWIND Spar with a 5 MW turbine using coupled HAWC2 and Simo-Riflex codes with two control strategies as traditional conventional control and estimator-based control. It was stated that with the conventional control for FOWTs, there might be a negative damping problem that reduces a platform's fatigue life. According to their research, the fatigue life of the HYWIND platform was highly dependent on the environment and blade pitch control. In contrast, with estimator-based control, there were improvements in the lifetime of the rotor and the tower. Etemaddar et al. (2014) examined the effects of controller faults on fatigue damage of an OC3 HYWIND spar with an NREL 5 MW turbine. They concluded that blade composite material has greater fatigue life compared to steel. A comparison of the behavior of controller faults was also carried out for an onshore turbine and an OC3 HYWIND Spar (Etemaddar et al., 2014).

Coupled dynamic response in survival conditions of a Spar with 5 MW NREL wind turbine is studied using coupled HAWC2 and Simo-Riflex codes. This research concludes that steady wind agitates the pitch natural frequency (resonance) dominantly, whereas turbulent wind excites the surge and pitch DOFs (Karimirad & Moan, 2011). A feasibility study for implementing a Spar-type floater on moderate water depth is conducted using HAWC2 and Simo-Riflex, where the structure is shortened and modified with a smaller mass providing a decreased cost (Karimirad

& Moan, 2012a; Karimirad, 2013). The details of the coupling using a dynamic link library and the numerical methodology can be found in Karimirad & Moan (2012).

An initial concept for a floating VAWT with a Darrieus-type rotor and spar-type platform, DeepWind concept/project, is designed and verified using HAWC2 (Vita et al., 2012). Within this project, a numerical model for a floating VAWT was also developed simultaneously. The simulation challenges for integrating a floating VAWT to HAWC2 are mainly the blade and controller/drivetrain instabilities discussed in detail in Verelst et al. (2015).

A triple spar floating structure and DTU 10 MW RWT is modeled using coupled WAMIT and HAWC2 tools to investigate the substructural flexibility and its effects on the wind turbine response (Borg et al., 2017).

Previous modeling studies using HAWC2 for FOWTs considered only linear wave hydrodynamics. Xu et al. (2019) applied a fully nonlinear wave methodology for an OC4 semisubmersible FOWT generating the wave field in a 2D numerical wave tank to investigate the effects of nonlinearity on the FOWT behavior and related forces. Within this study, there was a difference in the wave spectrum's energy distribution, and greater shear force and bending moment at the tower base were obtained for linear waves. Due to the wave frequency load domination, similar heave and pitch responses were obtained. On the other hand, the linear model underestimated the surge response and mooring tension due to the effects of low-frequency loads on those parameters (Xu et al., 2019).

A combined wind wave energy device P80 platform semisubmersible concept from FPP is modeled with WAMIT-HAWC2 coupled code (Voltá et al., 2020). Unlike the previous concepts discussed in this chapter, P80 is a wave-wind combined energy device that could support one turbine with 5-10 MW and WECs of 2-3.6 MW. The authors provided a simplified approach for design iteration and suggested that wind-wave misalignment should also be modeled for this platform. For the cases where the platform reached its highest response in pitch and heave, the tower top

acceleration exceeded the design limit. Therefore, the aerodynamic damping direction is essential for this design for platform pitch DOF.

OpenFAST (previously known as FAST) is developed by NREL in Colorado. The code also models onshore and offshore turbines and includes various submodules to introduce multiphysics modeling, which is crucial for FOWT numerical modeling. The code was initially developed for the onshore turbines; with increasing interest in offshore turbines, the software was extended, and hydrodynamic capabilities were added to model OWTs and FOWTs. Previously, the code has been used and validated by a significant number of scholars.

One of the first coupled FOWT models with FAST was a TLB with 500 kW HAWT, where a method was developed for the coupled analysis of FOWTs for the first time (Withee, 2004). The efforts to develop a methodology for FOWT modeling continued with state-of-the-art TLP designs (Jonkman, 2009; Matha, 2010). Roddier et al. (2010) worked on a semisubmersible design, WindFloat, which could accommodate a 5 MW or larger wind turbine without significant modifications in the design. During the testing and model verification of this concept, it was determined that minor oscillations with longer periods resulted in a decreased power production due to the control system.

A Dutch tri-floater semi-submersible with NREL 5 MW turbine is modeled using Aquaplus for hydrodynamics and FAST for the coupled analysis. The moorings were computed using Orcaflex. The effects of four different hydrodynamic cases are compared based on the linear potential flow solution with the addition of nonlinear Froude-Krylov forces, excluding Morison loads on brace elements, and a fully linear model with a damping plate. It is observed that the difference is slight for smaller wave heights. In some cases, a greater response is observed for nonlinear Froude Krylov forces within the same magnitude. The wave directionality models result in increased translational motion in translational DOFs and decreased motion in rotational DOFs (Philippe et al., 2014). The effects of non-linear hydrostatics and wave forces of FOWTs during extreme seas are investigated by coupled FAST-

Simdyn model. The relation of negative damping due to using conventional land-based control (constant power control) on FOWTs and large amplitude motions area studied(Jose et al., 2020). In addition to the work of Philippe et al. (2014), the effects of wind speed are also considered. It is found that the greater wind speed with waves yields greater heave and pitch motion compared to the fully linear hydrodynamic modeling. It is noted that this phenomenon is not dependent on the negative damping problem on FOWTs.

Validation of a FAST model with experimental data is carried out for DeepCWind semisubmersible by Coulling et al. (2013), including the second-order hydrodynamics using Newman's method, and it was found that the second-order difference frequency forces have a significant effect on the global response of the structure especially when there is no wind. The second-order difference frequency for the wave-only FAST model improved the correlation of experiment data and the numerical model in surge DOF and mooring tensions. Although there is a deviation in the low-frequency responses, this might be due to the quad-drag selection for the numerical model. For a wave wind coexistent case, the effects of second-order waves are slight. Since, during the parked turbine case, the primary driving force is the hydrodynamics, second-order wave forces should be considered (Coulling et al., 2013). A methodology for computing second-order forces is applied to OC3 Hywind Spar and UMaine TLP (Roald, 2013). The results of the numerical models provide that the effects of second-order forces for the OC3 Hywind spar were negligible. However, there were some excitations in the natural frequencies of the platform. For the next concept, UMaine TLP, the effects of the second-order forces were higher with greater motion. Especially in heave DOF, the second-order sum frequency forces govern the global motion. The aerodynamics dominate the motion for the low-frequency range of OC3 Hywind Spar; therefore, difference frequency forces can be neglected.

Second-order forces were also computed for the OC4 semi-submersible using two approaches, (DIFFRAC+aNySIM) and (WAMIT+FAST) combination with overall agreements for two methods (Gueydon et al., 2014). Due to the design ideas behind

the OC4 semi-submersible, to have a pitch natural period above the high energy wave region in its operational state, the structure has a small righting moment and hence second order difference frequency forces with longer periods have in heave, pitch, and surge DOFs have greater effects on the structure. Since the additional damping during the linear potential flow solution was not considered in QTF computation, this might cause the amplification of the motions. In addition to the effects on the global response of the FOWTs, with the current methods for estimating difference frequency second order loads, there is an underprediction (Simos et al., 2018) which might affect the accuracy of the ultimate and fatigue loads on the system (Robertson et al., 2020).

CHAPTER 3

THEORETICAL BACKGROUND

Considering their multidisciplinary nature, to fully understand the behavior of FOWTs, one should have knowledge about at least the aerodynamics, structural dynamics, and hydrodynamics of a floating body and the relevant loads on the structure. In this chapter, the fundamentals of wave theory are initially given to present a basis for further numerical modeling of hydrodynamics. Irregular waves and spectrum concepts are provided to visualize the stochastic nature of ocean waves. Potential flow theory, an efficient approach for the FOWT hydrodynamics, and the basis of this thesis are described in detail. Finally, the loads the structure is exposed to during its operational life due to the environmental parameters are discussed.

3.1 Fundamentals of Wave Theory

3.1.1 Small Amplitude Wave Theory (Regular Waves)

Wave motion can be represented by the small amplitude wave theory, a straightforward solution based on sinusoidal waves (Kamphuis, 2000). The coordinate axis used for this theory is chosen as the x-axis direction in wave propagation, and the y-axis is the perpendicular horizontal plane. The z-axis is upwards vertically. The water surface for small amplitude wave theory could be represented as,

$$\eta = a\cos(kx - \omega t) = a\cos(\frac{2\pi x}{L} - \frac{2\pi t}{T}) \tag{3.1}$$

$$k = \frac{2\pi}{L}\ and\ \omega = \frac{2\pi}{T} \tag{3.2}$$

In this equation, η represents the wave elevation, a is the wave amplitude, where x is the wave propagation distance, L is the wavelength, T is the wave period, k is the wave number, and ω represents the angular wave frequency.

3.1.2 Irregular Waves

Regular waves can be generated in the wave tanks to assess relevant parameters, including response amplitude operator (RAO) and natural frequencies. However, irregular waves and wave spectrums should be included in the analysis to represent the ocean. The wave spectrum is crucial in defining all possible sea states; in other words, describing the sea surface as a combination of stochastic events is essential (Holthuijsen, 2007). The moving surface elevation could be represented by the sum of multiple harmonic waves with random phase and a constant amplitude given below as:

$$\eta(t) = \sum_{i=1}^{N} a_i \cos(2\pi f_i t + \alpha_i) \tag{3.3}$$

In this equation, N represents the number of frequencies, amplitude a_i and phase f_i are random variables.

Two primarily used wave spectrum types are Pierson-Moskowitz (Pierson & Moskowitz, 1964) and Joint North Sea Wave Project (JONSWAP) (Hasselmann et al., 1973) JONSWAP Spectrum is an empirical spectrum that is the outcome of an extensive measurement project in the North Sea. JONSWAP spectrum is the modified form of the Pierson-Moskowitz spectrum as being a non-fully developed, fetch-limited version, meaning wave growth continues for the JONSWAP spectrum.

$$S_j(f) = \alpha g^2 (2\pi)^{-4} f^{-5} \exp\left[-\frac{5}{4}\left(\frac{f}{f_{peak}}\right)^{-4}\right] \gamma^{exp\left[-\frac{1}{2}\left(\frac{f/f_{peak}}{\sigma}\right)^2\right]} \tag{3.4}$$

In this equation of the complete expression of the JONSWAP spectrum, α represents the energy scale parameter, f_{peak} is the frequency scale, and finally, γ, σ_a, and σ_b

($f \leq f_{peak}\ \sigma = \sigma_a\ and\ f > f_{peak}\ \sigma = \sigma_b$) are the shape parameters where their average values are (Holthuijsen, 2007):

$$\gamma = 3.3, \sigma_a = 0.07\ and\ \sigma_a = 0.09 \tag{3.5}$$

Although JONSWAP Spectrum was created from a limited region, it gives accurate results for the universal problems for various wind conditions as well as storms and hurricanes, making the JONSWAP spectrum an attractive design spectrum for engineers (Holthuijsen, 2007). Hence, in this study JONSWAP spectrum is used to define the irregular sea state.

3.1.3 Potential Flow Theory

Potential flow is a flow condition in which a velocity potential can be defined. The theory assumes that the flow is irrotational and, hence, inviscid, which yields that the viscous effects are neglected (Birk, 2019). The velocity field might be represented by velocity potentials. For the incompressible flows outside the boundary layer, viscous effects might be neglected, and the Navier-Stokes Equations could be described as Euler equations.

Potential flow theory has a practical application for offshore waters. By assuming irrotational flow, the effect of viscosity is not considered. Additional damping might be added to the system to include the effects of viscosity.

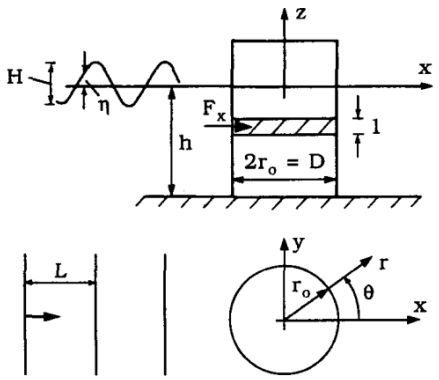


Figure 7 Coordinate system and definition of a vertical cylinder system (Sumer & Fredsøe, 2006)

Considering large cylinders (D/L>0.2), the diffraction effects around the body become essential. For Keulegan Carpenter (KC) number smaller than two, the body remains in an unseparated flow region, the effects of the boundary layer on the structures remain insignificant, and the viscosity effects could be neglected. Hence, the potential flow equations can be applied to the body.

Potential flow equations can be defined below using the coordinate system and the definitions described in Figure 7. Let us define velocities as:

$$u_i = \frac{\partial \emptyset}{\partial x_i}, v_i = \frac{\partial \emptyset}{\partial y_i} \text{ and } w_i = \frac{\partial \emptyset}{\partial z_i} \tag{3.6}$$

Additionally, the continuity equation could be written using the velocity potentials, satisfying the Laplace equation.

$$\nabla^2 \emptyset = \frac{\partial^2 \emptyset}{\partial x^2} + \frac{\partial^2 \emptyset}{\partial y^2} + \frac{\partial^2 \emptyset}{\partial z^2} = 0 \tag{3.7}$$

Using the kinematic bottom condition at the bottom and assuming an impervious seabed,

$$w_i = \frac{\partial \emptyset}{\partial z_i} = 0 \; at \; z = -h \tag{3.8}$$

And having the dynamic free surface condition with constant pressure (Linearized Bernoulli Equation at the free surface),

$$\frac{\partial^2 \emptyset}{\partial t^2} + g\frac{\partial \emptyset}{\partial z}=0 \text{ at z=0 (Free Surface)} \tag{3.9}$$

Additionally, considering the linear nature of the potential flow function, the total potential flow could be written as below:

$$\emptyset = \emptyset_i + \emptyset_s \tag{3.10}$$

In this equation, the total velocity function is written as the sum of the incident and scattered part of the potential functions. Here, the scattered amount includes the effects of refraction and diffraction from the body. $\emptyset_i$ which is the incident potential function for undisturbed wave could be written as:

$$\emptyset_i = -i\frac{gH}{2\omega}\frac{\cosh(k(z+h))}{\cosh(kh)}e^{i(kx-\omega t)} \tag{3.11}$$

Equation 3.11 satisfies the Laplace equation and the boundary equations above for the total potential. The angular frequency, ω in Equation 3.11 could also be written as:

$$\omega^2 = gk\tanh(kh) \tag{3.12}$$

Furthermore, the equations for the linear wave theory using the potential function for surface elevation and velocities in x and z directions can be written as:

$$\eta = -\frac{1}{g}\left(\frac{\partial \phi}{\partial t}\right)_{z=0} = \frac{H}{2}\cos(\omega t - kx) \tag{3.13}$$

$$u = \frac{\partial \emptyset_i}{\partial x} = \frac{\pi H}{T}\frac{\cosh(k(z+h))}{\sinh(kh)}\cos(\omega t - kx) \tag{3.14}$$

$$w = \frac{\partial \emptyset_i}{\partial z} = \frac{\pi H}{T}\frac{\sinh(k(z+h))}{\sinh(kh)}\sin(\omega t - kx) \tag{3.15}$$

In Equation 3.13, η is the surface elevation, u is the velocity in the x-direction, w is the velocity in the z-direction, T is the wave period, ω is the angular frequency, and

k is the wave number given in Equation 3.2. Potential flow around a body could be solved using those equations. The detailed potential flow analytical solution for linear (sinusoidal) waves can be found in Sumer & Fredsøe (2006).

For larger structures like FOWT platforms, potential flow solvers promise an alternative, powerful analytical solution. Although the limitations include considering irrotational flow assumption and neglecting the effects of viscosity, potential flow solution applies to deep-water bodies. If necessary additional damping could be added to tune the model.

3.1.4 Second Order Stokes Waves

Linear wave theory (sinusoidal waves) provides an efficient approach to wave mechanics problems with less computational cost than higher-order solutions. However, it is crucial to capture the nature of the "real" wave (Svendsen, 2006), including second-order effects and its effects on the offshore structures instead of sinusoidal waves with equal crests. Although the second-order contributions are smaller than the first-order solution, combinations of two approximations result in a steeper crest and shallow trough similar to ocean waves (Chakrabarti, 2005). This thesis does not consider the effects of the second-order waves.

3.2 Hydrodynamics of Floating Body

3.2.1 Equation of Motion

The hydrodynamics of the floating platform is similar to the moored motion of the ships, where there are six DOF motions. The characteristic DOFs of floating body motion on the water can be named as surge in longitudinal horizontal motion (x direction), sway in lateral motion perpendicular to surge (y direction), heave in the vertical direction (z-direction), pitch in rotational motion about the lateral axis (Rx), roll in rotational motion about the longitudinal axis (Ry) and finally yaw in rotational

motion about z direction (Rz). The motion of FOWTs is coupled in 6 DOFs where the general equation of motion could be written as (Chakrabarti, 2005; Goda, 2008):

$$\sum_{j=1}^{6}\{(M_{kj}+m_{kj})\ddot{x}_j + N_{kj}\dot{x}_j + C_{kj}\dot{x}_j|\dot{x}_j| + B_{kj}x_j + R_{kj}(x_j)\} = X_k(t)$$

$$k = 1,2,3,..6 \qquad (3.16)$$

In Equation 3.16, k represents the 6 DOFs, and j is the coupled DOF of k for the coupled motion. x_j corresponds to the related displacement in DOF j. M_{kj} refers to the inertia matrix where it stores the inertia in the k direction in the presence of motion in j DOF. m_{kj}, corresponds to the added mass. The term added mass is the fluid resistance to the floating body motion in k DOF while the platform moves in the j direction. The wave-damping coefficient is represented by N_{kj} and the nonlinear damping force (e.g., Drag force) is given as C_{kj}. The restoration force coefficient due to the buoyancy is presented as B_{kj} and the nonlinear effect because of the mooring system is given as $R_{kj}(x_j)$. $X_k(t)$ on the right-hand side is the external force the floating structure is exposed to, including current, wind, and wave loads. Equation 3.16 is modified to have the same naming as the FOWT literature. The added mass term is presented as A_{kj}, the hydrostatics matrix is shown as C_{kj} (includes buoyancy and mooring effects - $B_{kj}x_j \; and \; R_{kj}(x_j)$ terms) and the radiation damping is given as B_{kj}, which includes wave damping (N_{kj}) and nonlinear damping force (C_{kj}) in Equation 3.16.

3.3 Load Description

Offshore wind turbines strongly interact with the environment, where the resulting loads are mainly due to wind, waves, and currents. The following section provides the theoretical background of the environmental loads.

3.3.1 Hydrodynamic Loads

Similar to coastal engineering problems, the method should be chosen carefully considering the structure's flow conditions and dimensions to calculate the forces on the offshore structures. Due to waves, tides, and currents, an offshore structure may be exposed to hydrodynamic loads. Since we are interested in the deep water and the project location is in the Black Sea, only hydrodynamic loads due to waves are considered in this thesis. The loads due to waves could be classified as forces due to undisturbed oscillatory flow, radiation forces due to relative movement of the structure and flow, and diffraction forces due to diffracted waves. For those components, contributions of linear and nonlinear effects establish the hydrodynamic loads. These are the combination of linear hydrostatics, linear excitation, linear radiation, and nonlinear effects. Incident waves create linear excitation, and linear radiation is created due to the platform motion and the outgoing waves (Jonkman, 2010).

3.3.1.1 Morison's Equation

For structures with smaller KC numbers with negligible diffraction effects, the Morison equation provides a solution for the load calculation around the structures for the drag and inertia terms separately. The inertia term consists of hydrodynamic force and Froude-Krylov force, where the total inline force per unit length could be written as (Sumer & Fredsøe, 2006):

$$F = \frac{1}{2}\rho C_D U|U| + \rho C_m A\dot{U} + \rho A\dot{U} \tag{3.17}$$

In equation 3.17, the first term is the drag force, the second is the hydrodynamic mass force, and the last is named the Froude-Krylov force. By organizing Equation 3.17, the Morison equation could be written as below:

$$F = \frac{1}{2}\rho C_D U|U| + \rho C_M A\dot{U} \tag{3.18}$$

$$C_M = C_m + 1 \tag{3.19}$$

where U is the inline velocity, $\dot{U}$ is the time derivation of velocity, C_M is the inertia coefficient, and C_D is the drag coefficient. Values of C_M and C_D depend on the flow conditions considering KC and Re numbers, and the reference values could be found in the literature (Sumer & Fredsøe, 2006).

3.3.2 Aerodynamic Loads

The aerodynamic forces due to air-structure interaction on the blades and turbine could be investigated in three main areas as steady aerodynamic forces due to mean wind speed, periodic aerodynamic loads induced due to wind shear, misaligned wind, shadow effects, and rotor rotation, and randomly fluctuating loads due to random events as turbulence and system dynamics (Matha, 2010). The steady aerodynamic loads can be computed with Blade Element Momentum Theory, where the thrust and the generated power could be calculated. Blade element momentum theory (BEMT) is the most often used aerodynamic model and provides good accuracy with decreased computational cost. Blade element theory, the first part of BEMT, divides the blades into small aerodynamically independent elements as 2-D airfoils and calculates the aerodynamic loads on the elements separately, considering the local forces. Ensuring the conservation of momentum, the second part of BEMT, also named momentum theory, guarantees that the force exerted by the air on the rotor equals the loss of momentum. The usage of these two theories results in an iterative loop where the aerodynamic forces and the induced velocities can be calculated (Moriarty & Hansen, 2005).

3.3.3 Other Loads

Environmental loads on offshore structures are not limited to hydrodynamic and aerodynamic loads. Additional considerations may include sea ice, current, earthquake, and marine growth, considering the site's environmental parameters.

Since there is no sea ice in our possible offshore wind farm area and the tidal effects are negligible for the area, those additional forces are not discussed further. For the earthquake loads, as given by Caceoğlu et al. (2022), the earthquake risk is not crucial for the area. However, as the offshore wind industry expands through earthquake-prone regions, the effect of the earthquake loads on the FOWTs should be investigated for potential sites.

This chapter presents the theoretical background behind this thesis, starting from the linear wave theory. Regular and irregular waves are discussed. The linear potential flow theory and second-order waves are given. The environmental loads that a FOWT is exposed to during its lifetime are discussed briefly, including hydrodynamic and aerodynamic loads.

The next chapter focuses on the numerical model and methodology details. The components of the numerical model, including the turbine and the platform configurations, are given. The commercial and open-source codes used in the coupled analysis are discussed with the theories and limitations. The selected project location properties and the extreme value analysis for the area are given in detail. Finally, the numerical model comparison tests are provided for the platform concepts to define the system characteristics.

CHAPTER 4

NUMERICAL MODELLING AND METHODOLOGY

As described in Chapter 3, the global response of FOWTs includes the coupling of turbine aerodynamics and platform hydrodynamics. The coupling should be included in the analysis process to understand the structure. To fully represent this coupling, experimental research about FOWTs requires expensive laboratory facilities, including a wave flume and a wind tunnel. Numerical studies provide an efficient and accurate solution. This study uses numerical methods to carry out a dynamic analysis of FOWTs.

As mentioned in Chapter 1, three different platform types are selected and modeled in this work using HAMS and AQWA. The dynamic responses of those platforms are simulated in the operational conditions for a chosen site. Chapter 4 provides essential information about the numerical models, the properties of the turbine, the platform designs, the modeling considerations, and the project location. The model parts discussed are the DTU-10 MW reference wind turbine (RWT), Nautilus DTU-10, OO-Star DTU-10, and CENTEC TLP. Detailed flowchart of this thesis is shown below in Figure 8, where the methodology and tools are presented. The figures used to prepare Figure 8 are taken from OO-Star System (Dr.techn. Olav Olsen AS, 2018), the Nautilus platform (Galván, Sánchez-Lara, et al., 2018), the CENTEC TLP system (Uzunoglu & Guedes Soares, 2020), and Fast diagram (Matha, 2010).

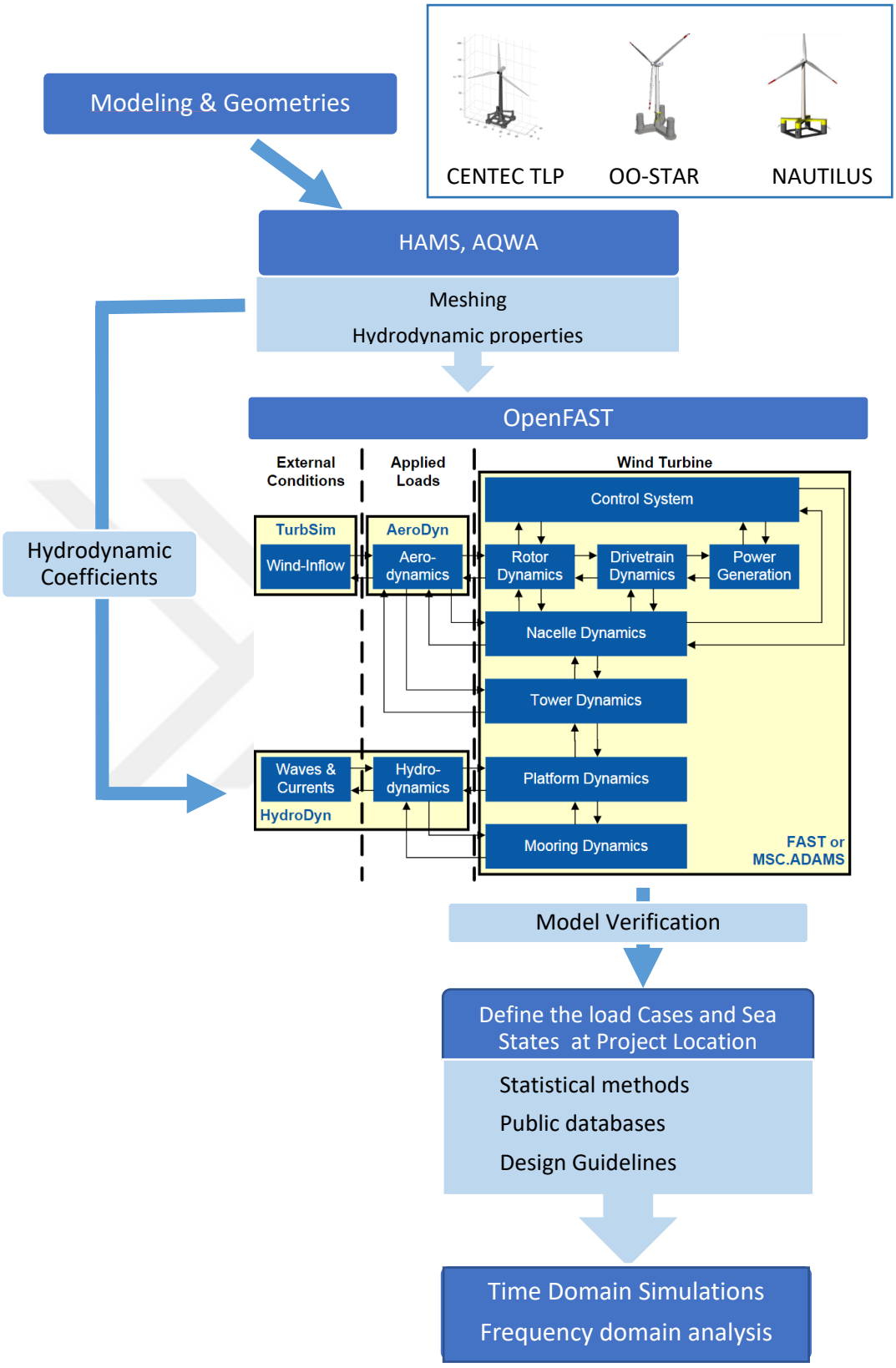


Figure 8 Overall flowchart of the thesis presenting the methodology and tools

4.1 DTU 10 MW Reference Wind Turbine (RWT)

DTU 10 MW is a publicly available horizontal axis wind turbine having 10 MW rated power and three blades. DTU 10 MW RWT is developed upscaling the NREL 5MW RWT as a basis for future designs' aerodynamic and structural validation. Although the design concept is similar, there are differences due to DTU 10MW RWT being designed for an offshore environment. As can be seen in Bak et al. (2013), the International Electrotechnical Commission (IEC) turbulence class is changed to 1A for the offshore environment with high wind and high turbulence wind climate, the hub height is lowered, the drivetrain concept is changed to medium speed, and blades have prebend for tower clearance purposes during the upscaling process by DTU team. As seen from Figure 16, the annual mean wind speed for the possible offshore wind farm site in Kıyıköy is around 8.5 m/s at hub height which counts for class 2 turbine, and the turbulence class can be selected as class B for the chosen area (Zhang, 2015). Hence, a different turbine design might be considered for future studies for Kıyıköy. However, DTU 10 MW was used in this thesis to carry out the numerical analysis. The design parameters of DTU 10 MW RWT are summarized in Table 4, and further design details of DTU 10MW RWT can be found in Bak et al. (2013).

Table 4 Overall design parameters of DTU 10MW RWT. (Borg, Manuel, Collu, &Liu, 2015)

Design Properties	**Value/Type**	**Unit**
Rotor Orientation	Clockwise rotation-upwind	[-]
Control	Variable speed, Collective pitch	[-]
Cut in wind speed	4.0	[m/s]
Cut out wind speed	25.0	[m/s]
Rated wind speed	11.4	[m/s]
Rated power	10.0	[MW]
Number of blades	3.0	[-]

Table 4 (continued)

Rotor diameter	178.3	[m]
Hub diameter	5.6	[m]
Hub height	119.0	[m]
Drivetrain	Medium speed, multiple-stage gearbox	[-]
Minimum rotor speed	6.0	[rpm]
Maximum rotor speed	9.6	[rpm]
Gearbox ratio	50.0	
Hub overhang	7.1	[m]
Shaft tilt angle	5.0	[deg]
Rotor precone angle	-2.5	[deg]
Blade prebend	3.332	[m]
Rotor mass	227.962	[kg]
Nacelle mass	446.036	[kg]
Tower mass	628.442	[kg]

4.2 Platform Types

4.2.1 Nautilus DTU-10 Floating Wind Turbine

Nautilus floating platform is an innovative smart semisubmersible platform design with a Platform Trim System (PTS) to decrease the wind-induced trim angle using an active ballast system (Galván, Sánchez-Lara, et al., 2018). The floating system is designed for the Gulf of Maine and has a water depth of 130 m (Yu, 2018). The RNA system has the DTU 10 MW RWT and DTU wind energy controller (Hansen & Henriksen, 2013) tuned for an offshore environment. The support system consists of the tower, platform, and Station Keeping System (SKS), which includes four

catenary mooring lines. The full Nautilus DTU-10 floating wind turbine system can be seen in Figure 9.

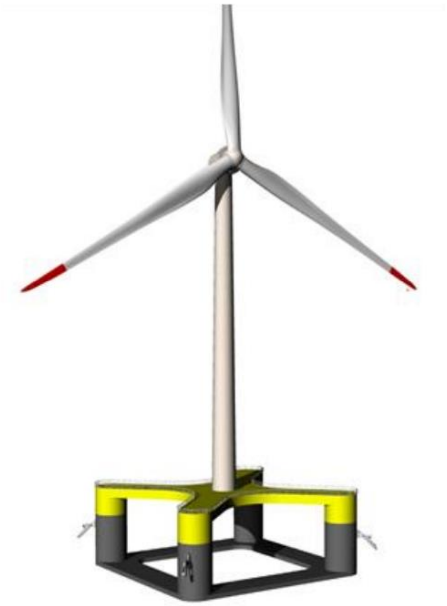


Figure 9 Nautilus DTU-10 FOWT concept (Galván, Sanchez-Lara, et al., 2018)

Since Nautilus floating substructure has an active ballast system, the relevant weight-dependent parameters can be modified concerning the changing wind and wave directions, including the mass, inertia, and draft-dependent parameters (Galván, Sánchez-Lara, et al., 2018). This modification also yields changes in the hydrodynamic parameters of the platform. Hence, different hydrodynamic models can be used for each simulation case considering the environmental parameters. Pegalajar-Jurado et al. (2018) applied an alternative approach where the hydrodynamic parameters of the platform are calculated assuming the fully loaded tank condition for all design load cases (DLCs). The same procedure is followed in this work, and the publicly available Nautilus DTU-10 FAST model from the Lifes50+ project (Galván, Sánchez-Lara, et al., 2018) is used without major modifications for hydrodynamic model comparison. The fully loaded ballast properties of the platform are given in Table 5.

Table 5 Nautilus platform properties with fully loaded ballast, including DTU 10 MW RWT (Yu, 2018)

Property	**Fully Ballasted Value**	**Unit**
Overall substructure mass (excl. tower, mooring)	7.781E06	[kg]
Center of Mass (CM) below MSL	14.283	[m]
Roll Inertia about CM	4.829E9	[kg.m^2]
Pitch Inertia about CM	4.829E9	[kg.m^2]
Yaw Inertia about CM	7.451E9	[kg.m^2]
Draft at equilibrium with moorings (no thrust)	18.333	[m]
Displaced water volume	9280.96	[m^3]

4.2.2 OO-Star DTU-10 Floating Wind Turbine

The OO-Star floating platform is semi-submersible with one central and three outer columns. The design is developed by Dr. techn. Olav Olsen AS (Dr.techn. Olav Olsen AS, 2018). The connection between the columns is ensured with a base pontoon and a bottom slab. The structure can be seen in Figure 10. The primary material type used in the platform is post-tensioned concrete. Three catenary mooring lines connect the structure to the seabed (Yu, 2018).

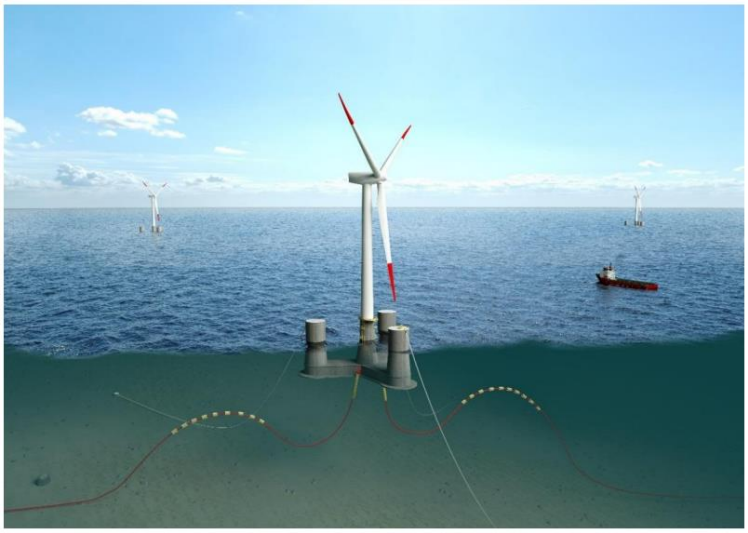


Figure 10 OO-Star FOWT concept (Dr.techn. Olav Olsen AS, 2018)

Considering the initial design from Dr. Olav Olsen (2018), modifications are made for the numerical modeling of OO-Star DTU 10 within the scope of the Lifes50+ project considering the capabilities of the numerical programs. The system is modeled using the environmental conditions of the Gulf of Maine and for 130 m water depth. There are two main approaches to modeling structural components: rigid and flexible. It is possible to model tower, blades, and mooring lines following a flexible approach in OpenFAST. Since rigid structure assumption might not be a practical application for some engineering problems, flexible modeling might be introduced to capture more realistic behavior. To implement this flexibility into the model, a semi-flexible approach was implemented within the Lifes50+ project (Pegalajar-Jurado, Madsen, Borg, &Bredmose, 2018), modifying the tower platform interface. The bottom part of the tower is modeled as part of the platform. The relevant drag coefficients are also included in the analysis for the viscous effects using Morison Equation, considering related KC and Re numbers (Yu, 2018).

In this study, the OO-Star DTU-10 model from the Lifes50+ project (Pegalajar-Jurado et al., 2018) employs the semi-flexible tower approach. The fast v8 model (input files) from the Lifes50+ project (Pegalajar-Jurado et al., 2018) is not modified for validation purposes. The public model is converted to an OpenFAST model. The hydrodynamics of the platform is modeled using HAMS (Liu, 2019) and AQWA

(*Aqwa Theory Manual*, 2013), and additional load cases and scenarios are simulated. The properties of the OO-Star DTU-10 model can be seen in Table 6.

Table 6 Properties of LIFES50+ OOS-Star platform properties with ballast (Yu, 2018)

Property	***Value***	***Unit***
Overall substructure mass (excl. tower, mooring)	2.1709E+07	[kg]
Center of Mass (CM) below MSL	15.225	[m]
Roll Inertia about CM	9.43E+09	[kg.m^2]
Pitch Inertia about CM	9.43E+09	[kg.m^2]
Yaw Inertia about CM	1.63E+10	[kg.m^2]
Tower base interface above MSL	11.0	[m]
Draft at equilibrium with moorings (no thrust)	22.0	[m]
Displaced water volume	2.3509E+04	[m^3]
Center of buoyancy below MSL	14.236	[m]

4.2.3 CENTEC TLP DTU-10 Floating Wind Turbine

Being a free-float capable TLP, CENTEC TLP combines two traditional stability approaches: it behaves as a barge platform during transportation and operates as a TLP after installation. Hence, the design was initially investigated as a barge for its dynamic performance. Later, the required conditions were checked considering the safety qualifications of a TLP, including no slack mooring, mooring breaking, and extreme surge displacement (Uzunoglu & Guedes Soares, 2020). CENTEC TLP is designed for Galicia, Spain, for a water depth of 150 m. The mass data of the installed system can be seen in Table 7.

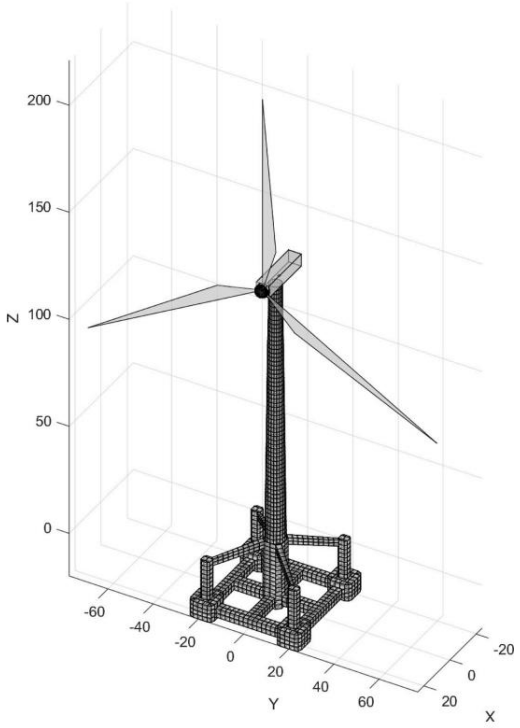


Figure 11 CENTEC TLP model with DTU 10 MT RWT in its installed draft (Uzunoglu & Guedes Soares, 2020)

In this work, the installed system is given in Figure 11, named CENTEC TLP DTU-10, for further convenience in the text. Since this work aims to simulate the operational conditions of the platform concepts in a specific site in the Black Sea, CENTEC TLP DTU-10 is modeled only in its operational condition where it is installed and operates as a TLP. Additionally, detailed geometric data and WAMIT hydrodynamic simulation results for the platform are provided by Dr. Emre Uzunoğlu for comparison purposes. The installed dynamic system properties, such as natural frequencies and mooring tensions, are shown in Table 8.

Table 7 Mass data for the CENTEC TLP (Uzunoglu & Guedes Soares, 2020)

Parameter	**Value**	**Unit**
Mass	2208.6	[t]
Center of gravity measured from the baseline	[0, 0, 8.36]	[m]
Roll Inertia	6.90E08	[kg.m^2]
Pitch Inertia	6.90E08	[kg.m^2]
Yaw Inertia	1.04E09	[kg.m^2]
Draft when installed	20	[m]

DTU 10 MW RWT and its tower are implemented (Bak et al., 2013) with Basic DTU Wind Energy Controller (Hansen & Henriksen, 2013) for the CENTEC TLP OpenFAST model. The tower is modeled as a rigid structure to ensure compatibility with the modeling approaches of the other two platform concepts. Relevant hydrodynamic drag coefficients are applied to the platform sections according to flow conditions around the structure (Sumer & Fredsøe, 2006). A linear, fully potential flow solution is considered for hydrodynamic modeling. Since no experimental data is available, and the system's natural frequencies comply with the values in the reference model (Uzunoglu & Guedes Soares, 2020), no additional damping is added to tune the model. Since complete details of the mooring system are unavailable, the missing parameters are selected from a similar six-strand independent wire rope core (IWRC) mooring material.

Table 8 Installed properties of the CENTEC TLP (Uzunoglu & Guedes Soares, 2020).

Parameter	Value	Unit
Installation Depth	150	[m]
Surge and sway natural frequencies	35.71	[s]
Heave natural frequency	2.08	[s]
Roll and Pitch natural frequencies	4.83	[s]
Yaw natural frequency	17.83	[s]
Mooring line tensions at fairleads, upwind	3597	[kN]
Mooring line tensions at fairleads, downwind	3553	[kN]

4.3 Numerical Modelling Tools

The modeling approach of two hydrodynamic modeling software, AQWA, and HAMS is conducted to compare the modeling capabilities of open-source and commercial hydrodynamics solvers. Results are compared to previously modeled, available WAMIT runs. The outputs from these three solvers are used as input to the hydrodynamic module of OpenFAST for coupled analysis of three platform concepts. The results are compared to the previous studies. Section 4.3 presents the software/codes properties and modeling approaches of the software/codes used. The detailed process of the numerical modeling can be seen in Figure 12.

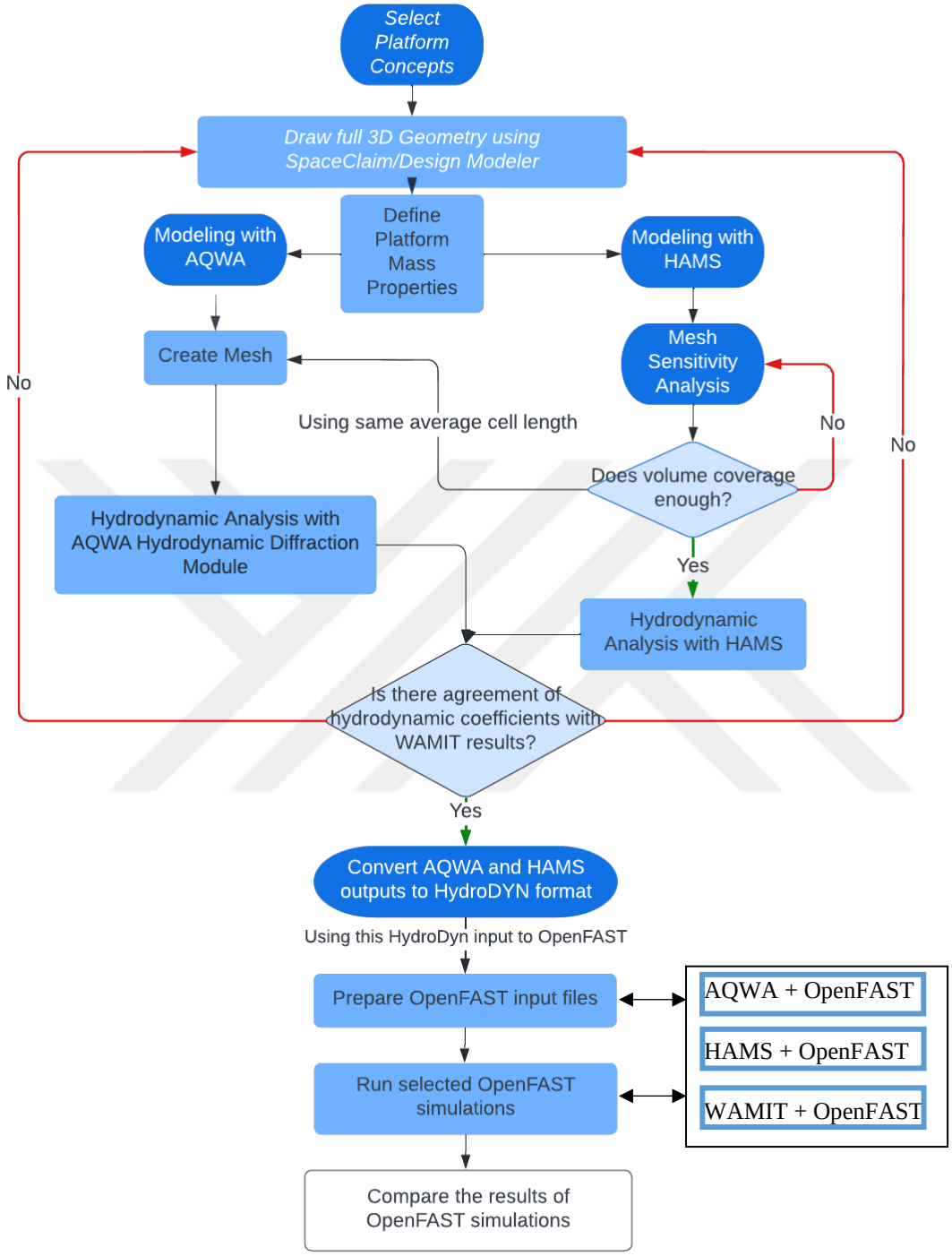


Figure 12 Flowchart of the numerical part of this thesis for hydrodynamic solution

4.3.1.1 An Overview of AQWA

As mentioned in Chapter 3, potential flow theory could provide an efficient solution for large bodies (D/L>0.2) where the KC number is smaller than two, and there is no flow separation. On the other hand, it neglects the viscosity effects and related viscous damping. For smaller bodies, Morison's concept includes those effects. AQWA, which has wide industrial applications, combines the Morison Equation approach and 3D radiation theory with the potential flow approach. In addition to its capabilities as a combined Morison equation and potential flow solver, it has two main subsystems: hydrodynamic diffraction and hydrodynamic response. The hydrodynamic diffraction system is used to compute the hydrodynamic properties, including added mass and radiation damping, and carry out a hydrostatic analysis. The hydrodynamic response submodule/subsystem of AQWA is used to model the dynamic response of the floating bodies. This subsystem takes the hydrodynamic properties of the system as input from the hydrodynamic diffraction module. For the time domain or frequency domain analyses, mooring lines or connections of the two floating bodies could be added to this module. The effects of second-order stokes waves also can be modeled, and the output can be transferred as a full quadratic transfer function (QTF) matrix to OpenFAST.

In this thesis, only the Hydrodynamic Diffraction module of AQWA is used to compute the hydrodynamic properties of the platforms. The output of the diffraction module is used as an input to OpenFAST.

4.3.1.2 An Overview of HAMS

As an alternative to the commercial hydrodynamic solvers, e.g., WAMIT (Lee, 1995), hydrodynamic analysis of marine structures (HAMS) is an opensource frequency domain potential flow solver for computing hydrodynamic parameters, including added mass and radiation damping and wave excitation forces (Liu, 2019). Those hydrodynamic parameters computed by HAMS might be used as an input to

the time domain solvers as OpenFAST, which is selected for the scope of this thesis to carry out coupled analysis of a FOWT.

Being a linear potential flow solver, the discussions given in Section 3.1.3 are also valid for the theory behind HAMS. Additionally, the Sommerfeld radiation condition can be given as follows:

$$\lim_{R\to\infty}\left[\sqrt{vR}\left(\frac{\partial\phi}{\partial R}\right)-iv\phi\right]=0 \tag{4.1}$$

This boundary condition applies to only the scattered potential in Equation 3.10, whereas Equation 4.5 shows the gradual decay of scattered velocity potential. By detailing the total velocity potential for six DOFs and the diffraction component, the velocity potential can be written as:

$$\phi=\phi_0+\phi_7-i\omega\sum_{k=1}^{6}\zeta_k\phi_k \tag{4.2}$$

In Equation 4.6, the ζ_k represents the magnitude of the oscillatory motion in six DOFs and ϕ_k is the unit magnitude of radiation potential in six DOFs (Liu, 2019). For the linear wave theory, the incident wave potential for finite depth could be given below:

$$\phi_0=-\frac{igA}{\omega}\frac{\cosh k(z+h)}{\cosh kh}e^{ik(x\cos\beta+y\sin\beta)} \tag{4.3}$$

The radiated and diffracted velocity potentials on the surface of a submerged body can be solved using Green's theorem with mixed source/dipole boundary integral equations (Liu, 2019; Liu, 2021). The numerical solution for this problem may encounter errors named irregular frequencies due to the interaction of the water plane section of buoyant bodies and free water surface. In HAMS, the irregular frequencies are eliminated by assuming zero velocity potentials on the internal water plane (Liu, 2019). For instance, the same geometry files are initially used for HAMS and AQWA models for hydrodynamic modeling, where the body is cut from the mean water level. Comparing the outputs of two codes for CENTEC TLP, the results were similar for most wave frequencies. However, there were some irregular wave frequency results in the AQWA outputs due to the water and structure interaction in

the mean water level cut. Hence for modeling with AQWA, the body meshes with full z-dimension. For the modeling of the Nautilus platform, there were still irregular frequencies, even with the full z-dimension model. Hence those frequencies are removed from the outputs.

4.3.2 OpenFAST

Including the coupling of the turbine and the platform, the dynamic response of the FOWTs can be modeled using OpenFAST. OpenFAST, previously known as FAST, is a comprehensive open-source code to simulate the coupled dynamic responses of HAWTs. The code includes the modules capable of simulating aerodynamics, hydrodynamics, control, and structural dynamics for coupled time-domain simulations. During its development phase, it transformed from FASTV8 to OpenFAST, which consists of an improved open-source developer space. OpenFAST (after FASTV8) behaves as a driver code with the submodules to enhance efficiency. The full submodules of the code can be seen in Figure 13.

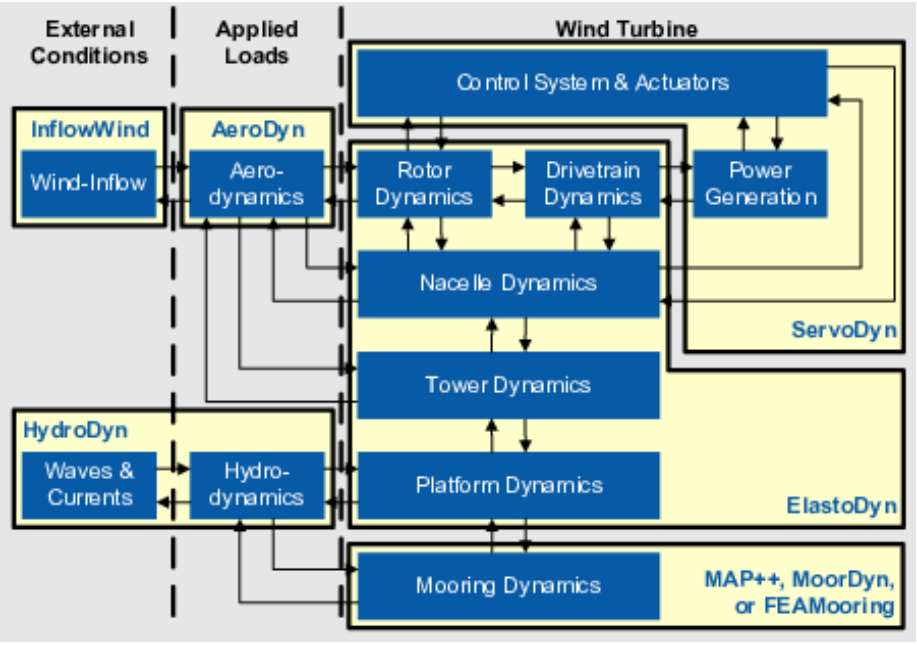


Figure 13 Submodules of FAST (Matha, 2010)

The submodules of OpenFAST are named ElastoDyn for the structural analysis, HydroDyn for the time domain hydrodynamic analysis, AeroDyn for the turbine aerodynamics, and ServoDyn for the control of the turbine. Four options for the mooring modeling can be selected: MAP++, FEAMooring, MoorDyn, and Orcaflex. The inflow wind velocities can be computed with the InflowWind option. Additionally, the performance of an individual turbine and the related loads in a farm can be modeled with the FAST Farm module, including the wind farm's wake meandering effects, atmospheric boundary layer, and wake deficits. In this thesis, only the single FOWT system is investigated where the wind farm effects are not considered, and the focal point is the hydrodynamics of the platforms. A detailed description of the hydrodynamic time-domain solver HydroDyn is given below.

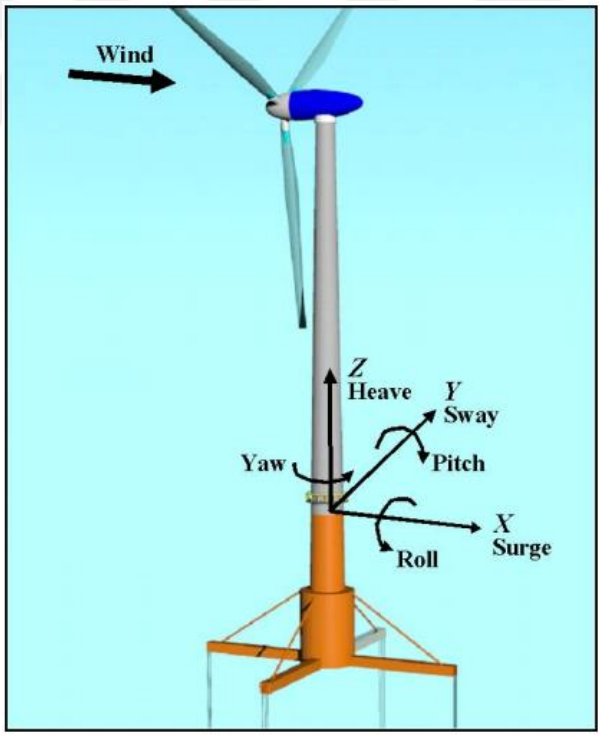


Figure 14 The global coordinate system for the Hydrodyn Module for a FOWT (Jonkman, Robertson, &Hayman, 2016)

Coupled with OpenFAST code, Hydrodyn is a tool capable of time domain hydrodynamic analysis of bottom fixed offshore turbines and FOWTs. The global coordinate system for the Hydrodyn module is shown in Figure 14. In this sign convention, surge represents the translation in the main wind direction (in the x-axis), sway represents the translation in the transverse main wind direction (in the y-axis), heave represents the vertical direction (z-axis), Roll represents rotation about the x-axis, pitch represents a rotation in the y-axis. Yaw represents the rotation about the z-axis. The same coordinate system is also used in further analyses in this thesis.

Hydrodyn includes alternative methods for hydrodynamic load calculations, including potential flow theory, strip theory, and a hybrid method (Jonkman et al., 2016). This thesis considers only the potential flow theory for validating the numerical models using three hydrodynamic solvers.

Modeling of second-order waves is also possible with the Hydrodyn module using the first-order solution and adding the extra energy component to the spectrum. The second-order solution may capture real surface wave shapes and related wave loads (Jonkman et al., 2016). Second-order potential flow terms are computed using full QTF matrices by a hydrodynamic solver as WAMIT, AQWA. QTF matrices input HydroDyn/OpenFAST to include second-order hydrodynamic effects.

4.4 Project Location

For the application of three floater concepts, the location is in Kıyıköy in the southwestern part of the Black Sea. The decision is given considering a recent offshore wind farm site selection study in Turkey (Caceoğlu et al., 2022). The criteria considered in this paper include wind energy potential, water depth, regional population, energy sufficiency, economic activities including fishing, shipping routes, tourism, and ecological factors such as bird migration and high biodiversity areas. Although it is “the second best site” as an offshore wind farm site according to this study (Caceoğlu et al., 2022), considering the aim of this thesis, Kıyıköy is

chosen as the application site due to the scope is the modeling of FOWTs and Kıyıköy has relatively deepwater suitable for floating platforms. Additional reasons might be given: lower marine trading density, shorter grid connection length, and the lowest earthquake risk among the sites. The earthquake response of the FOWTs is another high-interest research area with greater uncertainties and the need for better understanding. In this thesis, earthquake loads are not considered; hence, the site chosen with the least earthquake risk.

A sketch of the selected wind farm location is presented in Figure 15. This study analyses a 100 m depth location at the northeastern polygon (shown in dark green) in Figure 15 and the selected point is marked with a red dot. Figure 15 is prepared based on the suitable offshore wind farm sites in Turkey (Caceoğlu et al., 2022), where the potential site has various water depths. Figure 15 shows the area's detailed bathymetry for selecting site parameters and FOWT installation location.

The grid resolution is crucial to determine the water depth contours in the selected area and adequately define the site parameters. Also, for detailed planning of an offshore wind farm, multiple points should be considered with different water depths and site parameters. In this thesis, only one point is selected in the possible project location in Figure 15, and the related environmental site parameters are considered in the modeling. As a publicly available bathymetry, EMODnet bathymetry (EMODnet Bathymetry Consortium, 2020) is used to prepare Figure 15. The reason for using EMODnet bathymetry (EMODnet Bathymetry Consortium, 2020) instead of GEBCO bathymetry data (British Oceanographic Data Centre, 2003) is that the grid resolution of 7.5 arcseconds for EMODnet data and 15 arcseconds for GEBCO bathymetry.

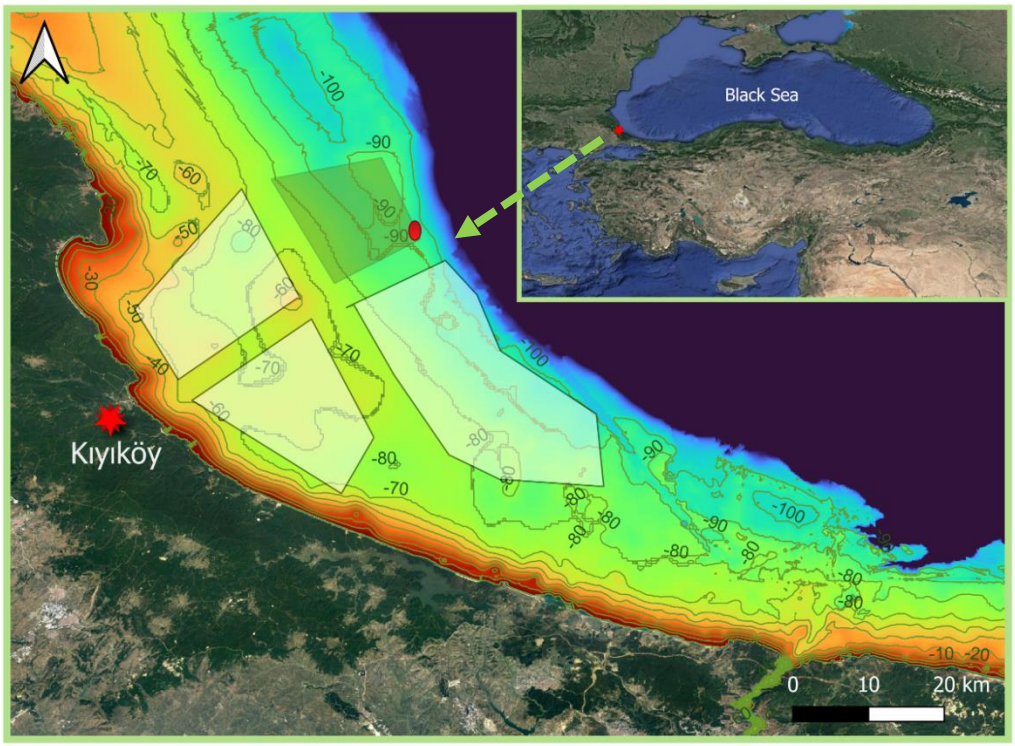


Figure 15 Detailed bathymetry and selected location for the FOWT modeling

In the previous site selection study for this area (Caceoğlu et al., 2022), the wind criteria were based on the annual average data from the Global wind atlas (Global Wind Atlas, 2022), and the wave parameters were not taken into consideration. In this thesis, the metocean parameters are computed for the dynamic analysis of the platform concepts. Wave parameters for extreme value analysis are chosen from the Copernicus Database (Staneva et al., 2020). In this database, the spectral wave model is forced by the ERA5 wind fields (Hersbach et al., 2018). To ensure the consistency between the extreme values of the wind and wave parameters 42-year hourly ERA5 (Hersbach et al., 2018) wind dataset from 1979 to 2020 is used.

The annual mean wind speed data graph is prepared for 100 m using ERA5 hourly wind data (Hersbach et al., 2018) to present the area's wind source, which can be seen in Figure 16. As can be seen from Figure 16, the annual mean wind speed at 100 m is greater than 7 m/s for the given period, which is the wind resource

requirement for a highly efficient wind farm operation, according to ESMAP (2019). Hence the selected area initially provides a promising wind farm location.

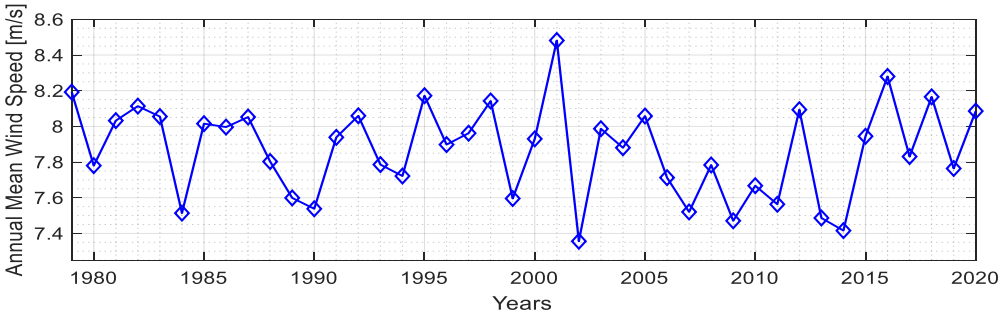


Figure 16 Annual mean wind speed values at 100 m for the potential site in Kıyıköy

For the metocean parameters computations, the return period is chosen as 50 years because the safety class of the FOWTs is defined as a normal safety class due to outcomes of a probable failure being primarily economic, and the lifetime of the modeled platforms is 25 years (Krieger et al., 2015).

Current and water level effects are not considered in this study due to the lower tidal ranges in the Black Sea, whose magnitude is centimeters (Medvedev et al., 2016). Using the data available for wave and wind parameters, operational load cases, including extreme cases, are prepared, and the three FOWT concepts are modeled for the region. A single location is chosen at 100 m depth and 40 km from the Kıyıköy region's coastline. Related metocean parameters are computed using the extreme value analysis, and the details will be given in Section 4.4.1.

For the application of FOWT projects, bathymetry (seabed topography) is essential, especially for the mooring, riser design, and the analysis of the seabed-riser interaction (Chakrabarti, 2005). Detailed geotechnical survey data is unavailable for the selected reference site. However, most of the chosen area's sediment type is fine mud (EMODnet, 2022). For the mooring design, the required parameters, including shear strength profile and frictional coefficients, might be estimated from previous studies. In this work, the design of the mooring lines is not conducted.

4.4.1 Extreme Value Analysis

To analyze the platform concepts for the Kıyıköy region, determining the metocean parameters with a 50-year return period is crucial. A non-directional analysis is conducted for the extreme value calculation. The first step for this analysis is the sampling of the wave data. In this work, the annual maxima method is used for sampling, where the highest significant wave height is sampled for each year. The annual maxima method also satisfies the requirement for being statistically independent (Goda, 2008). After the significant wave height data sampling, different distributions are implemented (graphically fitted), including Gumbel, Fishet-Tipper II, Weibull, and Lognormal distribution. Using the wave data for the Kıyıköy region from the Copernicus database (Staneva et al., 2020) and wind data from the ERA5 dataset (Hersbach et al., 2018), the Gumbel distribution was selected as the best-fitting function among the distribution types implemented. It covered all the data points for the 42-year data with a 90% confidence interval.

Table 9 Results of the extreme value analysis for significant wave height using Gumbel distribution

Return Period [Year]	**Lower Limit H_s [m]**	**H_s [m]**	**Upper Limit H_s [m]**	**T_p [s]**
5	5.59	5.95	6.31	12.76
10	5.99	6.47	6.94	13.3
20	6.36	6.96	7.56	13.79
50	6.83	7.59	8.36	14.41
100	7.19	8.07	8.96	14.86

Table 10 Results of the extreme value analysis for wind speed at 10 m using Gumbel distribution

Return Period [Year]	Lower Limit Ws [m/s]	Ws [m/s]	Upper Limit Ws [m/s]
5	18.26	18.79	19.33
10	18.92	19.63	20.34
20	19.55	20.44	21.33
50	20.35	21.48	22.62
100	20.95	22.27	23.59

The best fit functions are fitted to the graphical data. For H_s and wind speed at 10m, Gumbell distribution is fitted graphically to the annual extreme data, and metocean parameters are calculated for different return periods. The results of the extreme values analysis can be seen in Table 9 for H_s, and for wind speed, values at 10 m height can be seen in Table 10. Since the wind speed of interest is at hub height, which is 119 m for DTU 10 MW RWT, values in Table 10 are used to calculate the wind speed at hub height.

Table 11 Scatter Table H_s vs T_p for Kıyıköy region

Significant Wave Height, H_s [m] \ Peak Period, T_p [s]	<2.0	3.0	4.0	5.0	6.0	7.0	8.0	9.0	10.0	11.0	12.0	13.0	Total %
0.5	0.2	10.21	9.86	8.48	4.79	0.90	0.10	0.04	0.02	0.00	0.00	0.00	34.57
1.0	0.00	1.15	11.73	9.32	9.30	5.37	0.62	0.14	0.01	0.00	0.00	0.00	37.64
1.5	0.00	0.00	0.51	4.74	4.34	3.37	1.00	0.38	0.06	0.00	0.00	0.00	14.41
2.0	0.00	0.00	0.00	0.37	2.67	2.40	0.78	0.39	0.14	0.01	0.00	0.00	6.76
2.5	0.00	0.00	0.00	0.00	0.44	1.65	0.62	0.33	0.13	0.03	0.00	0.00	3.19
3.0	0.00	0.00	0.00	0.00	0.02	0.58	0.52	0.31	0.12	0.02	0.00	0.00	1.57
3.5	0.00	0.00	0.00	0.00	0.00	0.09	0.32	0.28	0.11	0.04	0.00	0.00	0.84
4.0	0.00	0.00	0.00	0.00	0.00	0.00	0.10	0.23	0.10	0.03	0.01	0.00	0.47
4.5	0.00	0.00	0.00	0.00	0.00	0.00	0.01	0.14	0.10	0.03	0.01	0.00	0.29
5.0	0.00	0.00	0.00	0.00	0.00	0.00	0.00	0.02	0.09	0.03	0.00	0.00	0.15
5.5	0.00	0.00	0.00	0.00	0.00	0.00	0.00	0.00	0.04	0.02	0.00	0.00	0.07
6.0	0.00	0.00	0.00	0.00	0.00	0.00	0.00	0.00	0.01	0.01	0.01	0.00	0.02
6.5	0.00	0.00	0.00	0.00	0.00	0.00	0.00	0.00	0.00	0.01	0.01	0.00	0.02
7.0	0.00	0.00	0.00	0.00	0.00	0.00	0.00	0.00	0.00	0.01	0.00	0.00	0.01
7.5	0.00	0.00	0.00	0.00	0.00	0.00	0.00	0.00	0.00	0.00	0.00	0.00	0.00
8.0	0.00	0.00	0.00	0.00	0.00	0.00	0.00	0.00	0.00	0.00	0.00	0.00	0.00
Total %	0.17	11.36	22.10	22.91	21.56	14.36	4.06	2.24	0.94	0.24	0.05	0.01	100

The joint probability distribution of significant wave heights (H_s) and peak periods (T_p) are used frequently for determining sea states. The scatter table presents the joint probability distribution of those variables for the Kıyıköy region in Table 11. Table 11 shows that the highest occurrence sea state has H_s and T_p values of 0.5-1 meters and 3-4 seconds. The uncolored regions are the values that are not observed in the area. Table 12 presents the joint probability distribution of the wind speed at hub height (W_s) and the peak period (T_p). Table 12 shows that the highest occurrence parameters have T_p between 3-4 s and a wind speed of 6.1-8.1 m/s.

Table 12 Scatter table for Kıyıköy region for wind speed at hub height

Wind Speed at Hub Height, W_s [m/s] \ Peak Wave Period, T_p [s]	< 2.0	3.0	4.0	5.0	6.0	7.0	8.0	9.0	10.0	11.0	12.0	13.0	Tot%
2.0	0.03	0.83	0.99	0.97	0.80	0.41	0.08	0.03	0.01	0.00	0.00	0.00	4.16
4.0	0.06	2.40	3.17	2.95	2.64	1.21	0.23	0.10	0.03	0.00	0.00	0.00	12.78
6.1	0.05	2.94	4.82	4.44	3.77	1.88	0.38	0.15	0.05	0.01	0.00	0.00	18.49
8.1	0.03	2.57	5.22	4.84	4.01	2.22	0.47	0.19	0.05	0.02	0.00	0.00	19.61
10.1	0.01	1.58	4.00	4.31	3.83	2.28	0.49	0.23	0.08	0.02	0.00	0.00	16.83
12.1	0.00	0.63	2.17	2.82	2.99	2.18	0.52	0.25	0.11	0.01	0.00	0.00	11.70
14.1	0.00	0.25	1.06	1.51	1.99	1.91	0.62	0.30	0.12	0.03	0.00	0.00	7.79
16.2	0.00	0.12	0.47	0.70	0.97	1.38	0.58	0.32	0.13	0.02	0.00	0.00	4.68
18.2	0.00	0.03	0.14	0.26	0.40	0.62	0.42	0.30	0.11	0.03	0.01	0.00	2.32
20.2	0.00	0.01	0.05	0.07	0.12	0.18	0.20	0.23	0.12	0.04	0.01	0.00	1.03
22.2	0.00	0.00	0.01	0.02	0.03	0.05	0.06	0.11	0.09	0.04	0.01	0.00	0.43
24.3	0.00	0.00	0.00	0.01	0.01	0.02	0.01	0.02	0.03	0.02	0.00	0.00	0.13
26.3	0.00	0.00	0.00	0.00	0.00	0.00	0.00	0.00	0.00	0.01	0.01	0.00	0.03
28.3	0.00	0.00	0.00	0.00	0.00	0.00	0.00	0.00	0.00	0.00	0.00	0.00	0.01
30.3	0.00	0.00	0.00	0.00	0.00	0.00	0.00	0.00	0.00	0.00	0.00	0.00	0.00
Tot%	0.17	11.36	22.10	22.91	21.56	14.36	4.06	2.24	0.94	0.24	0.05	0.01	100.0

For the calculation of extreme wind speed, the ERA5 hourly wind dataset is used (Hersbach et al., 2018). ERA5 is an hourly reanalysis database that covers the period 1959 to 2022 with a horizontal grid size of 0.25 degrees. Wind speed data at 10 m above water level is extracted at the selected reference location in the x (eastward) and y (northward) directions. The wind speed components are combined, and the extreme value analysis is conducted similarly to the waves. The extreme wind speed values at 10 m above still water level are calculated with a 50-year return period

using the Gumbell distribution. Since the extreme wind speed values are calculated for 10 m height, they should be converted to wind speed at hub height.

$$U_{50\,years}(z) = U_{50\,years}(h)\left[\frac{z}{h}\right]^{\alpha} \tag{4.4}$$

The wind speed at hub height can be calculated by using Equation 4.4. From Table 2-1 at the guideline for the Environmental Conditions and Environmental Loads (DNV GL, 2014), the parameter α, the power law exponent, is selected as 0.12 for the open sea environment with waves.

Another critical issue in computing the wind speed at hub height is the data from the ERA5 hourly averaged wind speed data. On the other hand, a 50-year return period of 10-minute averaged wind speed data should be used for the design load cases. To compute 10 min averaged wind speed at hub height, the Frøya wind model is recommended for offshore locations (DNV GL, 2014).

$$U(T,z) = U_0 * \left\{1 + C * \ln\frac{z}{H}\right\} * \left\{1 - 0.41 * I_v(z) * \ln\frac{T}{T_0}\right\} \tag{4.5}$$

$$C = 5.73 * 10^{-2}\sqrt{1 + 0.148U_0} \tag{4.6}$$

$$I_v = 0.06 * (1 + 0.043 * U_0) * \left(\frac{z}{H}\right)^{-0.22} \tag{4.7}$$

Derived from the Frøya wind model, Equation 4.5 is recommended for the conversion. In Equation 4.5, U_0 is the hourly averaged wind speed at 10 m where $T < T_0$, C and I_v parameters are given in Equation 4.6 and Equation 4.7. Due to the model's limitations, where it is calibrated only below 100 m, Equation 4.5 should not be used above 100 m (DNV GL, 2014). Considering this limitation, Equation 4.4 is selected for calculating wind speed at hub height without changing the averaging time. The load cases for modeling the three platform concepts are chosen considering the scatter tables (Table 11 and Table 12) and the outputs of the extreme value analysis for the 50-year return period. For the operational load cases, LC1 and LC2 represent the environmental parameters with higher occurrence during the 42 years. LC3 represents the above-rated wind speed load case, while LC4 is the extreme wind

speed load case where the turbine is parked and not operating. The load cases can be seen in Table 13.

Table 13 Load cases used in the analysis

Load Cases	H_s [m]	T_p [s]	W_s [m/s]
LC1	2	5	8.1
LC2	2.5	6	10.1
LC3	4	8	14.1
LC4	8	14	30.47

4.5 Model Comparison Tests

4.5.1 Free Oscillation (Free Decay) Tests

An undamped system with mass m and spring constant k experiences an inertia force due to its motion and a restoring force that withstands the wave excitation force (Chakrabarti, 2005). The forcing might be written as a harmonic force equal to the force computed using the airy (linear) wave theory. The force and the natural frequency of the system might be written as:

$$m\ddot{x} + kx = F_0 \cos \omega t \tag{4.8}$$

$$\omega_n = \sqrt{\frac{k}{m}} \tag{4.9}$$

Where m is the mass of the system, k is the spring constant, $\omega_n$is the undamped natural frequency, F_0 is the magnitude of the harmonic function for the force term with a frequency of ω. Physically, when a floating structure is released with an initial displacement, the body will have oscillatory motion, and the movement's frequency helps to define the system's natural frequency. The displacement for the system can be written as:

$$X = \frac{F_0/k}{\omega_n^2 - \omega^2} \tag{4.10}$$

As seen from Equation 3.13, when the frequency of the motion equals the natural frequency of the system, the denominator of the equation tends to infinity, and it is called resonance. Resonance is a devastating phenomenon for a floating body. During the design process, the environmental parameters should be examined carefully, and the resonant frequency and its relevant wave excitation range should be avoided. In this work, the natural frequencies of the three platform concepts are validated, and their performance in the Black Sea environment is examined.

This thesis also conducts free decay tests for the three platform concepts OO-Star, Nautilus, and CENTEC TLP. The results of the free decay tests without wind for the Nautilus DTU-10 system compared to three cases (AQWA+OpenFAST), (HAMS+OpenFAST), and (WAMIT+OpenFAST) can be seen in F'gure 17. As can be seen from Figure 17, for heave DOF, there is a good agreement for three hydrodynamic solvers. For surge and yaw DOFs, (AQWA+OpenFAST) and (WAMIT+OpenFAST) have good agreement on the time series. However, (HAMS+OpenFAST) model presents undamped behavior compared to other cases. The three cases almost match in pitch DOF. This thesis aims not to tune the model according to the test/benchmark case. Hence no additional damping has been added to the HAMS model. The numerical models can be tuned with additional damping considering the experimental free decay tests for the projects with actual experimental data.

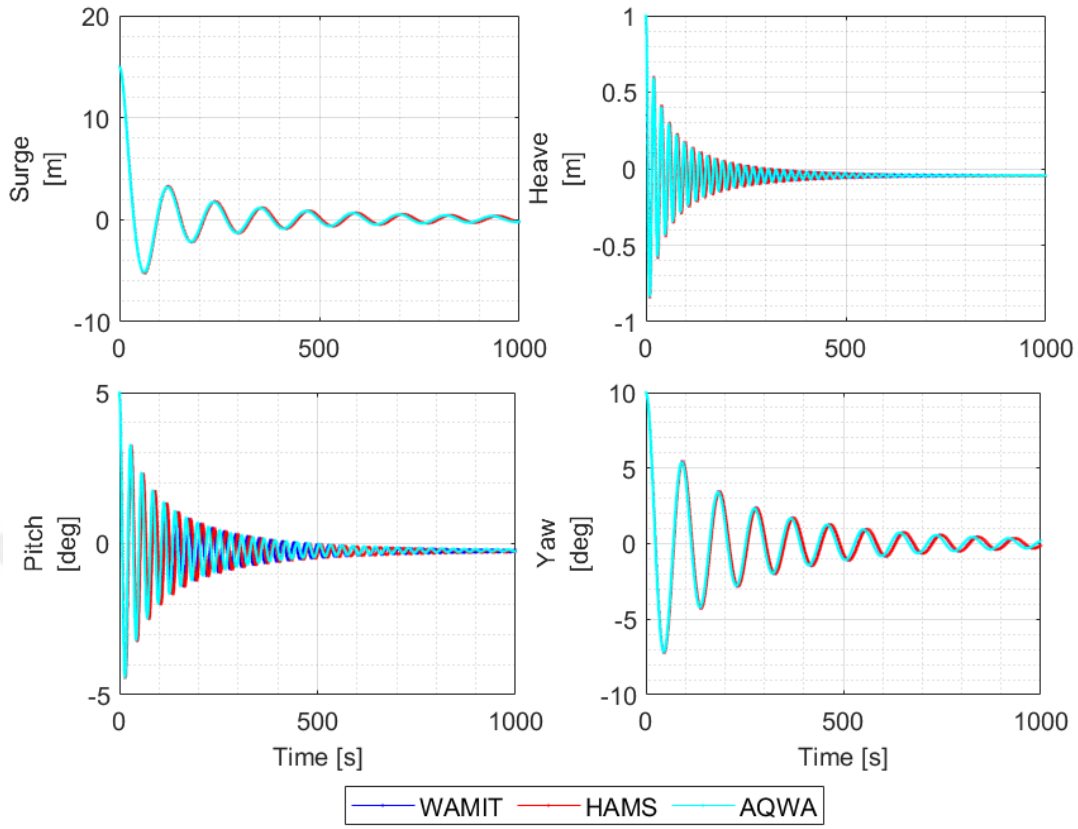


Figure 17 Free oscillation (decay) tests for the Nautilus platform with three different hydrodynamic models

4.5.2 Regular Wave Test

Regular wave tests are crucial for understanding the hydrodynamic behavior of the platform without the presence of wind coupling. Additionally, it might be an indicator of hydrodynamic model verification. In Figure 18, the regular wave simulation of the Nautilus platform is given where the simulation length is 1800 s and the first 600 seconds are extracted for further post-processing. The wave amplitude is taken as 3 m, and the period is 10 s. As can be seen from Figure 18, the three hydrodynamic solvers present the same dynamic response.

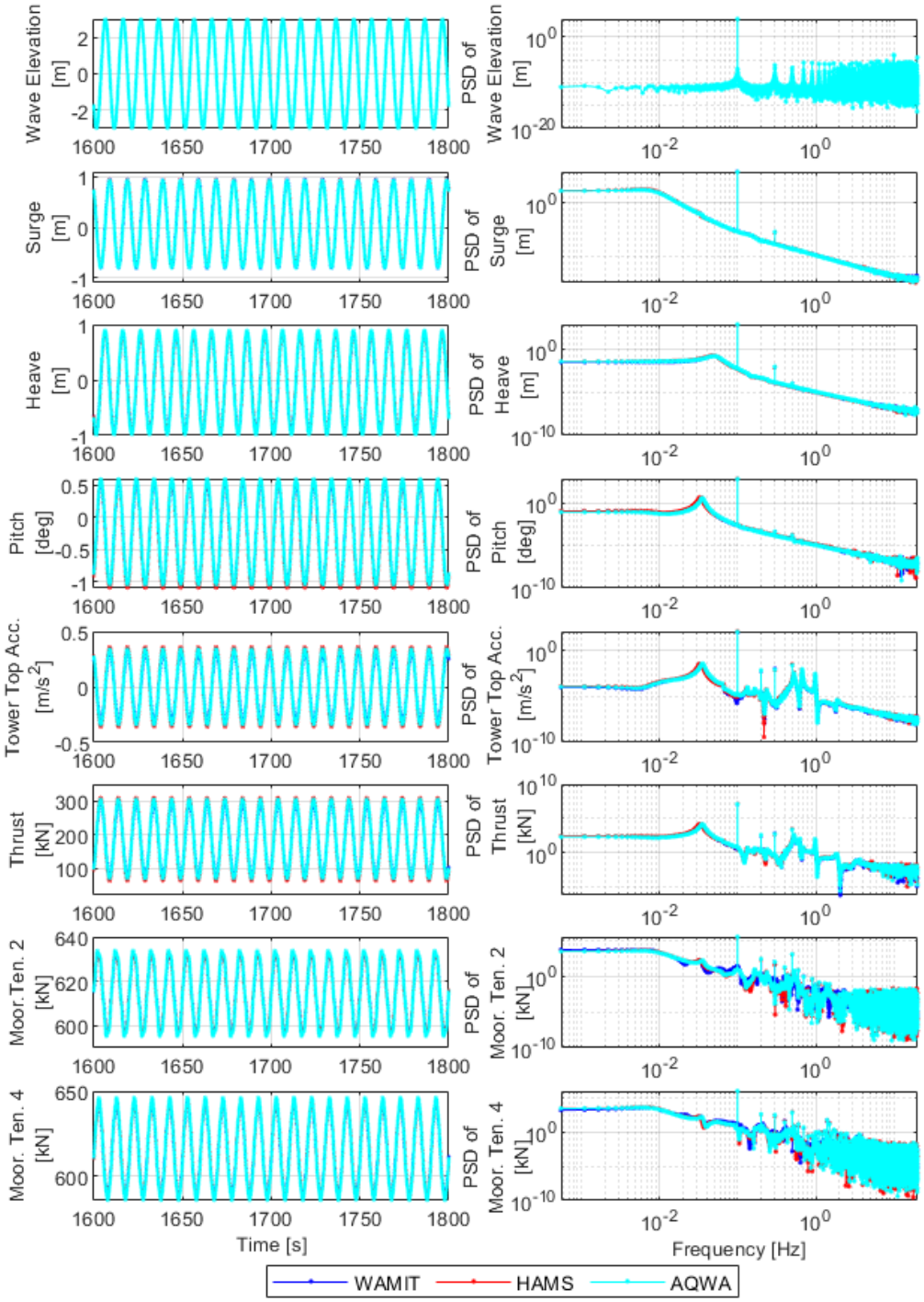


Figure 18 Regular wave responses of the Nautilus system modeled with three hydrodynamic solvers coupled with OpenFAST

Response Amplitude Operator (RAO) is a transfer function that ensures a prediction for a floating body motion. RAOs can be calculated to understand the behavior of the structure (Chakrabarti, 2005). The RAOs for the Nautilus platform without wind excitation is computed using white noise waves with 8000 seconds simulation length.

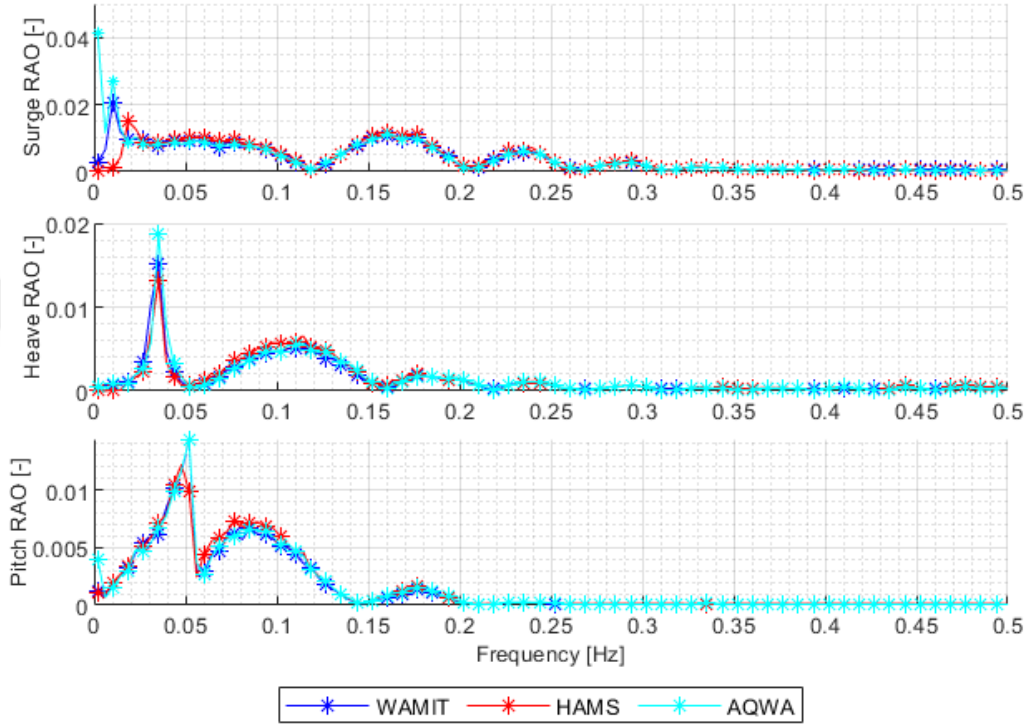


Figure 19 RAOs for Nautilus platform without wind excitation

Figure 19 presents the RAO for the Nautilus platform computed by three hydrodynamic solvers coupled to OpenFAST, including (WAMIT+OpenFAST), (HAMS+OpenFAST) and (AQWA+OpenFAST) cases. As seen in Figure 19, for heave and pitch DOFs, there is a good agreement between the three models. For the surge DOF, in the HAMS model, the peak frequency of the system is shifted to the right for a small amount. AQWA has a more prominent peak due to the data's post-processing.

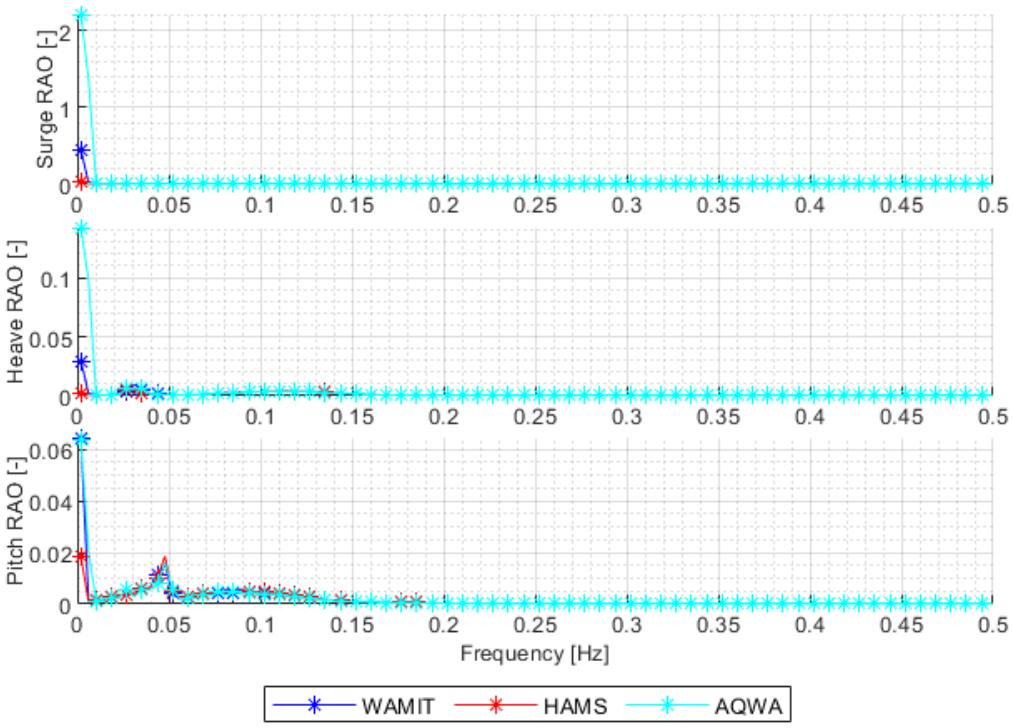


Figure 20 RAOs for OO-Star platform without wind excitation

Using three numerical models as (WAMIT+OpenFAST), (HAMS+OpenFAST), and (AQWA+OpenFAST) cases, the RAO of the OO-Star system is calculated. The related graphs can be seen in Figure 20. As can be seen in Figure 20, there are some disagreements at the smaller frequencies, significantly closer to zero frequency. It might be due to computational errors or binning during the post-processing. Heave value obtained from (WAMIT+OpenFAST) has a slightly higher magnitude than other models at the peak. In the case of (HAMS+OpenFAST), the model has a slightly higher value at the peak in pitch.

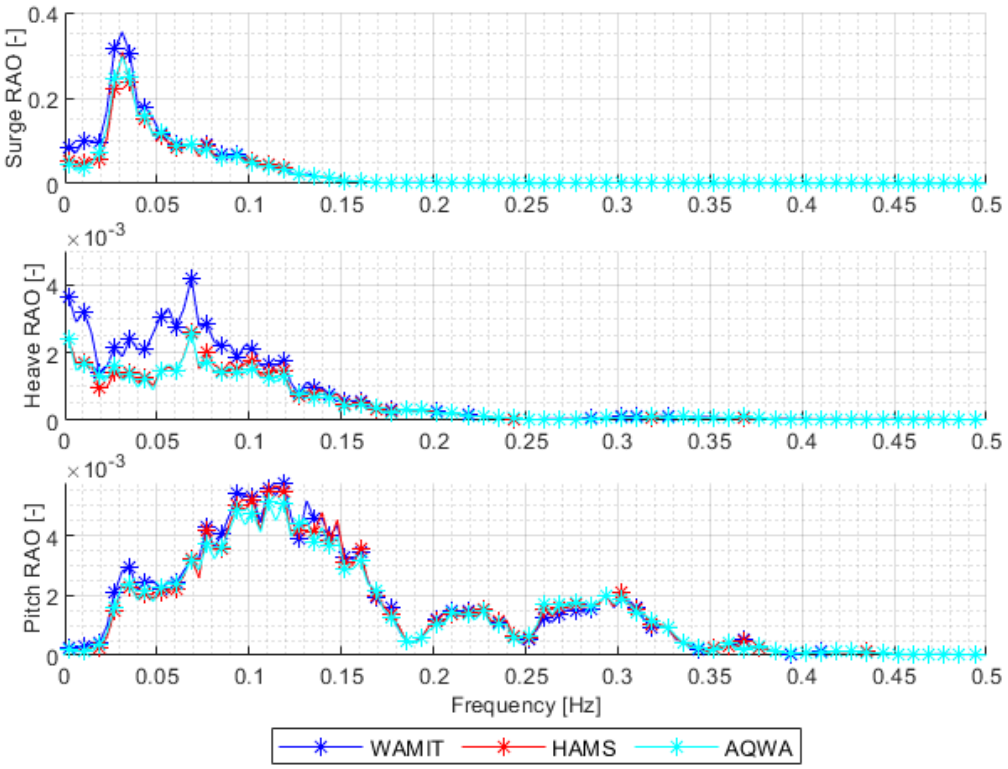


Figure 21 RAOs for CENTEC TLP without wind excitation

The RAOs for CENTEC TLP computed as the previous concepts can be seen in Figure 21. As can be seen from Figure 21, the magnitudes of RAO are smaller compared to RAO of OO-Star and Nautilus in heave and pitch DOFs. The peaks in three DOFs in the surge, heave, and pitch are at the same frequencies for each DOF for the three models. After discussing the fundamental simulations/tests to understand hydrodynamic behavior, the results of the numerical simulations are discussed in Chapter 5.

CHAPTER 5

RESULTS AND DISCUSSION

In this chapter, the results of the numerical simulations are presented together with the relevant discussion. Initially, the publicly available Fast v8 models from the Lifes50+ project are used for Nautilus DTU-10 and OO-STAR DTU-10 systems (Galván et al., 2018; Pegalajar-Jurado et al., 2018). The public models are converted into OpenFAST v3 due to the more outstanding hydrodynamic capabilities of the latter, which are then used for modeling purposes. The OpenFAST v3 model for the CENTEC TLP is prepared.

Within the scope of this thesis, a comparison of the first-order hydrodynamic modeling capabilities of HAMS, AQWA, and WAMIT software coupled with OpenFAST is conducted. The hydrodynamic coefficients added mass (A_{ij}), radiation damping (B_{ij}), wave excitation forces (X_i), and hydrostatics (C_{ij}) are computed using HAMS and AQWA. Results are compared to WAMIT output from the previous studies for OO-Star, Nautilus, and CENTEC TLP. Free decay tests are conducted to compute natural frequencies using the hydrodynamic coefficients obtained from three hydrodynamic solvers as input to OpenFAST. Regular wave tests (without wind condition) and irregular wave tests (with the wind) are conducted, and dynamic responses of the three platform concepts are compared to the relevant studies (Galván et al., 2018; Pegalajar-Jurado et al., 2018; Uzunoglu & Guedes Soares, 2020). The effects of the hydrodynamic solver on the global response of the system and power generation are investigated. Three FOWT designs are modeled considering the environmental conditions of Kıyıköy, the Black Sea, to evaluate whether they apply to a region in Turkey.

5.1 Numerical Model Verification

In this section, hydrodynamic coefficients of the three platform concepts are obtained using an open-source hydrodynamic code, HAMS, and mesh sensitivity analysis is carried out. The results of the mesh sensitivity simulations are compared to publicly available WAMIT output from the Lifes50+ project for the OO-Star (Pegalajar-Jurado et al., 2018); Nautilus (Galván, Sánchez-Lara, et al., 2018) platforms and the CENTEC TLP (Uzunoglu & Guedes Soares, 2020).

Table 14 Cell numbers and % volume for Cases of mesh sensitivity analysis with y symmetric geometry

		Average Cell Length [m]	**Cell Number**	**Volume %**
OO-Star	Case 1	2.50	863	99.22
	Case 2	2.22	1093	99.67
	Case 3	2.05	1271	99.82
	Case 4	1.77	1723	99.85
	Case 5	1.50	2773	99.98
Nautilus	Case 1	2.46	611	95.29
	Case 2	1.77	1160	97.14
	Case 3	1.55	1575	98.61
	Case 4	1.00	3437	99.40
	Case 5	0.60	9794	99.72
CENTEC TLP	Case 1	2.42	490	88.22
	Case 2	1.79	784	94.21
	Case 3	1.59	1149	95.47
	Case 4	1.05	2608	98.07
	Case 5	2.00	766	91.96

A mesh sensitivity analysis is conducted for the HAMS model to represent the platform geometry well. As seen in Table 14, the finer mesh (Case 5) gives a better representation of the volume of the body. For the hydrodynamic analyses of the platform concepts OO-Star and Nautilus platforms, Case 5 and Case 4 are selected, which are the finer meshes. There are 4 mesh cases chosen for the Nautilus model due to a dramatic increase in the computational time for finer mesh and less improvement in the volume. The properties of Case 5 are given for the Nautilus platform in Table 14. However, Case 5 is not used further for the simulations. As can be seen in Figure 22, Nautilus Case 4 mesh has 2.62 s computational time per cell. For OO-Star and CENTEC TLP models, the finest mesh case (Case 5) has less computational time than Case 4 of Nautilus mesh which is 1.75 s and 2.58 s per cell, respectively. Since the volume coverage of Case 4 and Case 5 meshes of the Nautilus model are almost the same, which are 99.40 % and 99.72 %, the simulation of Case 5 for the Nautilus platform is not completed. At the beginning of this study, the aim was to create similar-sized mesh cases for three platforms and compare them. However, due to differences in the geometry, to represent the volume of each concept properly, different mesh case sizes are used. The same mesh as the WAMIT output (Uzunoglu & Guedes Soares, 2020) is used for the HAMS model for a better comparison with WAMIT.

For the AQWA model, mesh sensitivity analysis is not conducted. The AQWA mesh cases are defined using the average cell length of the HAMS mesh cases (see Table 14 for further details). The WAMIT outputs of the Lifes50+ project (Galván et al., 2018; Pegalajar-Jurado et al., 2018) are used as a benchmark and compared to two other hydrodynamic solvers. Since the mesh size is not publicly available for the benchmark cases, a comparison of the mesh size is not possible between WAMIT and other hydrodynamic models. It is assumed that there is no mesh dependency in WAMIT models, and WAMIT outputs are compared to the most refined mesh case. Another variable here is the number of frequency points. For HAMS models, 200 frequency steps are chosen, and for AQWA models, 100 frequency steps are chosen as the maximum number of frequencies that can be chosen in AQWA.

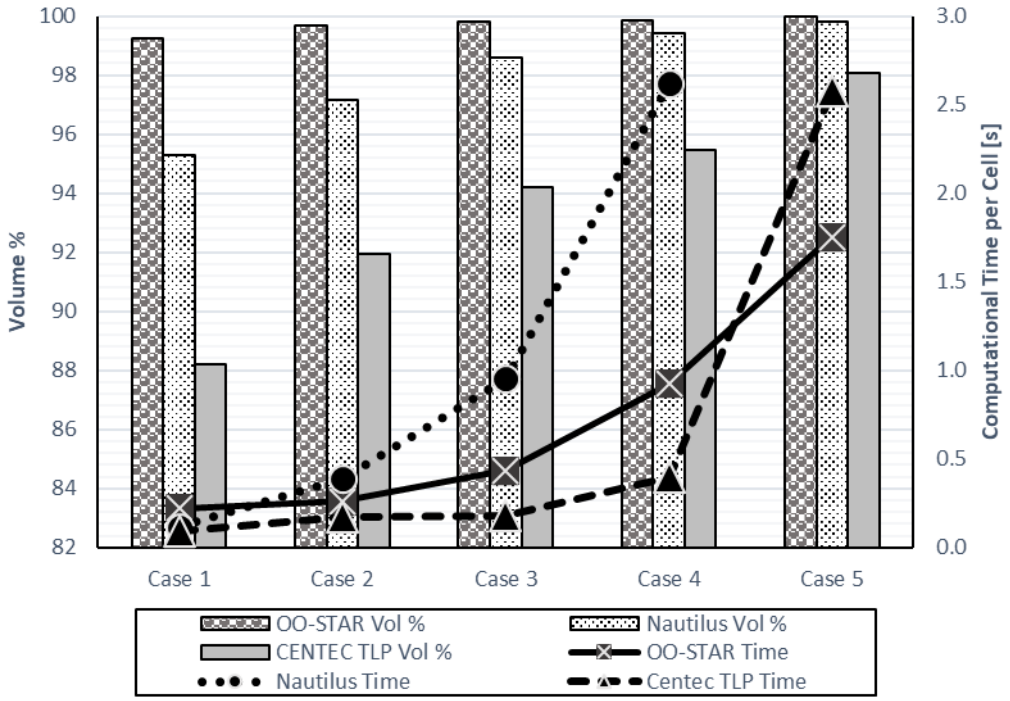


Figure 22 Percent volume and computational time for mesh sensitivity analysis

The mesh sensitivity analysis results can be seen in Figure 22, where the three platform concepts are studied. For this comparison, the mesh is created using CAD software, and HAMS solved the hydrodynamics of the platform. Detailed convergence graphs of the OO-Star platform concept can be seen in Appendix A for the added mass.

It can be seen from Figure 22 that even the coarsest case of the OO-Star platform represented the volume well with 99.22% coverage. Refining mesh size resulted in a slight increase in the volume coverage, from 99.22% to 99.96% for the coarsest and finest case. Refining the mesh resulted in a more significant increase in computational time. For the OO-Star platform, the computational time increased from 0.22 s per cell to 1.75 s per cell from coarsest (Case 1) to most refined mesh (Case 5), with average cell lengths of 2.5 m and 1.5 m. Meshes for Case 1 and Case 5 can be seen in Figure 23.

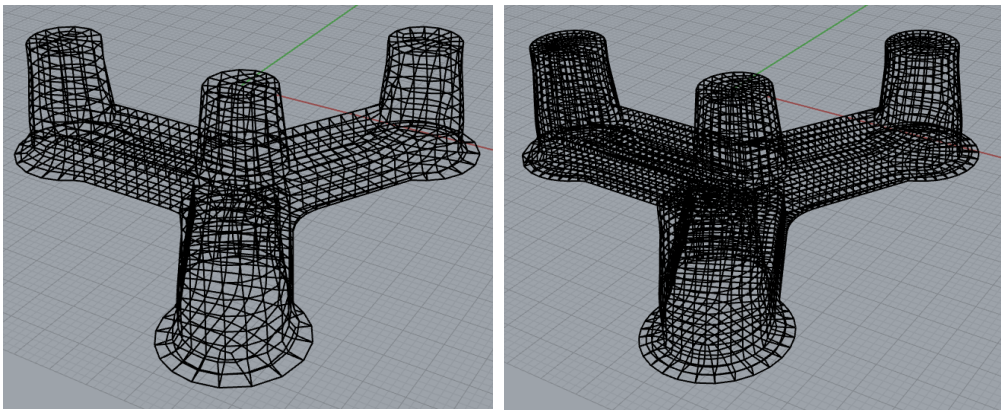


Figure 23 Case 1 mesh with 2.5 m average cell length on the left and on the right Case 5 mesh with 1.5 m average cell length on the right for OO-Star platform

CENTEC TLP's volume coverage ranges from 88.22% to 98.086 % from the coarsest (Case 1) to the finest case (Case 4). From Case 1 to Case 4, the volume coverage increases steadily. As can be seen in Figure 22, computational time increased dramatically compared to the increase in volume coverage from Case 1 to Case 4, which is 0.09 s per cell to 2.58 s per cell. Dr. Emre Uzunoğlu provided the mesh file of the CENTEC TLP WAMIT simulation. Therefore, this mesh file is used (Case 5) to compare results obtained from HAMS and WAMIT. Since this work aims to compare the HAMS and WAMIT codes, comparing Case 5 and WAMIT output (original) is crucial. In the next section, a comparison of hydrodynamic coefficients and natural frequencies of the platform concepts computed by three different hydrodynamic solvers and OpenFAST can be found. Dynamic responses of the platforms are also investigated and compared for relevant load cases from the Lifes50+ project (Galván et al., 2018; Pegalajar-Jurado et al., 2018), which are selected for the Gulf of Maine and operational conditions of CENTEC TLP (Uzunoglu & Guedes Soares, 2020) which are chosen for Galicia, Spain.

5.1.1 OO-STAR

This subsection gives the system behavior calculated by three hydrodynamic solvers and OpenFAST. The results presented here follow the same coordinate system in

Figure 14. The minus sign in the physical parameters indicates the opposite direction according to this sign convention.

The simulated load cases for benchmark comparison are given in Table 15. The same load cases from the Lifes50+ project are used for OO-Star and Nautilus platforms. The modeled LCs for this platform are named LC12 (Operational), LC17 (Ultimate), and LC18 (Extreme) conditions. For CENTEC TLP, the load cases used for benchmark comparison are rated, above rated, and extreme. The extreme cases for both comparisons have 50-year extreme wind and wave parameters.

Table 15 Benchmark load cases modeled

Benchmark Load Cases	**Wind Speed [m/s]**	**Wave Height [m]**	**Peak Wave Period [s]**
Operational (LC12)	13.9	3.04	9.5
Ultimate (LC17)	22.1	10.9	16
Extreme (LC18)	44	10.9	16
Rated	11.4	4	10
Above Rated	22.4	8	11.5
Extreme	47.5	12.5	14.3

Natural Frequencies

In Table 16 and Figure 24, the natural frequencies of the OO-Star platform are given for different code combinations, including (WAMIT+OpenFAST), (AQWA+OpenFAST), (HAMS+OpenFAST), and (WAMIT+FASTv8) (Galván et al., 2018; Pegalajar-Jurado et al., 2018) simulation results.

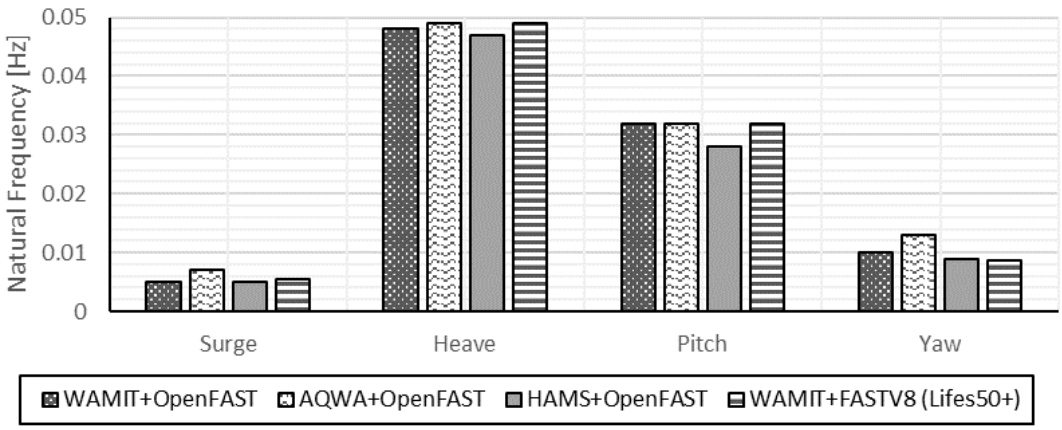


Figure 24 Natural frequencies of OO-Star computed with OpenFAST using input from different hydrodynamic models

Figure 24 and Table 16 present the natural frequencies of the OO-Star system computed using OpenFAST. Calculation of the natural frequencies is also possible in AQWA; however, to have better consistency, natural frequencies are computed with OpenFAST and using free decay tests for models in still water without wind. The last combination (WAMIT+FAST v8) is not calculated since it was taken from the reference (Pegalajar-Jurado et al., 2018). As seen in Figure 24, the natural frequencies computed agree well with the benchmark case. Although both models use the same WAMIT input, there are minor differences between (WAMIT+OpenFAST) and (WAMIT+FASTv8) cases, especially in surge and yaw DOFs which might be caused by the greater hydrodynamic modeling capabilities of OpenFAST. In the case of OO-star, all DOFs except yaw, HAMS have slightly smaller natural frequencies than WAMIT results.

Table 16 Natural frequencies of OO-Star platform.

Natural Frequencies [Hz]	**WAMIT OpenFAST**	**AQWA OpenFAST**	**HAMS OpenFAST**	**WAMIT FASTV8 (Lifes50+)**
Surge	0.005	0.005	0.005	0.0055
Heave	0.048	0.049	0.047	0.0490
Pitch	0.032	0.032	0.028	0.0320
Yaw	0.010	0.010	0.009	0.0086
Tower	0.747	0.747	0.743	0.7860

Hydrodynamic Coefficients

Figure 25 presents the hydrodynamic coefficients of the OO-Star platform computed by three potential flow solvers. Overall, there are slight differences in the parameters compared. For surge and heave DOFs, the deviations are more visible for frequencies smaller than 1 rad/s (6.28 s) for three hydrodynamic coefficients. Added mass of the pitch DOF has slightly different values comparing the three hydrodynamic solutions. The difference is visible for pitch-added mass in the AQWA solution. The values of the other DOFs are very similar for added mass.

Additionally, for the AQWA solution, smaller irregular peaks can be seen, mostly larger than 2 rad/s (3.14 s). However, smaller frequency steps might solve this issue where the maximum frequency steps (100) are already used for AQWA in this study. For HAMS, there is an option to remove these irregular frequencies during the computation. For the AQWA solution, the irregular peaks are removed manually before using as input to OpenFAST. For radiation damping, the three models have good agreement. Only at the peaks are slight deviations, and some irregular peaks can be seen in yaw radiation damping for AQWA. For wave excitation forces, the deviations can be seen at smaller frequencies (smaller than 0.5 rad/s), and some irregular peaks can be seen for AQWA.

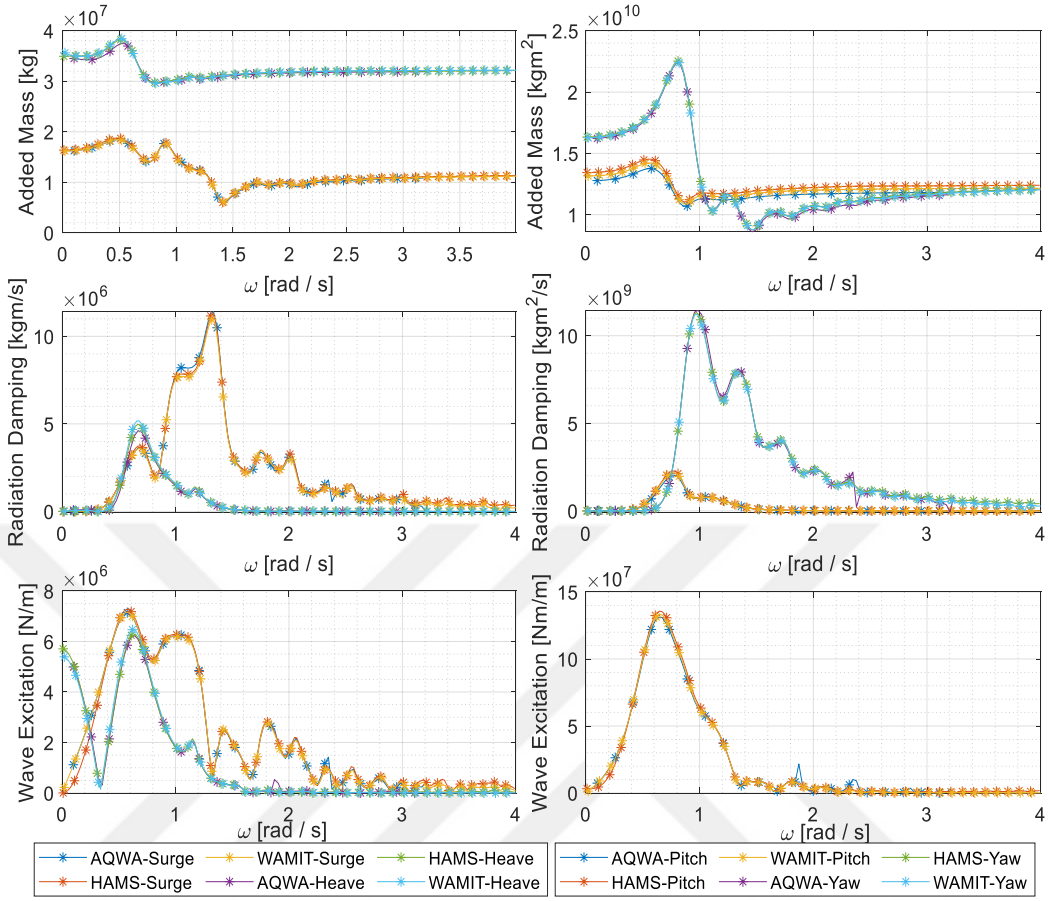


Figure 25 Hydrodynamic coefficients of OO-STAR computed by three potential flow solvers

Operational Load Case

Dynamic responses of the OO-Star platform concept in its operational conditions for the Gulf of Maine with a wind speed of 13.9 m/s, H_s of 3.04 m, and T_p of 9.5 s are modeled using three numerical model combinations ((WAMIT+OpenFAST), (AQWA+OpenFAST), (HAMS+OpenFAST)). The three models are simulated using the same wave seed and wind seed. The wave direction is chosen as zero degree, and the effects of wave direction or wind/wave misalignment are not considered. The simulation duration is 5400 s, and the first 600 s are excluded from the post-processing. The same conditions apply to the other load cases simulated. The environmental parameters given are the LC 12 for the Lifes50+ project, and it was chosen to compare the model results with the Lifes50+ project. Overall, the

system's response is similar to the project in the time series. Figure 27 and Table 17 show that the difference is more evident for pitch DOF motion for (HAMS+OpenFAST) model than the other two combinations (19.6 % higher than WAMIT output and 31.4 % higher than AQWA).

Table 17 Maximum and minimum responses of OO-Star system in operational sea states with a comparison of three potential flow solvers

	Surge [m]	**Heave [m]**	**Pitch [deg]**	**Tow. Top. Acc.[m/s2]**	**Thrust [kN]**	**Gen. Pow. [kW]**	**Mooring 1 [kN]**
Min							
WAMIT	8.67	-0.60	-1.51	-0.82	542.90	8147	1976
HAMS	8.51	-0.57	-1.92	-0.89	427.30	8174	1976
AQWA	8.66	-0.58	-1.49	-079	552	8157	1975
Mean							
WAMIT	13.78	0.01	3.22	0.00	1251.76	9999.08	2294
HAMS	13.43	0.01	4.05	0.00	1290.78	9997.93	2299
AQWA	13.79	0.01	3.20	0.00	1250.72	9999.12	2294
Max							
WAMIT	20.27	0.60	8.68	0.78	2434	12020	2858
HAMS	19.12	0.58	10.56	0.76	2484	12130	2922
AQWA	20.33	0.58	8.62	0.77	2425	12030	2855

Here in Table 17, *Tow. Top. Acc.* is the horizontal tower top acceleration in x direction (in line with the wave and wind direction), *Gen. Pow.* is the generated power and *Mooring 1* is the mooring tension in the given mooring line in the structure.

Additionally, comparing the tower top acceleration, (HAMS+OpenFAST) differs from (WAMIT+OpenFAST) and (HAMS+OpenFAST) models. There is a slight difference in generated power and rotor thrust in the three models. However, (HAMS+OpenFAST) model has the smallest minimum rotor thrust (427.30 kN). The mooring tensions obtained are almost identical in the three models. (HAMS+OpenFAST) the model has a slightly smaller maximum surge and slightly

larger pitch motion than other solvers. Since surge and pitch DOFs are coupled, this might be expected for the HAMS solution. The differences in surge and pitch DOFs are more visible in Figure 28 in the time series than in Figure 27. However, for the power spectral densities, the difference is not significant. The difference in the frequency domain is negligible for the other parameters. The difference in the surge and pitch motion might also cause a change in the aerodynamics of the turbine. Hence, as shown in Figure 27, there are slight differences in the rotor speed, thrust, and generated power. The mooring line configuration of the OO-Star system can be seen in Figure 26.

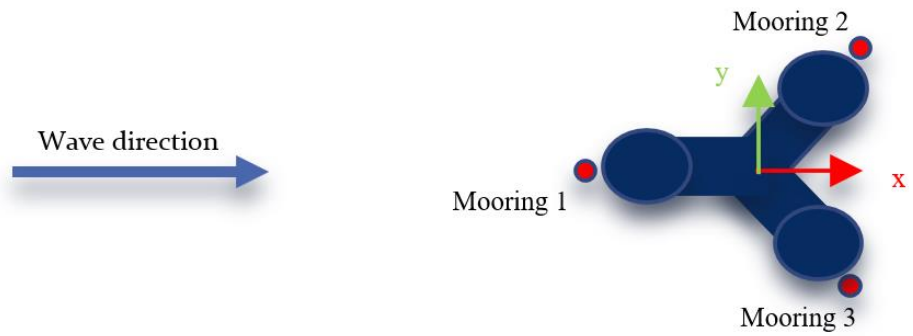


Figure 26 Mooring line configuration of OO-Star system

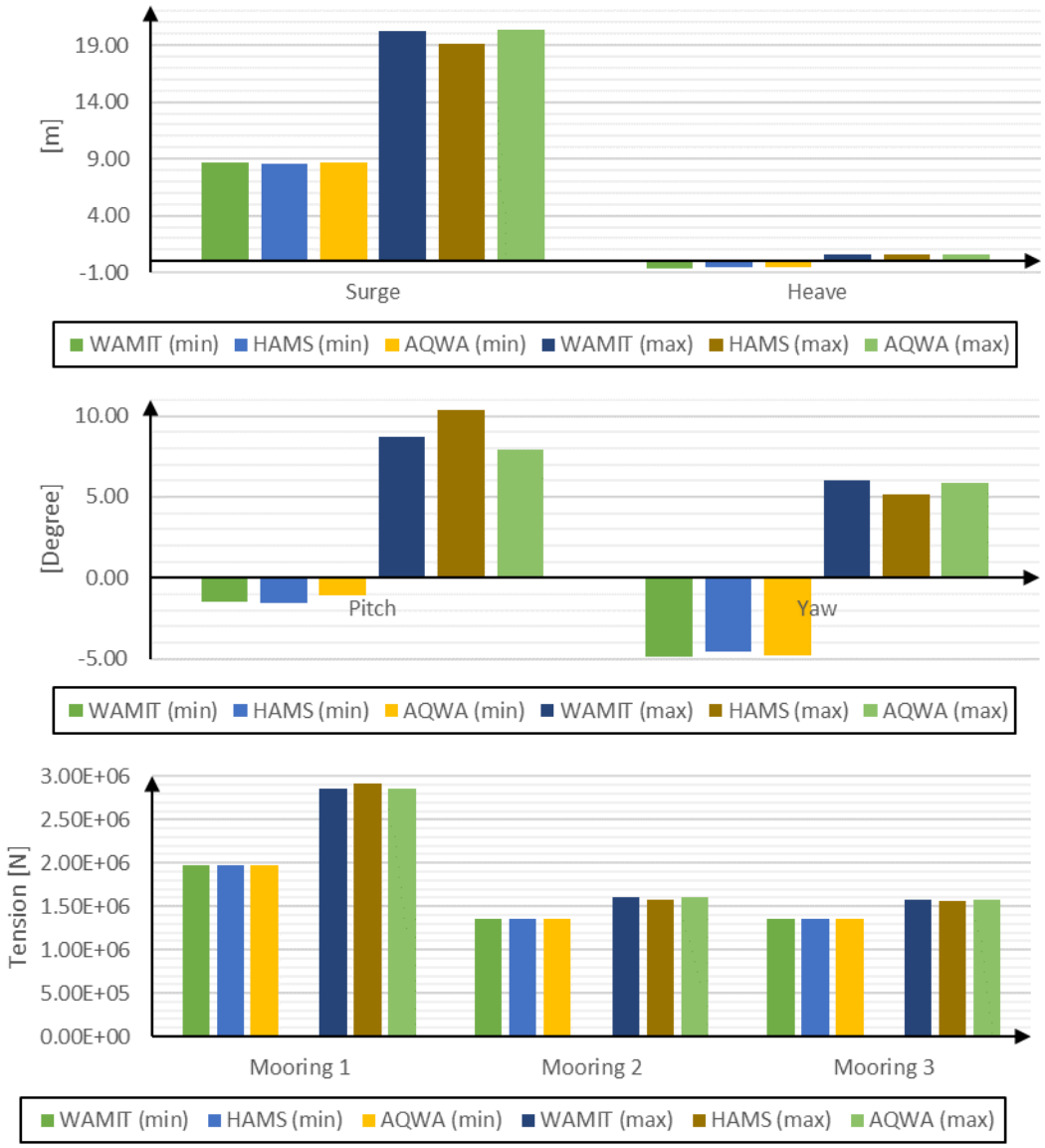


Figure 27 Maximum and minimum values of the OO-Star system in operational sea states

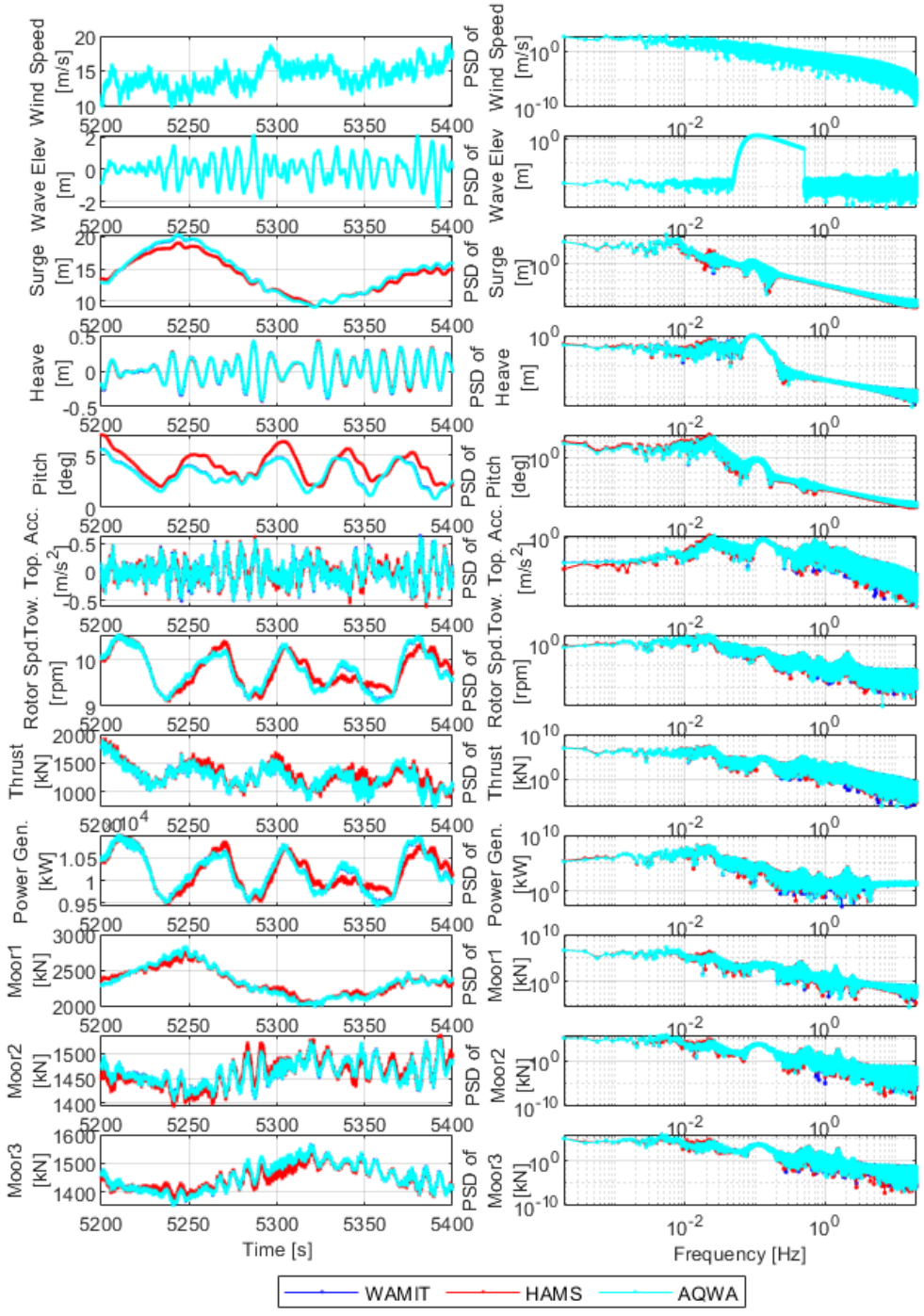


Figure 28 Dynamic response of OO-Star in operational condition

Here in Figure 28, *wave elev.* represents the wave elevation, *Tow. Top. Acc.* is the horizontal tower top acceleration in x direction (in line with the wave and wind direction), *rotor spd.* is the rotor speed, *power gen.* is the generated power, and

Moor.1 is the mooring tension in the given mooring line in the structure. For OO-Star, mooring 1 is in the wave direction, and two other moorings are aligned 120 degrees apart from mooring 1 (See Figure 26).

Ultimate Limit State

To verify the models against the Lifes50+ project (Pegalajar-Jurado et al., 2018), ultimate (LC 17) and extreme responses (LC 18) are also modeled and compared. The ultimate response LC has a wind speed of 22.1 m/s, H_s of 10.9 m, and T_p 16 s. All simulations have the same setup as the previously discussed operational load case for the OO-Star platform.

Table 18 Maximum and minimum responses of ultimate sea states of OO-Star DTU 10 system with a three potential flow solvers comparison

	Surge [m]	**Heave [m]**	**Pitch [deg]**	**Tow. Top. Acc. [m/s2]**	**Thrust [kN]**	**Gen. Pow. [kW]**	**Moor. 1 [kN]**
Min							
WAMIT	2.79	-4.17	-1.05	-1.48	127.10	8337	1353
HAMS	2.88	-4.19	-0.66	-1.43	162.30	8353	1373
AQWA	2.80	-4.14	-1.15	-1.49	139.60	8331	1358
Mean							
WAMIT	9.50	0.04	2.07	0.00	850.42	9999.88	2025
HAMS	9.24	0.04	2.59	0.00	871.68	9999.94	2027
AQWA	9.50	0.04	2.06	0.00	849.93	9999.87	2025
Max							
WAMIT	16.31	4.38	5.69	1.38	1529.00	11650	2621
HAMS	15.83	4.33	6.24	1.44	1509.00	11590	2610
AQWA	16.27	4.30	5.65	1.36	1528.00	11660	2631

As can be seen from Table 18 and Figure 29, the three models have similar surge motions (2.79 m – 2.88 m), where (HAMS+OpenFAST) is slightly smaller. The difference between the models is more visible for the pitch DOF in the case of the (HAMS+OpenFAST) model than in other models. For maximum pitch value,

(HAMS+OpenFAST) is 9.6 % higher than (WAMIT+OpenFAST) and 10.5 % higher than (AQWA+OpenFAST).

As expected, the tension in the mooring is greater for mooring 1 (2610 kN – 2631 kN) in all combinations, which is in the wave direction. Further comparing the models, (HAMS+OpenFAST) has the largest minimum rotor thrust (162.30 kN) and minimum tension at mooring 1.



Figure 29 Maximum and minimum values of OO-Star system in ultimate sea states

As can be seen in Figure 29 and Figure 30, the three solvers have good agreements except for the slight differences in surge and pitch DOFs. Similar to the operational load case (LC12), the hydrodynamic solver has a more negligible influence on the system's aerodynamic behavior than its hydrodynamic behavior.

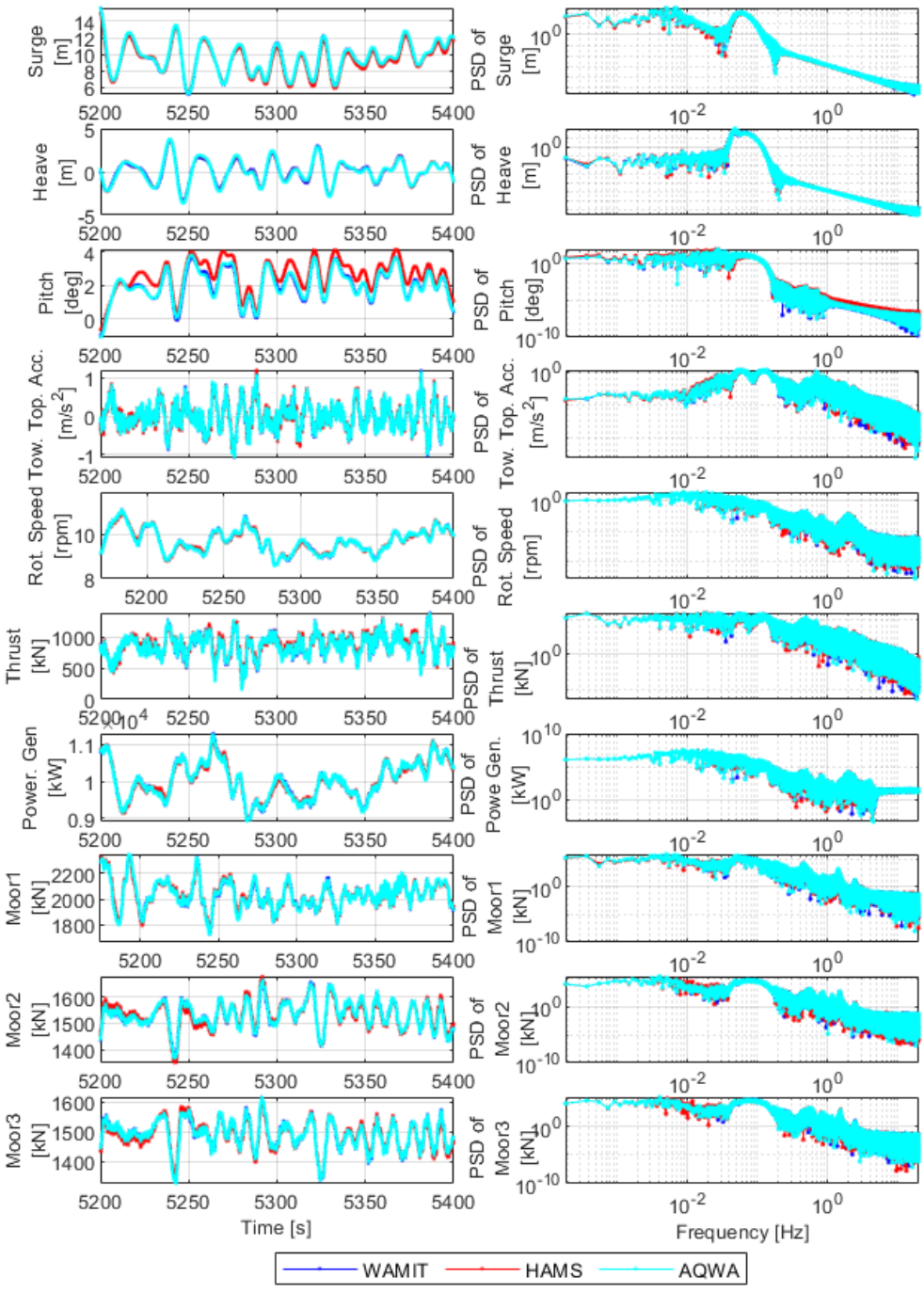


Figure 30 Ultimate response of OO-Star system

Extreme Load Case

The last LC comparison from the Lifes50+ project is the extreme case where the wind speed is 44 m/s, H_s is 10.9 m, and T_p of 16 s with a parked turbine and feathered blades. As can be seen from Figure 31 and Figure 32, similar to the previous load cases, there are minor differences in the surge and pitch DOFs which cause slight deviations in the tower top acceleration and the rotor thrust. Since the turbine is parked, the mean rotor thrust (317 kN) is smaller than in the ultimate case (857 kN).



Figure 31 Maximum and minimum OO-Star system response in extreme sea states

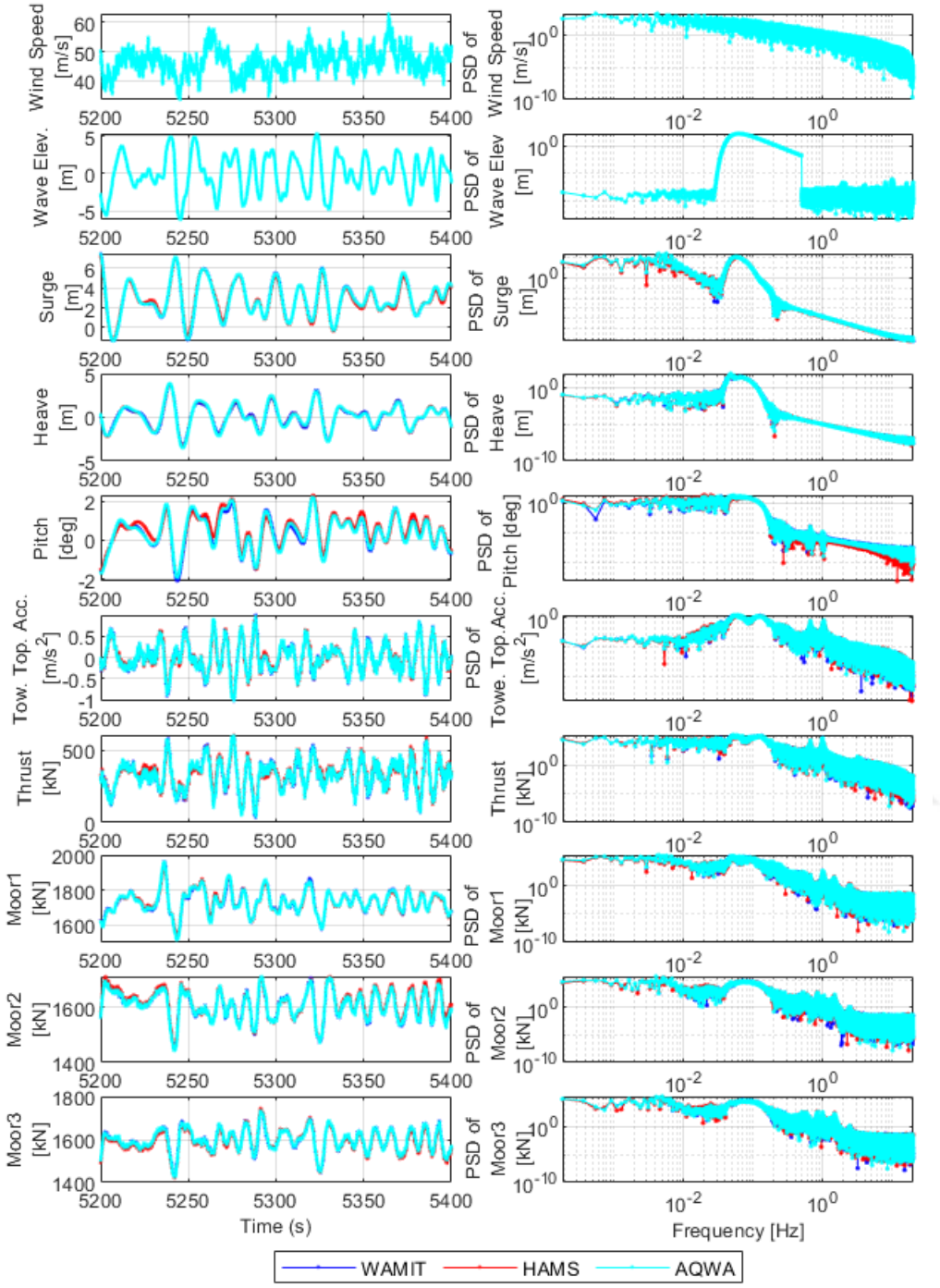


Figure 32 Responses of the OO-Star system in extreme load case

5.1.2 NAUTILUS

In this subsection, the response of the Nautilus system computed by three hydrodynamic solvers and OpenFAST are given.

Natural Frequencies

Natural frequencies of the Nautilus platform computed by three hydrodynamic solvers and OpenFAST combinations are given. The same combinations and references explained in the OO-Star system are used. Calculated values can be seen in Figure 33 and Table 19.

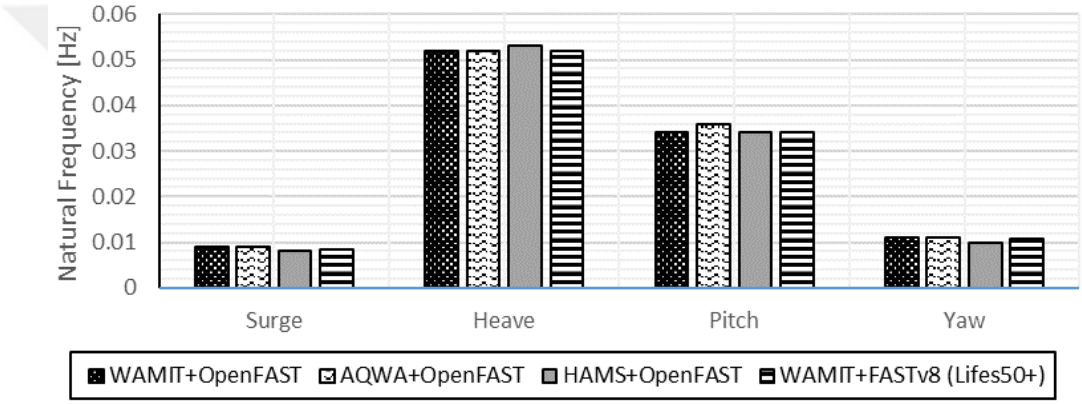


Figure 33 Natural frequencies of Nautilus computed with OpenFAST using input from different hydrodynamic models

As mentioned in the previous concept, free decay tests were carried out to calculate natural frequencies in OpenFAST. (WAMIT+FASTv8) the combination is not calculated since it is taken from the reference (Yu, 2018). Figure 33 shows an agreement with the natural frequencies of the benchmark case with slight differences. Heave and tower natural frequencies are slightly higher in (HAMS+OpenFAST) model (2% higher) than other models. Moreover, (AQWA+OpenFAST) and (WAMIT+OpenFAST) models have good agreement apart from the pitch DOF.

Table 19 Natural frequencies of the Nautilus platform

Natural Frequencies [Hz]	(WAMIT+ OpenFAST)	(AQWA+ OpenFAST)	(HAMS+ OpenFAST)	(WAMIT+ FASTv8) (Lifes50+)
Surge	0.009	0.009	0.008	0.0085
Heave	0.052	0.052	0.053	0.0518
Pitch	0.034	0.036	0.034	0.0340
Yaw	0.011	0.011	0.010	0.0107
Tower	0.530	0.532	0.528	0.5230

Hydrodynamic Coefficients

Figure 34 compares hydrodynamic coefficients added mass, radiation damping, and wave excitation force computed using three hydrodynamic solvers. As can be seen from Figure 34, surge added mass is almost the same for the three hydrodynamic solvers. For heave, (AQWA+OpenFAST) and (WAMIT+OpenFAST) models have a good agreement, and the results of the (HAMS+OpenFAST) models are slightly smaller. For the added mass comparison OO-Star model has almost identical added masses except for the frequencies smaller than 1 rad/s for heave and pitch DOFs. In the Nautilus concept, the agreement is not as great as OO-Star; the reason for this might be the volume coverage difference (OO-Star 99.98% and Nautilus 99.40%). For heave and yaw DOFs, the difference is more visible. The Nautilus platform AQWA model has better agreement with the WAMIT model in heave but not in yaw DOFs. Radiation damping is well captured within the outputs of three hydrodynamic solvers. A minor deviation can be seen in the AQWA model for frequencies smaller than 1.5 rad/s, especially in heave and pitch DOFs. For wave excitation forces, the differences in the hydrodynamic solvers are more visible for smaller frequencies of heave and pitch DOFs.

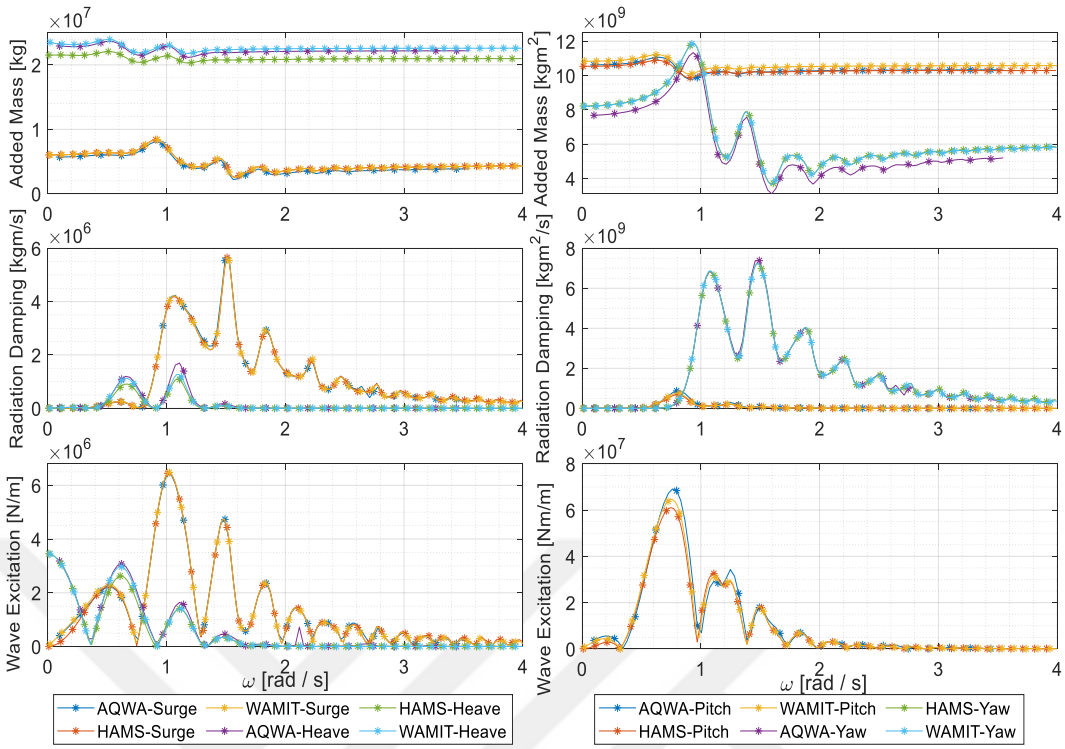


Figure 34 Hydrodynamic coefficients of the Nautilus platform

Operational Case

The same LCs are simulated as the OO-Star platform for comparison with the Lifes50+ project. The first LC to be simulated is the operational case with 13.9 m/s wind speed, 3.04 m H_s, and 9.5 T_p. The outputs of this simulation can be seen in Table 20 and Figure 36. As can be seen from Figure 36, the maximum and minimum values of the motion and mooring tensions are almost identical for the three cases (AQWA+OpenFAST), (HAMS+OpenFAST) and (WAMIT+OpenFAST) models. A slight difference in heave DOF ((HAMS+OpenFAST) is 7% smaller for minimum and maximum values) and a more significant difference in maximum and minimum values of pitch motion could be observed. The mooring configuration of the Nautilus system can be seen in Figure 35, where moorings 2 and 3 are in the upstream wave direction.

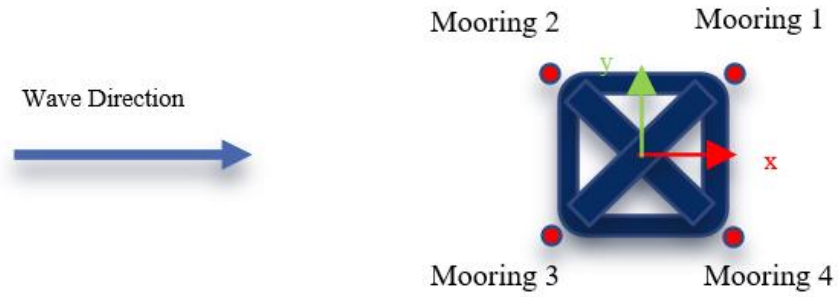


Figure 35 Mooring configuration of the Nautilus platform where wave direction is zero (head wave)

As can be seen from Table 20 and Figure 36, the simulation results have good agreement. (HAMS+OpenFAST) model has a slightly higher maximum and slightly lower minimum surge motion, whereas it has a smaller minimum heave motion and larger minimum tower top acceleration (26.9 % greater in magnitude than (WAMIT+OpenFAST).

Table 20 Maximum and minimum values of the operational sea states of Nautilus DTU 10 system with three potential flow solvers comparison

	Surge [m]	**Heave [m]**	**Pitch [deg]**	**Tow.Top Acc. [m/s2]**	**Thrust [kN]**	**Gen. Pow. [kW]**	**Mooring 2 [kN]**	**Mooring 4 [kN]**
Min								
WAMIT	9.74	-0.61	-5.95	-1.22	75.32	7479	817.10	358
HAMS	9.87	-0.57	-6.20	-1.55	88.90	7351	812.60	356.30
AQWA	9.77	-0.63	-5.18	-1.16	180	7506	822.30	359.90
Max								
WAMIT	27.22	0.37	5.67	1.32	2426	12520	1733	505
HAMS	27.33	0.35	6.02	1.35	2381	12480	1715	504.80
AQWA	27.22	0.38	5.11	1.301	2319	12250	1741	505.30

Table 20 shows the data for mooring 2 and mooring 4 are given (See Figure 35). Nautilus system has four mooring lines, mooring 2 is in the upwind direction (incoming wave direction), and mooring 4 is in the downwind direction. Mooring 2 (AQWA+OpenFAST) has a higher minimum and maximum tension values. (HAMS+OpenFAST) the model has slightly smaller minimum mooring tensions compared to (AQWA+OpenFAST) and (WAMIT+OpenFAST) values.



Figure 36 Maximum and minimum responses of Nautilus system in operational sea states

Time series and PSDs have good agreements, as seen in Figure 37. Smaller deviations in pitch, tower top acceleration, rotor speed, and rotor thrust can be seen for (HAMS+OpenFAST) and (AQWA+OpenFAST) models.

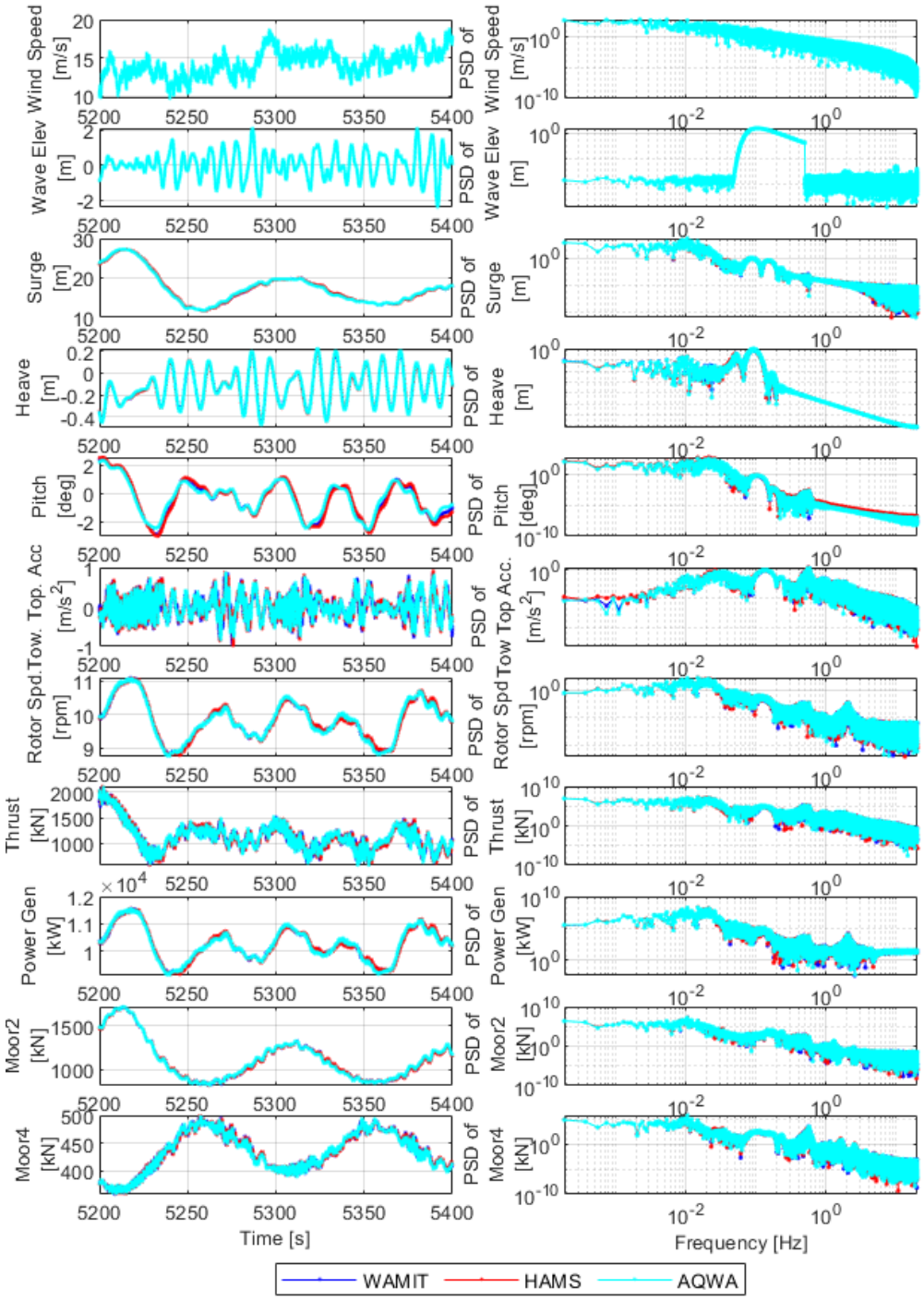


Figure 37 Operational response of Nautilus system

Ultimate Load Case for Nautilus Platform

The second LC for the Nautilus platform is the ultimate load case defined in the Lifes50+ project (LC 17) with 22.1 m/s wind speed, 10.9 m H_s and 16 s T_p. The results of the dynamic simulation of the Nautilus platform can be seen in Table 21 and Figure 38. As can be seen from Table 21, (HAMS+OpenFAST) model has greater minimum values in the surge, smaller minimum pitch, and tower top acceleration. (HAMS+OpenFAST) model has a greater minimum (6.82 %) and smaller maximum values (6.18 %) than the (WAMIT+OpenFAST) model in mooring line tension. (AQWA+OpenFAST) the model has similar results to the (WAMIT+OpenFAST) model. As can be seen from Figure 38, (AQWA+OpenFAST) and (WAMIT+OpenFAST) models have a good agreement for compared properties, whereas in the case of (HAMS+OpenFAST) there is a slight difference.

Table 21 Maximum and minimum responses of the ultimate sea states of Nautilus DTU 10 system with three potential flow solvers comparison

	Surge [m]	**Heave [m]**	**Pitch [deg]**	**Tower Top Acc. [m/s2]**	**Thrust [kN]**	**Pow. Gen. [kW]**	**Moor. 2 [kN]**	**Moor. 4 [kN]**
Min								
WAMIT	4.21	-3.03	-3.45	-1.54	32.32	7927	538.7	345.3
HAMS	5.76	-2.89	-3.96	-1.74	131.2	7786	628.4	385.4
AQWA	4.28	-3.06	-3.26	-1.54	2.29	7902	542.2	338.7
Max								
WAMIT	17.57	2.72	3.57	1.613	1549	12360	1368	637.7
HAMS	17.02	2.66	3.63	1.536	1675	12280	1276	556.6
AQWA	17.42	2.77	3.47	1.628	1558	12370	1381	636.2

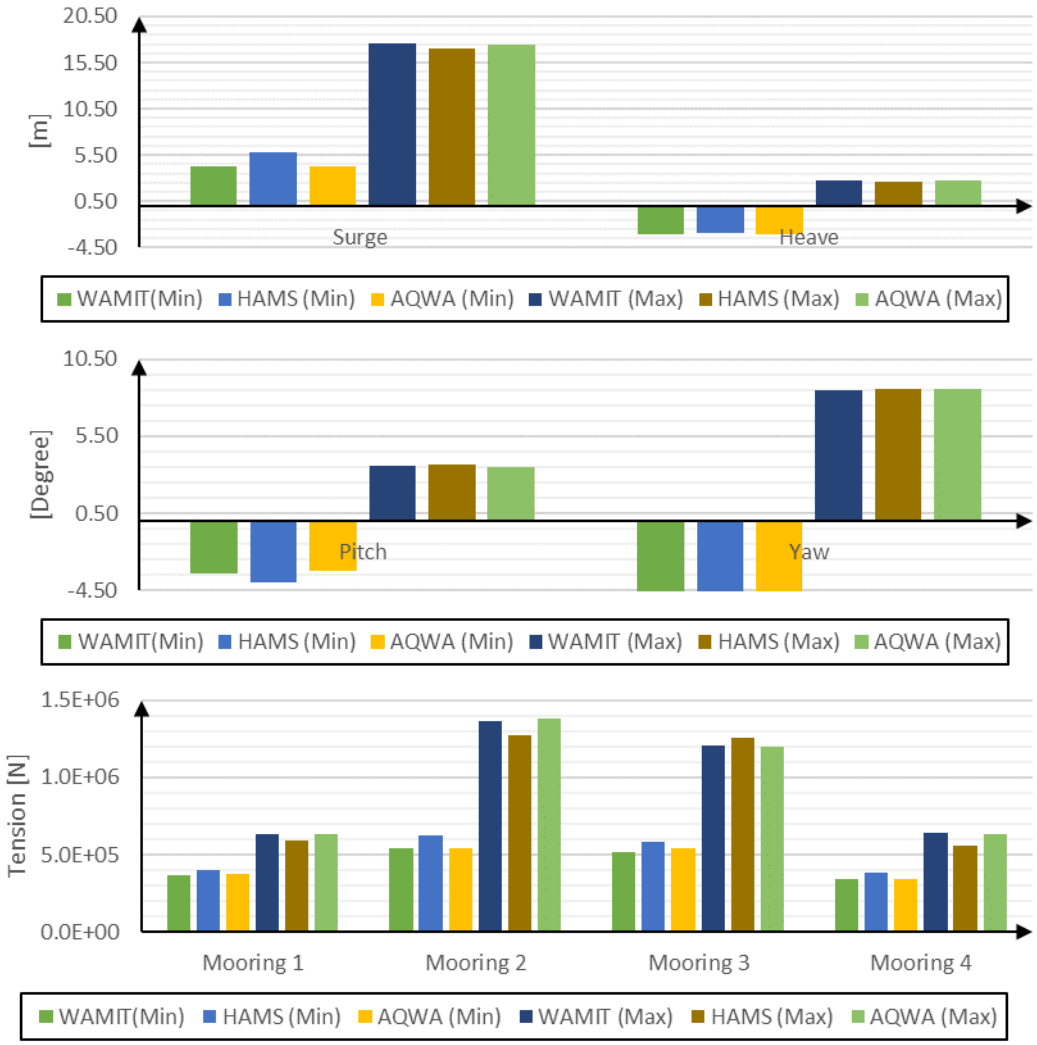


Figure 38 Maximum and minimum responses of Nautilus system in ultimate sea states

As seen in Figure 39, the difference in time and frequency domain are more significant in heave and pitch DOFs (HAMS+OpenFAST). Additionally, more minor deviations from the (WAMIT+OpenFAST) and other solvers can be observed at rotor speed, thrust, and the generated power. For larger frequencies, the deviation is also observed in the PSD graphs of that parameters.

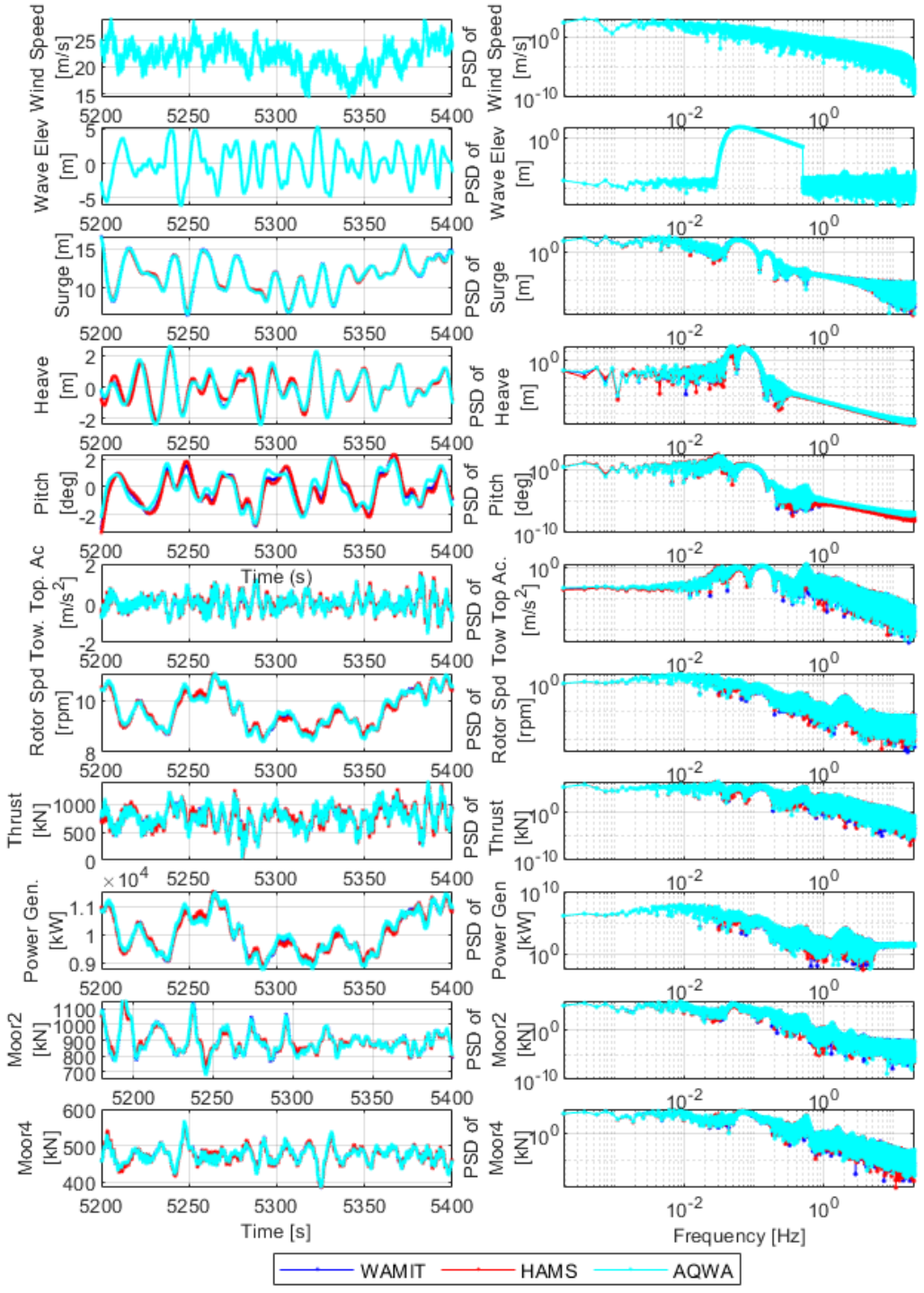


Figure 39 Response of the Nautilus platform in ultimate conditions

Extreme Conditions

The last LC comparison from the Lifes50+ project for the Nautilus system is the extreme case (LC18) with a parked turbine and feathered blades. As can be seen from Table 22 and Figure 40 (HAMS+OpenFAST) model has a smaller minimum surge, heave and tower top acceleration compared to other models. However, it has a smaller minimum thrust, minor maximum surge, maximum heave, and maximum tower top accelerations. The minimum mooring tensions are greater for the (HAMS+OpenFAST) simulation (2.86 % higher than the (WAMIT+OpenFAST) model). For this load case, (AQWA+OpenFAST) and (WAMIT+OpenFAST) have a good agreement.

Table 22 Maximum and minimum responses of the extreme sea states of Nautilus DTU 10 system with a three potential flow solvers comparison

	Surge [m]	**Heave [m]**	**Pitch [deg]**	**Tow. Top Acc. [m/s2]**	**Mooring 2 [kN]**	**Mooring 4 [kN]**
Min						
WAMIT	-5.00	-2.93	-2.05	-1.360	459.10	405.50
HAMS	-2.73	-2.79	-1.85	-1.260	483.90	432.70
AQWA	-4.93	-2.97	-1.84	-1.410	460.90	407.80
Max						
WAMIT	9.54	2.83	1.89	1.34	884.40	809.80
HAMS	8.19	2.76	2.02	1.24	916.90	816.70
AQWA	9.37	2.88	1.97	1.42	876.80	808.40

As seen from Figure 41, similar to the ultimate load case, there are deviations from the (WAMIT+OpenFAST) model. The difference is more visible in heave and pitch DOFs than in other DOFs. There is still a minor difference for tower top acceleration, but since the turbine is parked, it is less than the ultimate case.

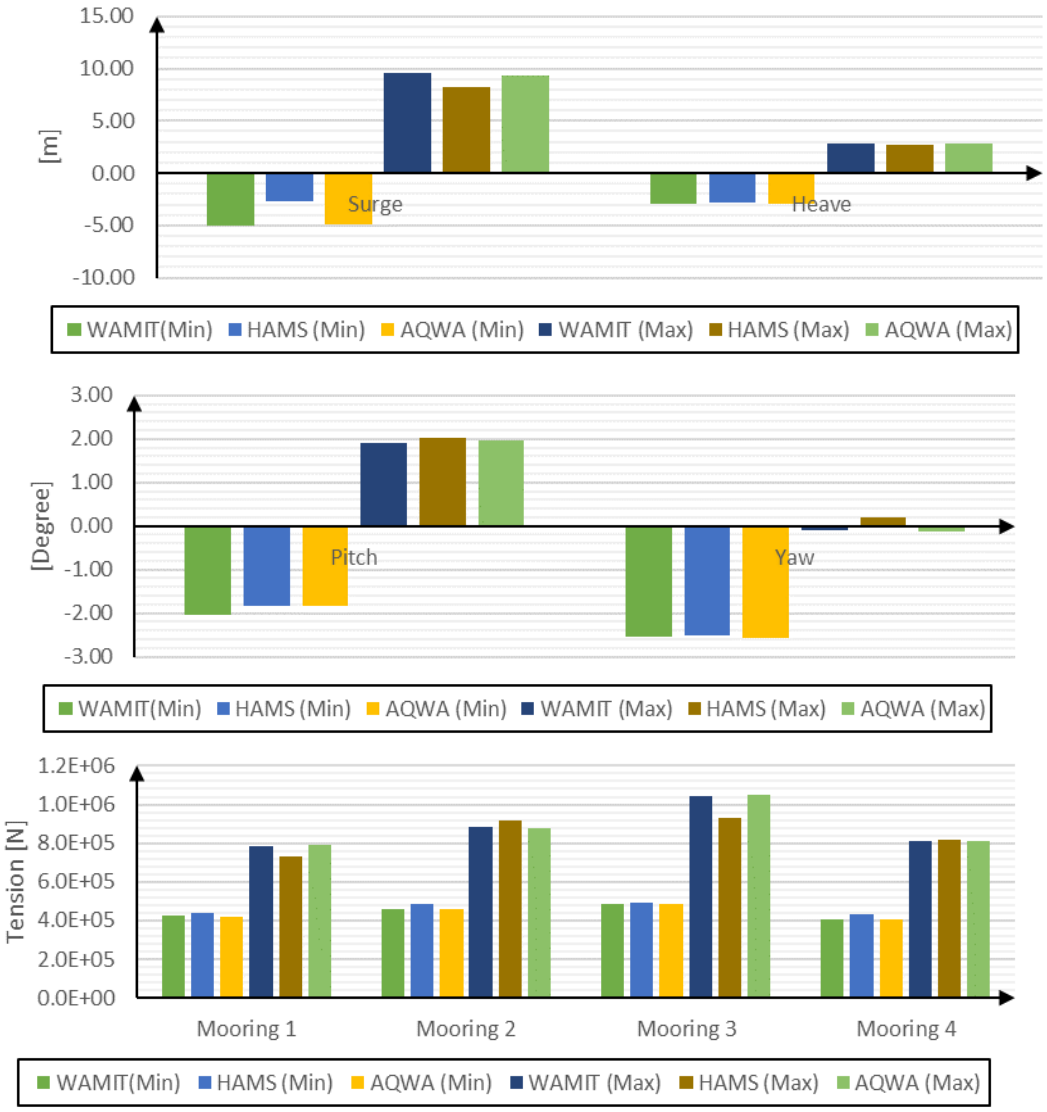


Figure 40 Maximum and minimum values of Nautilus system in extreme sea states

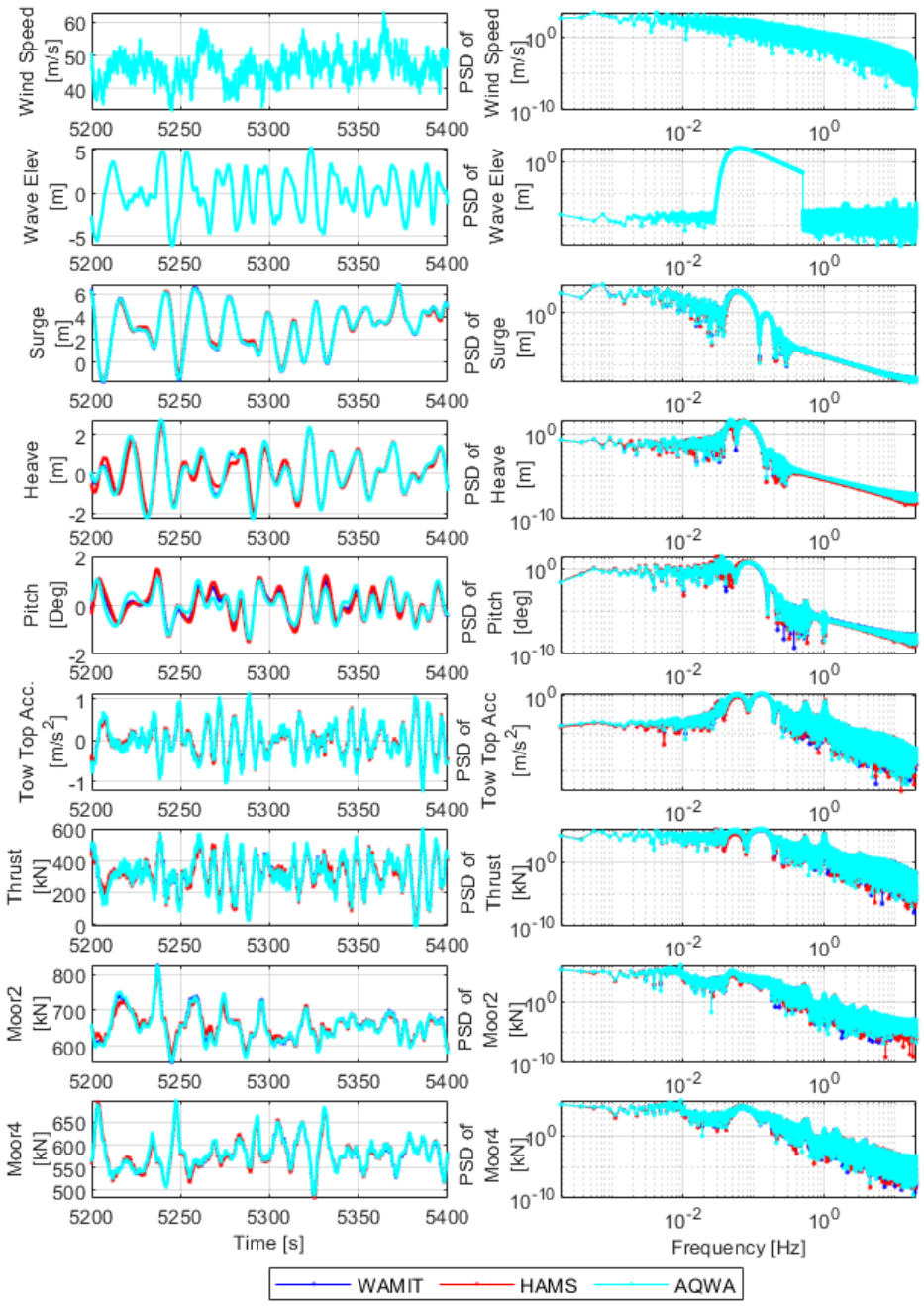


Figure 41 Extreme response of the Nautilus platform

5.1.3 CENTEC TLP DTU-10

This subsection presents the dynamic behavior of CENTEC TLP computed by three hydrodynamic solvers and OpenFAST.

Natural Frequencies

In Figure 42 and Table 23, the natural frequencies of the CENTEC TLP computed using the models ((WAMIT+OpenFAST), (AQWA+OpenFAST), (HAMS+OpenFAST). Computed values are compared with (WAMIT+FAST)) (Uzunoglu & Guedes Soares, 2020). The natural frequencies are obtained from free decay tests for models in still water without wind. (WAMIT+FAST) the combination was taken from the reference above. As can be seen from Figure 42, there is a good agreement except for pitch DOF. For pitch, the three modeled natural frequencies are similar. The pitch natural frequency taken from Uzunoglu & Guedes Soares (2020) is slightly different even from the (WAMIT+OpenFAST) model (24.15 % smaller). The reason might be either the calculation method of natural frequencies or different FAST (OpenFAST) versions.

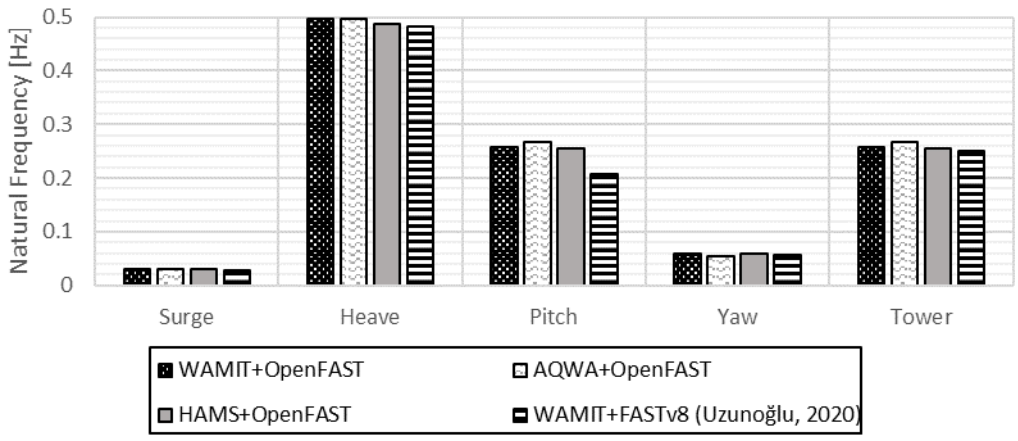


Figure 42 Natural Period of the CENTEC TLP

As can be seen from Table 23, (HAMS+OpenFAST) model has a slightly lower heave natural frequency than other models. Surge pitch and yaw DOFs have good agreement with (WAMIT+OpenFAST) model. (AQWA+OpenFAST) model has a

slightly lower yaw natural frequency than obtained from other models. The modeled tower natural frequencies have a good agreement but similar to the pitch DOF, and the tower natural frequency is slightly different from the benchmark case (WAMIT+FAST) (Uzunoglu & Guedes Soares, 2020). The reason for this difference might be due to the modeled tower. The tower properties of the CENTEC TLP are not publicly available. Hence to prepare an OpenFAST model, the tower of the DTU 10 MW turbine is used.

Table 23 Comparison of the natural frequencies of CENTEC TLP

Natural Frequencies [Hz]	**WAMIT OpenFAST**	**AQWA OpenFAST**	**HAMS OpenFAST**	**WAMIT FAST (Uzunoğlu, 2020)**
Surge	0.030	0.030	0.030	0.029
Heave	0.496	0.496	0.488	0.481
Pitch	0.257	0.256	0.255	0.207
Yaw	0.059	0.054	0.059	0.056
Tower	0.257	0.256	0.256	0.250

Hydrodynamic Coefficients

Figure 43 compares hydrodynamic coefficients added mass, radiation damping, and wave excitation force computed using two hydrodynamic solvers, HAMS and AQWA. The results are compared to WAMIT outputs from (Uzunoglu & Guedes Soares, 2020).

As can be seen from Figure 43, added mass, radiation damping, and wave excitation forces are almost the same for HAMS and WAMIT outputs. Both models have the same mesh. There is only a slight difference for higher frequencies (higher than 2 rad/s) for surge added mass and wave excitation. For AQWA models, the difference is greater compared to the HAMS output. The mesh used for AQWA is different, but a mesh sensitivity is conducted to have a similar mesh with HAMS and WAMIT models. The difference is more visible for heave and pitch added mass.

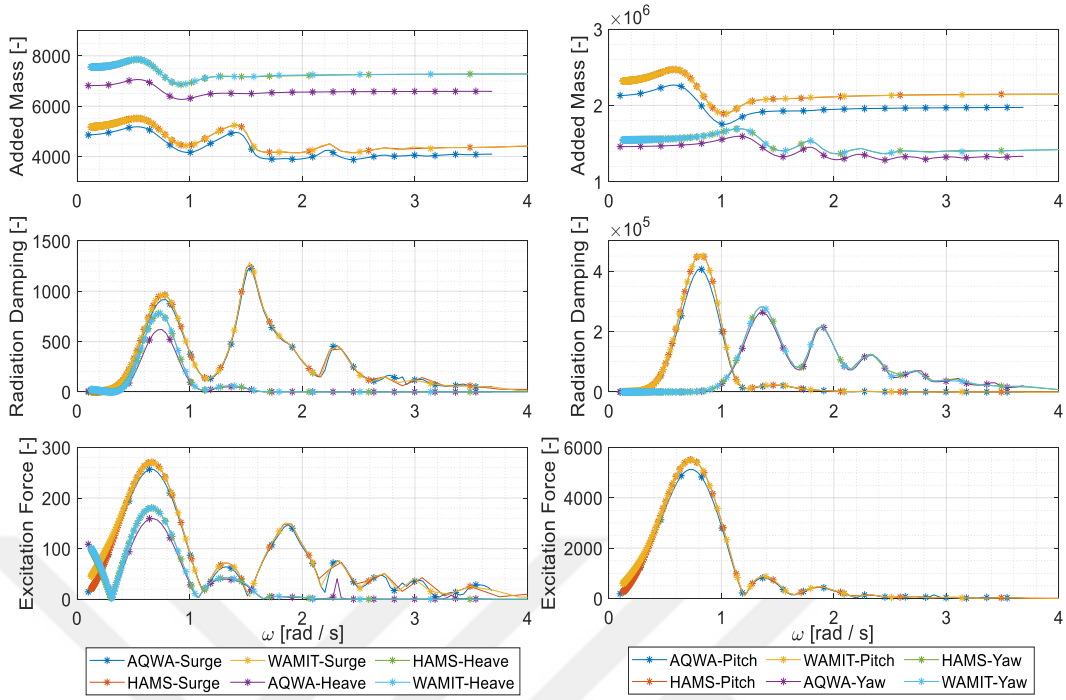


Figure 43 Hydrodynamic coefficients for CENTEC TLP

Rated Operational Condition

The benchmark load cases chosen for comparison are different for the CENTEC TLP compared to previous FOWT concepts studied in this thesis. The operational load case is the rated operational condition in Uzunoglu & Guedes Soares (2020), where the wind speed is lower than the rated wind speed. The rated operational condition is chosen for Galicia, Spain, where the CENTEC TLP is modeled in the reference above with a wind speed of 11.4 m/s, H_s of 4 m, and T_p of 10 s. CENTEC TLP is modeled using three numerical model combinations (WAMIT+OpenFAST), (AQWA+OpenFAST), and (HAMS+OpenFAST) using the same wave and wind seeds. Similar to the previous concepts, the wave direction is zero, and the wave/wind misalignment is not investigated.

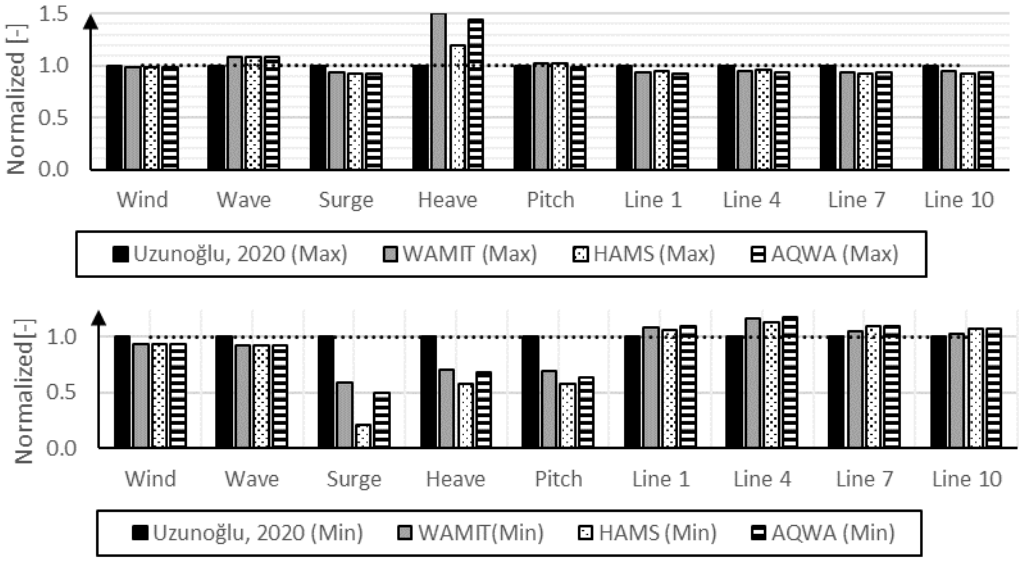


Figure 44 Normalized maximum and minimum responses for rated wind conditions

The outputs of the simulations are compared to the minimum and maximum values presented in Uzunoglu & Guedes Soares (2020). For those simulation results in the reference paper, 5 simulations of 1200 seconds in length with the different wave and wind seeds are modeled. The smallest and the largest value of each parameter is selected for a LC among 5 time series in Uzunoglu & Guedes Soares (2020). The comparison results are normalized for (HAMS+OpenFAST), (AQWA+OpenFAST) and (WAMIT+OpenFAST) models using the selected values in Uzunoglu & Guedes Soares (2020). The same presentation is also adopted for other load cases for CENTEC TLP. The simulations carried out in this thesis for this comparison have 5400 seconds simulation time and run for a single wave/wind seed. Same as the previous concepts first 600 seconds are excluded from the post-processing.

As can be seen in Figure 44, the normalized minimum and maximum wind speeds are different for modeled simulations and the benchmark case (Uzunoglu & Guedes Soares, 2020). The normalized minimum wind speed is slightly higher for the benchmark values. Normalized maximum wave height is higher for modeled cases, and minimum wave height is smaller than the benchmark value. The maximum pitch values have good agreements for (HAMS+OpenFAST), (AQWA+OpenFAST), and

(WAMIT+OpenFAST) simulation results and the benchmark value (the normalized values are almost 1 for all cases).

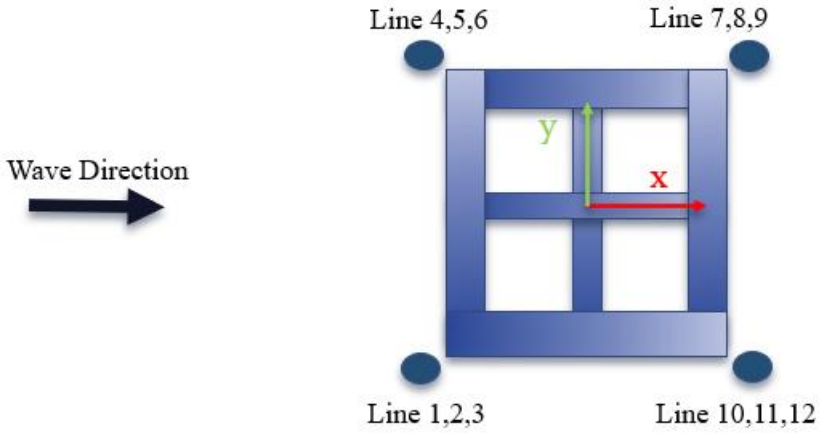


Figure 45 Top view and mooring configuration of CENTEC TLP

The maximum mooring tensions of the modeled cases are slightly lower. The minimum tensions are almost the same for (HAMS+OpenFAST) and (WAMIT+OpenFAST) and slightly higher than (AQWA+OpenFAST). The mooring configuration of the system can be seen in Figure 45. In the case of CENTEC TLP the minimum values of the surge, heave, and pitch differ between the modeled and benchmark case which might be caused by the differences in the wind/wave seeds, and limited data of the CENTEC TLP.

Table 24 Maximum and minimum responses of the rated conditions of CENTEC TLP

	Surge [m]	**Heave [m]**	**Pitch [deg]**	**Tow. Top Acc. [m/s2]**	**Mooring 1 [kN]**	**Mooring 7 [kN]**
Min						
WAMIT	-0.75	-0.19	-0.12	-1.51	3012	1861
HAMS	-0.74	-0.19	-0.12	-1.48	3027	1890
AQWA	-0.63	-0.19	-0.11	-1.47	3071	1938
Max						
WAMIT	7.45	0.08	0.45	1.78	5097	4067
HAMS	7.45	0.08	0.44	1.76	5075	4059
AQWA	7.37	0.07	0.43	1.75	5042	4023

The outputs of the rated operational condition simulation in the time and frequency domain are shown in Figure 46. As can be seen from Figure 46 and Table 24, the difference between the three coupled simulations is almost negligible. A slight difference in the peak magnitudes is observed in heave and pitch DOFs together with the moorings.

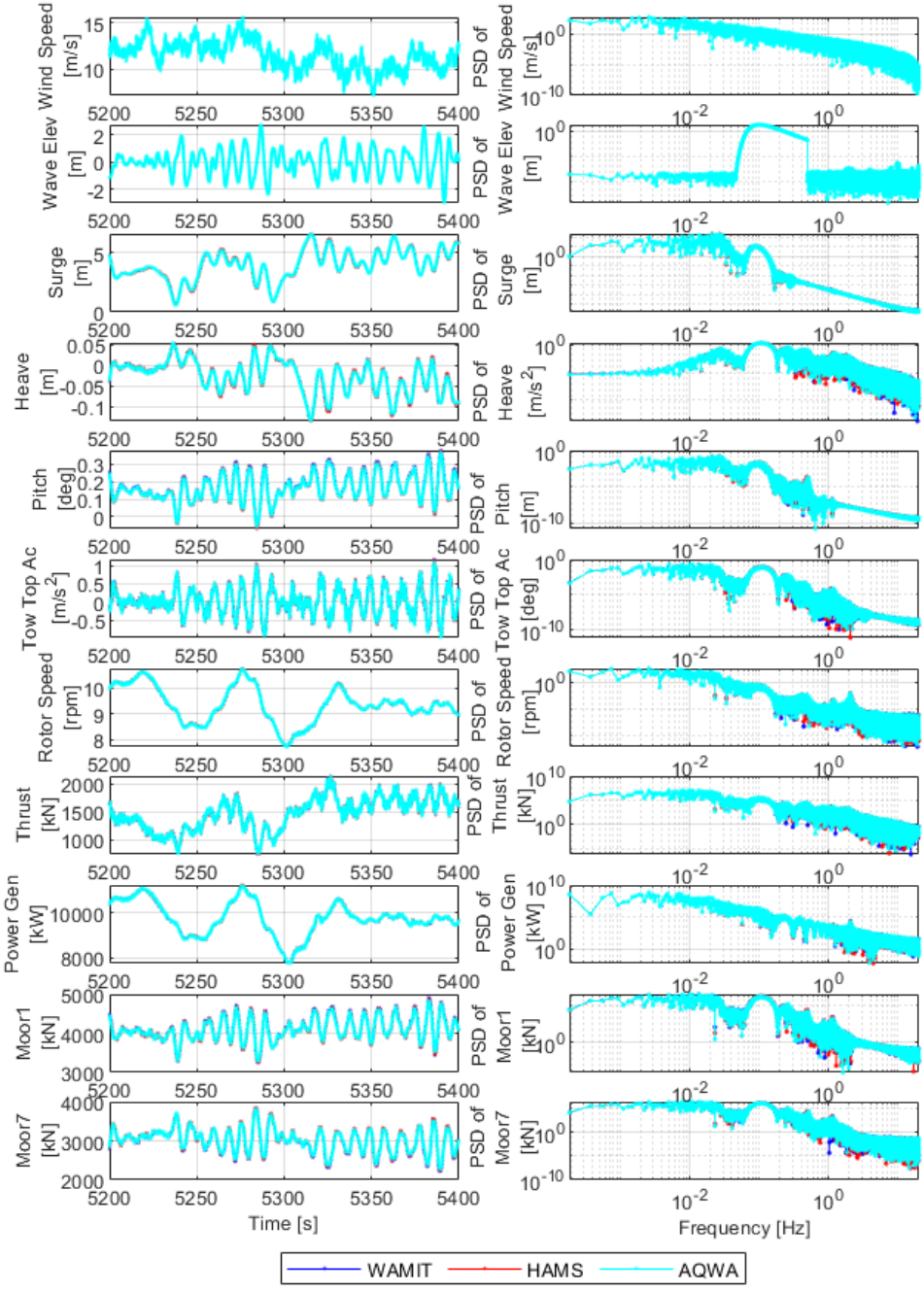


Figure 46 Dynamic responses of the rated operational case of CENTEC TLP

Mooring 1 and 7 are presented in Figure 46, where mooring 1 is in the upwind direction, and mooring 7 is in the downwind direction. Both moorings are located parallel to the x-axis. The difference can be seen in the frequency domain for larger frequencies in the PSD plots.

Above Rated Operational Conditions

The above-rated operational condition is chosen for Galicia, Spain, where the CENTEC TLP is modeled in the reference above with a wind speed of 22.4 m/s, H_s of 8 m, and T_p of 15 s. Except for the environmental parameters, the same simulation setup is used for the above-rated simulations. The normalized results of the above rated LC simulations can be seen in Figure 47. The maximum wind speed (approximately 0.97 for modeled cases) and significant wave height (approximately 1.05 for modeled cases) for this load case are almost identical (upper Figure 47). However, the minimum wind speed and wave speed are greater for the modeled cases (Lower Figure 47).

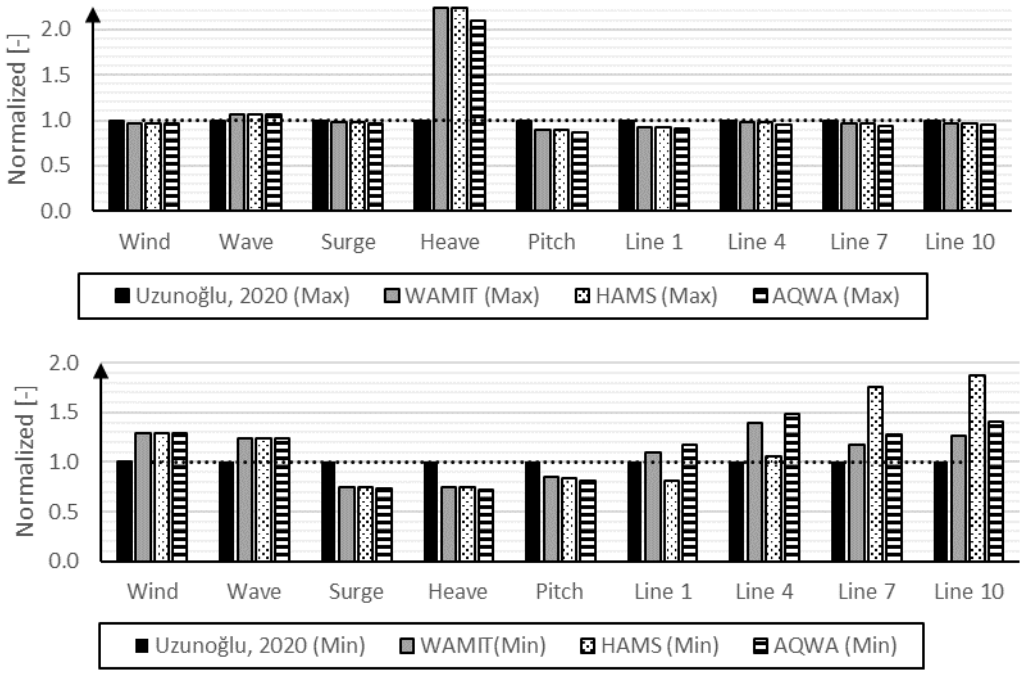


Figure 47 Normalized nondimensional maximum and minimum values for above-rated wind conditions

The modeled cases are slightly smaller for the maximum pitch DOF than the benchmark value (WAMIT+OpenFAST model 10% smaller). The maximum heave motion is significantly greater for modeled cases due to the differences in the mooring system. For the minimum responses, modeled surge, heave, and pitch motions are smaller than the benchmark. There are differences in the mooring line tensions.

The maximum and minimum responses of CENTEC TLP in the above-rated conditions are compared for (AQWA+OpenFAST), (HAMS+OpenFAST) and (WAMIT+OpenFAST) in (Uzunoglu & Guedes Soares, 2020). Minimum and maximum values of surge and heave motion are similar for the three models. The minimum pitch motion and tower top acceleration are greater in the (AQWA+OpenFAST) model. Minimum mooring tensions are also greater for the (AQWA+OpenFAST) model. (HAMS+OpenFAST) and (WAMIT+OpenFAST) models show good agreement. Figure 48 shows the modeled cases' time and frequency domain representations. As can be seen from Figure 48 and Table 25, three models show good agreement.

Table 25 Maximum and minimum responses of the above-rated conditions of CENTEC TLP

	Surge [m]	**Heave [m]**	**Pitch [deg]**	**Tow. Top Acc. [m/s^2]**	**Moor. 1 [kN]**	**Moor. 7 [kN]**
Min						
WAMIT	-2.29	-0.19	-0.43	-2.11	1877	1299
HAMS	-2.30	-0.19	-0.42	-2.11	1912	1317
AQWA	-2.25	-0.18	-0.40	-2.09	2009	1413
Max						
WAMIT	6.93	0.18	0.54	2.34	5627	5575
HAMS	6.92	0.18	0.53	2.33	5593	5548
AQWA	6.86	0.17	0.52	2.35	5469	5399

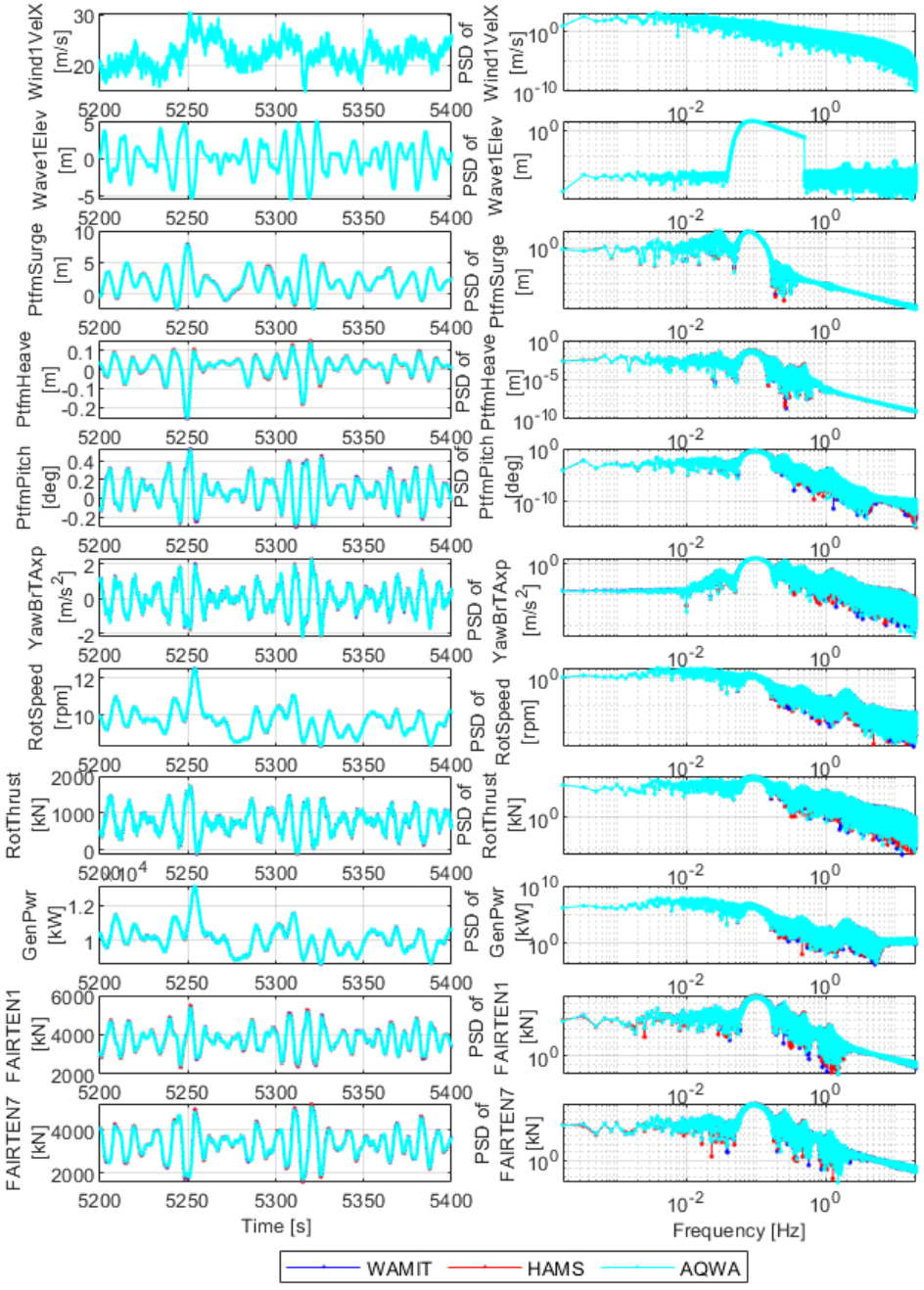


Figure 48 Above rated operational condition of CENTEC TLP

Extreme Conditions

The last modeled LC for CENTEC TLP is the extreme case where the wind speed is 47.5 m/s. H_s is 12.5 m and T_p of 14.3 s with parked turbine and feathered blades. As can be seen from Table 26, the maximum surge response is similar in the three models. (HAMS+OpenFAST) the model has a 5.9 % greater minimum surge response than the (WAMIT+OpenFAST) model. For heave and pitch, the responses are similar in the three models. The tower top acceleration is greater in (WAMIT+OpenFAST) model in minimum and maximum values. The minimum mooring tensions are 19.5 % greater for the (AQWA+OpenFAST) than for (WAMIT+OpenFAST) simulation. Maximum mooring tensions obtained from the (HAMS+OpenFAST) model have 13.7 % smaller tension in mooring 7 than (WAMIT+OpenFAST).

Table 26 Maximum and minimum responses to the extreme conditions of CENTEC TLP

	Surge [m]	Heave [m]	Pitch [deg]	Tower Top Acc. [m/s^2]	Thrust [kN]	Mooring 1 [kN]	Mooring 7 [kN]
Min							
WAMIT	-8.89	-0.61	-0.66	-1.72	-0.14	1013	494.10
HAMS	-9.41	-0.48	-0.66	-1.58	-0.15	1035	573
AQWA	-8.63	-0.59	-0.63	-1.66	-0.14	1211	686.90
Max							
WAMIT	11.32	0.22	0.64	1.18	0.15	5832	7124
HAMS	11.13	0.18	0.65	1.11	0.15	5763	6022
AQWA	11.03	0.20	0.624	1.13	0.15	5641	6896

5.2 Comparison of Platform Concepts

Motions in 6 DOF and mooring line tensions of the platform under realistic environmental sea conditions should be investigated to give an insight into the dynamic behavior of a floating wind turbine. Some studies on dynamic analysis of FOWTs keep the structural components the same apart from the platform types to investigate their responses, as Uzunoğlu (2019). Although there are differences in the environmental conditions where the platforms are designed, in this thesis, a similar approach (Uzunoğlu, 2019) is followed where the turbine and blades are the same for the three platform concepts. Tower modeling differs between the platform concepts (Pegalajar-Jurado et al. (2018) used a semi-flexible approach for the OO-Star platform, while Nautilus flatform stiff tower modeling is considered in Galván et al. (2018). The tower is also modeled as stiff for CENTEC TLP in this thesis. Considering the limitations above, for comparison of three platform concepts, natural periods are calculated from free decay simulations using (HAMS+OpenFAST) model, and the results are shown below in Table 27. Since the considered platform concepts are symmetric and incoming waves are in x direction, only natural periods of the surge, heave, pitch, and yaw are presented.

Table 27 Natural frequencies of the modeled three platform concepts computed by the (HAMS+OpenFAST) model

Natural Frequencies [Hz]	OO-STAR	Nautilus	CENTEC TLP
Surge	0.005	0.008	0.030
Heave	0.048	0.053	0.488
Pitch	0.032	0.034	0.255
Yaw	0.010	0.010	0.059

Comparing the natural frequencies in Table 27, CENTEC TLP has greater natural frequencies in heave and pitch, which means the platform might excite in waves with

shorter periods (2 s for heave and 3.92 s for pitch). The OO-Star platform provides the lowest surge frequency (0.005 Hz) among the platform types, followed by Nautilus (0.008 Hz) and CENTEC TLP (0.030 Hz). On the other hand, the heave, pitch, and yaw natural frequencies of the OO-Star and Nautilus concepts are similar, whereas the yaw of CENTEC TLP has a larger natural frequency (0.059 Hz).

Project Location of the Selected Platform Concepts

As can be seen from Table 28, the platform concepts are designed for the environmental conditions of two locations. The Tp_{50} values range from 8.36 to 12.5 seconds, and the water depth varies from 100 m to 150 m. Kıyıköy has the smallest Hs_{50}, and Galicia has the highest Hs_{50} value with 12.5 m. Considering the environmental parameters of Kıyıköy in Table 11 and Table 12, the area has less severe environmental conditions than the Gulf of Maine and Galicia. However, since the water depth has changed and different LCs are present for Kıyıköy, modeling the three concepts for the area and their behavior are investigated.

Table 28 Environmental conditions of platform concepts and selected region in Turkey

Selected Area	**Gulf of Maine, US**	**Galicia, Spain**	**Kıyıköy, Turkey**
Water Depth [m]	130	150	100
Hs_{50} [m]	10.90	12.50	8.36
Tp_{50} [s]	16	14.30	14.41
Ws_{50} [m/s]	44	47.50	30.47

The load cases used in the coupled simulation for the possible site in Kıyıköy are given in Table 29, where the LCs are selected using extreme value analysis in Chapter 4. The outputs of the LC simulations can be found on the next page. The naming of the LCs will be given below for the rest of this thesis for Kıyıköy.

Table 29 The load cases (LCs) selected for Kıyıköy

Load Cases	H_s [m]	T_p [s]	W_s [m/s]
LC1	2	5	8.1
LC2	2.5	6	10.1
LC3	4	8	14.1
LC4	8	14	30.47

Dimensions of the modeled platform concepts can be seen below in Figure 49 for a better comparison size of the modeled concepts. Detailed dimensions of the models can be accessed in the literature (Galván et al., 2018; Pegalajar-Jurado et al., 2018; Uzunoglu & Guedes Soares, 2020).

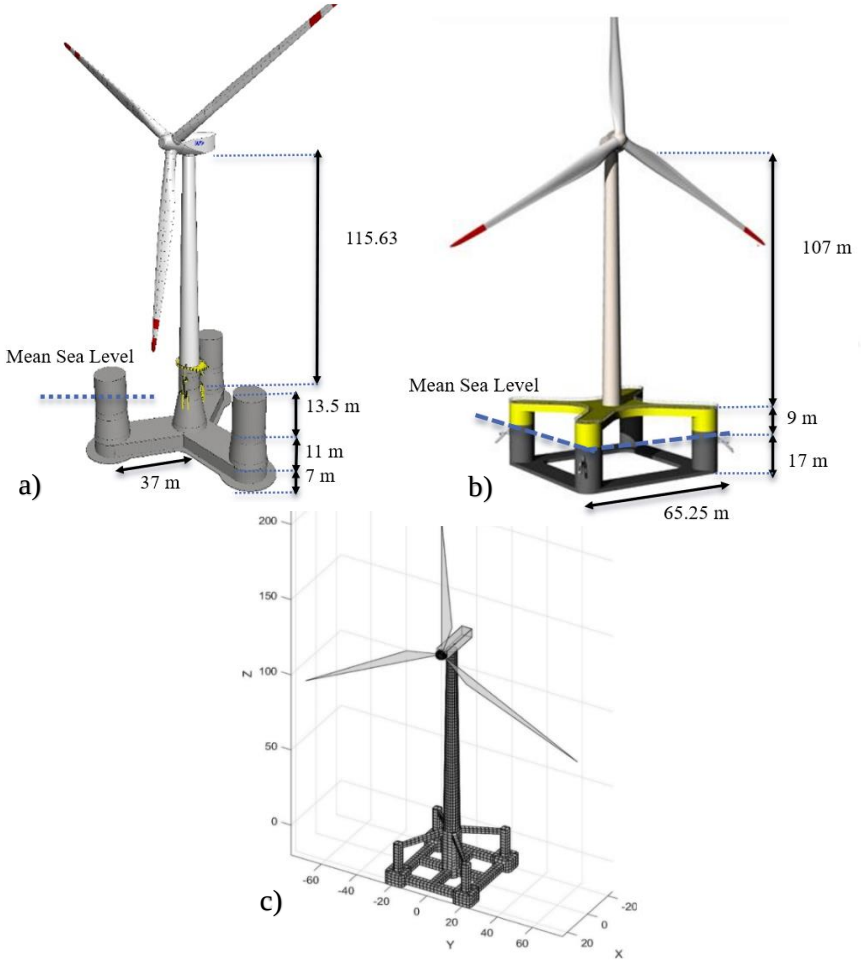


Figure 49 Dimensions of the selected concepts: a) OO-Star concept (Dr.techn. Olav Olsen AS, 2018)(Modified), b) Nautilus concept (Galván et al., 2018) (Modified), c) CENTEC TLP (Uzunoglu & Guedes Soares, 2020)

Simulation Results for LC1

The simulations' minimum, mean and maximum results in Kıyıköy are given in Figure 50, Figure 51, Figure 52, and Figure 53. The first two figures present the results for the operational conditions (LC1 and LC2) with rated wind speed. Figure 52 shows the results obtained for the above-rated wind condition, and Figure 53 presents the results of the LC4, which is an extreme load case. As can be seen from Figure 50, CENTEC TLP has less motion for the surge, heave, and pitch in the case of LC1 compared to other concepts. The average rotor thrust is similar for Nautilus and CENTEC TLP, where OO-Star has an 11.9 % higher average value than CENTEC TLP. The average power generated is similar in three concepts ranging from 3960 kW to 4038 kW. The mean mooring tension in CENTEC TLP is 3983 kN, whereas the mean mooring tensions in OO-Star and Nautilus are 1902 kN and 877 kN. Higher mooring tension is expected for a TLP due to its stabilization method.

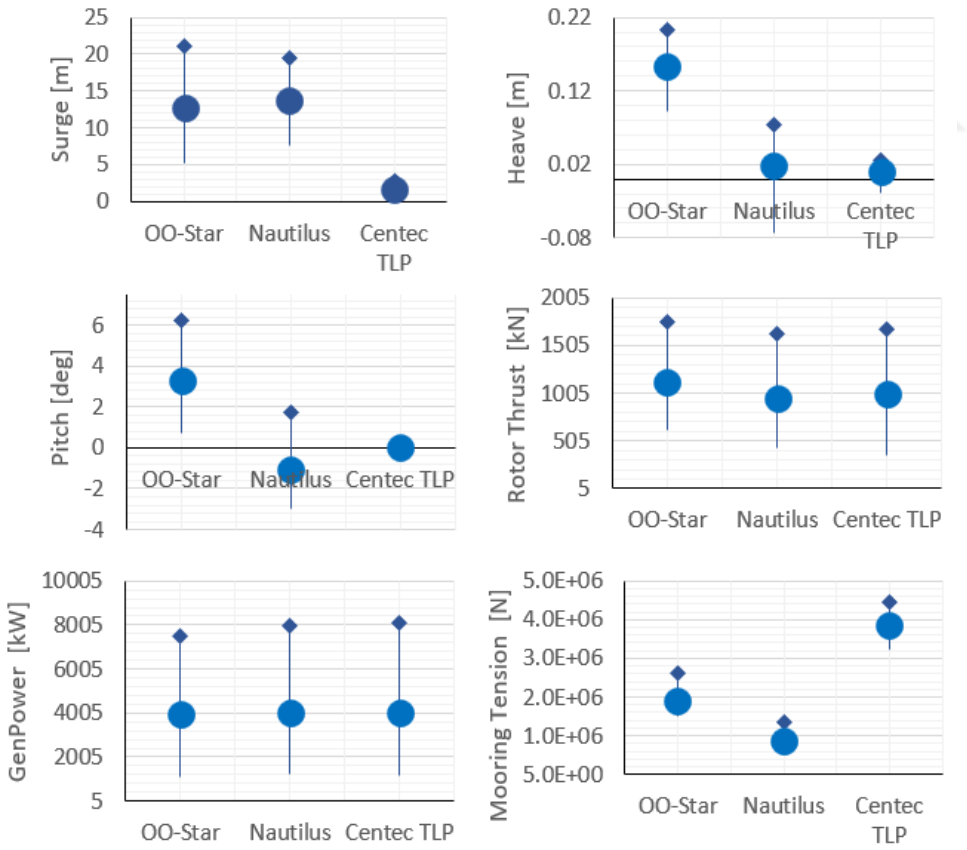


Figure 50 System behavior of the selected platforms in Kıyıköy for LC1

Simulation Results for LC2

As can be seen in Figure 51, the rotor thrust, and generated power are similar for the three platforms in the case of (LC2), whereas the mooring of CENTEC TLP has greater tension than other platforms. The same behavior is observed for the LC1, as seen in Figure 50. Compared to the previous LC, the mean surge is increased by 30 % for OO-Star, 26 % for Nautilus, and 50 % for CENTEC TLP. Mean Rotor thrust is increased by 40 % for OO-Star, 48.4 % for the Nautilus platform, and 39.65 % for CENTEC TLP compared to LC1, where the mean values are similar for the three concepts. However, for the Nautilus platform, the rotor thrust range is larger. Generated power has approximately the same range for all platform types, with a similar percentage increase from LC1 (83-85 %).

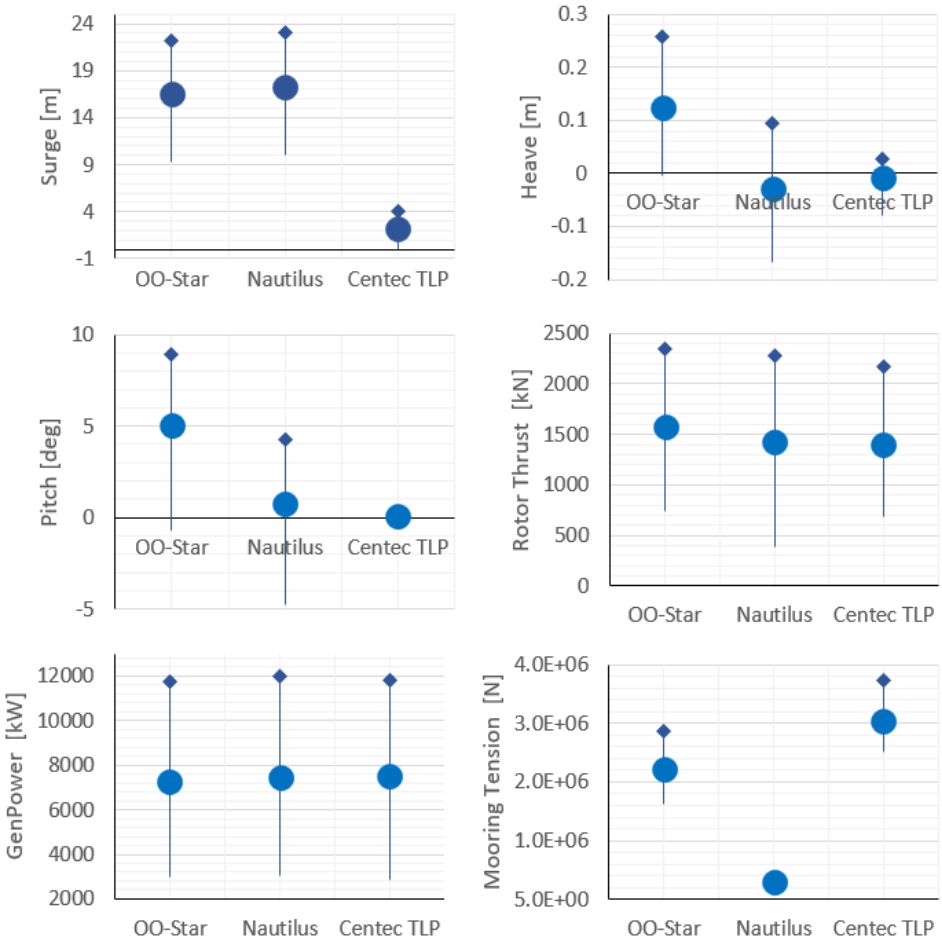


Figure 51 System behavior of the selected platforms in Kıyıköy for LC2

Simulation Results for LC3

The range of motion significantly increases in LC3 compared to LC1 and LC2. The general system behavior is similar, and there is greater energy production in LC3 with an average of 9998 kW compared to LC1 (7281 kW) and LC2 (3960 kW) for the OO-Star platform. Although the wind speed and generated power are greater than LC2, rotor thrust is 19.06 % smaller in OO-STAR, 23.78 % smaller in Nautilus, and 21.23 % smaller in CENTEC TLP. The reason is the increased pitch angle of the blades in LC3, which causes a decrease in rotor thrust and hence loads on the turbine (Kaya et al., 2022). Regarding platform motion, average surge motion decreased by 14.45 % compared to LC2 for the OO-Star platform, whereas heave response increased by 14.15 % compared to LC2. The pitch and yaw response of the platform also decreased. A similar motion is also present for the Nautilus platform.

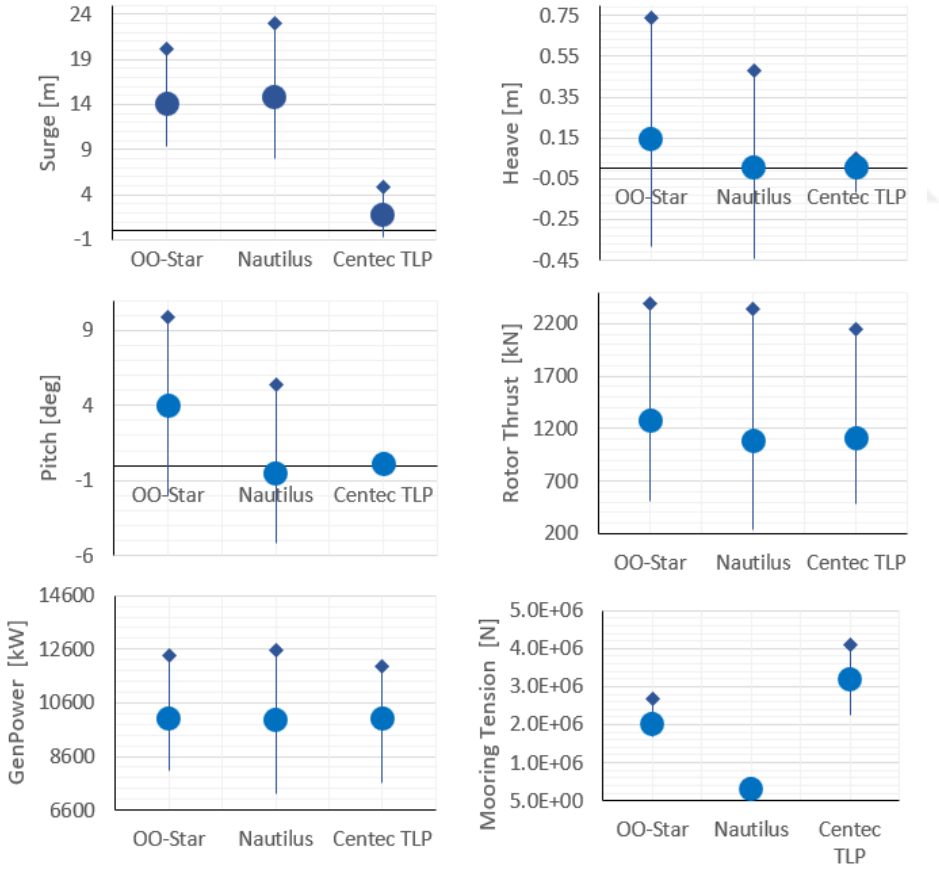


Figure 52 System behavior of the selected platforms in Kıyıköy for LC3

Simulation Results for LC4

Extreme wind and wave conditions are applied in the last simulation case for Kıyıköy (LC4). The turbine is in a parked position, and the blades are feathered. The simulation results can be seen in Figure 53. The generated thrust force is significantly less compared to previous LCs. Although the thrust on the turbine was lower in LC3 than LC2, the thrust force on the turbine is 80.39 % lower for OO-STAR, 78.38 % lower for Nautilus, and 77.41 % lower for CENTEC TLP in LC4 due to the parked turbine.

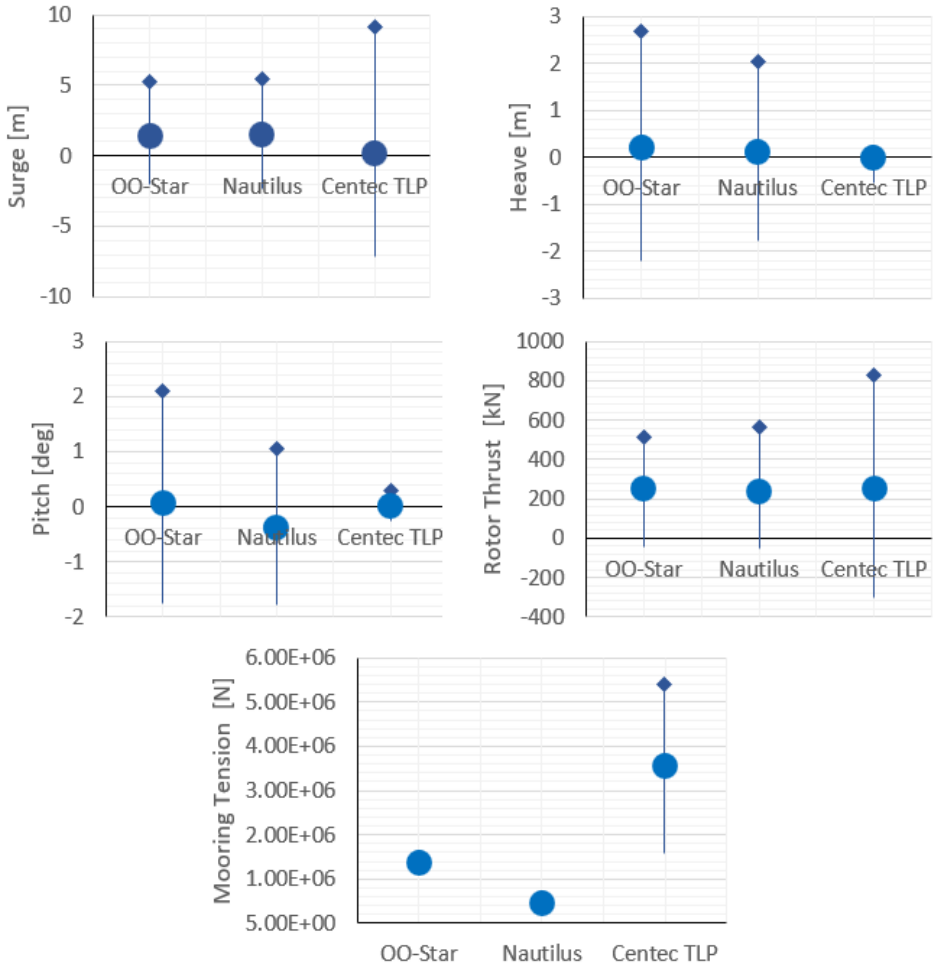


Figure 53 System behavior of the selected platforms in Kıyıköy for LC4

The rotor thrust comparison in Figure 53 also includes negative values. Since the thrust force presented here consists of the applied aerodynamic, gravitational, and inertial loads, negative thrust values can be expected.

As can be seen from Figure 53, The platform motions are wave dominated mostly where the surge and pitch motions are decreased for OO-Star and Nautilus platforms. However, there is a tremendous increase in surge motion for CENTEC TLP (90.65 % increase in maximum surge compared to LC3). There is an 11.81 % increase in mooring tension in the upwind direction for CENTEC TLP compared to LC3. For OO-STAR and Nautilus platforms, similar patterns also exist.

CHAPTER 6

CONCLUSION

The initial purpose of this thesis is to investigate the modeling capabilities of an open-source hydrodynamic solver, HAMS, as an alternative to hydrodynamic solvers (WAMIT and AQWA) in modeling FOWTs. For this purpose, three platform concepts, OO-Star (Pegalajar-Jurado et al., 2018), Nautilus (Galván et al., 2018), and CENTEC TLP (Uzunoglu & Guedes Soares, 2020), are modeled. As a first step, the hydrodynamic coefficients of the three platform concepts are calculated using the hydrodynamic solver only (AQWA and HAMS separately). Following this step, coupled analysis of modeled FOWTs is carried out using three configurations : *(i)* (AQWA+OpenFAST), *(ii)* (HAMS+OpenFAST), and *(iii)* (WAMIT+OpenFAST). Numerical simulations are carried out to assess the systems' dynamic behavior and obtain natural frequencies. Also, minimum, maximum and mean motion values are computed, and related power spectral densities are presented graphically. The effects of the hydrodynamic solver on the system's global response and power generation are investigated. Another goal of this thesis is to assess applicability of the three platform concepts for a potential site in Kıyıköy region in the Black Sea.

The main results of this thesis can be summarized in the following.

- For the hydrodynamic computations, the effect of the mesh is minimized by carrying out mesh sensitivity analysis. Since it is not possible to input mesh to AQWA, similar average cell size is used. Another limitation is that the mesh properties of the OO-Star and Nautilus platforms are not publicly available. However, with good volume coverage and fine mesh, it was possible to obtain accurate results for those platforms, especially for the hydrodynamic coefficients of OO-Star. There were slight differences in heave in the Nautilus platform, which might be caused by the modeling

differences in the heave plates. The same mesh file of the WAMIT simulation is used in HAMS simulations for CENTEC TLP. As seen in Chapter 5, the hydrodynamic coefficients of CENTEC TLP obtained from HAMS agree with WAMIT results substantially. The coefficients are almost equal to each other. There are slight deviations in frequencies greater than 2 rad/s.

- The coupled analysis and benchmark case comparison results showed excellent agreement on most simulations in time and frequency domains. With the increased severity of the load case, deviations from the benchmark case are observed.
- Three FOWT concepts previously designed for different locations are applied to the Kıyıköy in the Black Sea. The simulation results show that the three platform concepts are operable. The power generation of the turbines is similar; however, there are differences in motions and the loads on the structures. CENTEC TLP exhibits less motion compared to OO-Star and Nautilus platforms.
- The simulation results showed that Nautilus and OO-Star platforms are exposed to greater wave loads due to their size and present greater motion than CENTEC TLP for Kıyıköy LCs. The modeled platforms are initially designed for harsh environmental conditions compared to the Black Sea. Therefore, floater and mooring designs might be optimized for the Black Sea.
- More considerations should be included in the decision criteria to select an efficient platform concept for a region, including manufacturing details, installation, decommissioning, and materials. For instance, steel is expensive, and its manufacturing may require specific craftsmanship. Nautilus platform and CENTEC TLP are the steel platforms considered in this thesis. Since CENTEC TLP is the lightest platform among the three platform concepts discussed, it requires less steel material cost. Its lower draft and freely floating capability provide an efficient transportation option (Uzunoglu & Guedes Soares, 2020). Additionally, fatigue life should also be considered for steel structures, especially for moorings of CENTEC TLP. On the other

hand, OO-STAR is a concrete semisubmersible, where it might be cheaper in terms of material cost.

In the scope of this thesis, the possibility of using an open-source code in the hydrodynamic analysis of FOWTs is presented. Considering the outputs, the open-source code HAMS can produce the hydrodynamic coefficients such that almost the same results are obtained with the commonly used hydrodynamic software. Hydrodynamic coefficients obtained from previous steps are used as input to OpenFAST. The benchmark cases are modeled for the selected platform concepts. Finally, three platform concepts are modelled for the potential site in the Kıyıköy region in the Black Sea. Future recommendations of this thesis can be given as:

- Simulating more environmental conditions and DLCs, including installation and failure states
- Tuning control of the platforms for a better estimation of the power generation
- Designing mooring lines for the potential site
- Optimizing the floater considering the environmental parameters
- Investigating the second-order effects on the structure.

REFERENCES

ABS, A. B. of S. (2015). *Guide for building and classing floating offshore wind turbine installations*.

Aird, J., Gaertner, E., & Lackner, M. (2019). Dynamic prescribed-wake vortex method for aerodynamic analysis of offshore floating wind turbines. *Wind Engineering*, *43*(1), 47–63. https://doi.org/10.1177/0309524X18819897

Aqwa Theory Manual. (2013). 174.

Azcona, J., Bouchotrouch, F., González, M., Garciandía, J., Munduate, X., Kelberlau, F., & Nygaard, T. A. (2014). Aerodynamic Thrust Modelling in Wave Tank Tests of Offshore Floating Wind Turbines Using a Ducted Fan. *Journal of Physics: Conference Series*, *524*, 012089. https://doi.org/10.1088/1742-6596/524/1/012089

Azcona, J., Lemmer, F., Matha, D., Amann, F., Bottasso, C. L., Montinari, P., Chassapoyannis, P., Diakakis, K., Voutsinas, S., Pereira, R., Bredmose, H., Mikkelsen, R., Laugesen, R., & Hansen, A. M. (2016). *INNWIND-D4.2.4: Results of Wave Tank Tests*.

Bak, C., Zahle, F., Bitsche, R., Kim, T., Yde, A., Henriksen, L. C., & Natarajan, A. (2013). *Description of the DTU 10-MW Reference Wind Turbine* (DTU Wind Energy Report-I-0092; p. 138). DTU Wind Energy.

Bayati, I., Bernini, L., Facchinetti, A., Fontanella, A., Giberti, H., Zasso, A., & Belloli, M. (2018). *Hybrid HIL Testing of Floating Wind Turbines Within*

LIFES50+ Project. Conference of the Italian Association for Wind Engineering.

Bayati, I., Facchinetti, A., Fontanella, A., & Belloli, M. (2018). 6-DoF Hydrodynamic Modelling for Wind Tunnel Hybrid/HIL Tests of FOWT: The Real-Time Challenge. *Volume 10: Ocean Renewable Energy*, V010T09A078. https://doi.org/10.1115/OMAE2018-77804

Bayati, I., Facchinetti, A., Fontanella, A., Giberti, H., & Belloli, M. (2018). A wind tunnel/HIL setup for integrated tests of Floating Offshore Wind Turbines. *Journal of Physics: Conference Series*, *1037*, 052025. https://doi.org/10.1088/1742-6596/1037/5/052025

Birk, L. (2019). *Fundamentals of Ship Hydrodynamics: Fluid Mechanics, Ship Resistance and Propulsion* (1st ed.). Wiley. https://doi.org/10.1002/9781119191575

Bischoff Kristiansen, M. (2022). *Welcome to HAWC2*. Https://Www.Hawc2.Dk. https://www.hawc2.dk/hawc2-info

Borg, M., Bredmose, H., & Hansen, A. M. (2017). Elastic Deformations of Floaters for Offshore Wind Turbines: Dynamic Modelling and Sectional Load Calculations. *Volume 10: Ocean Renewable Energy*, V010T09A044. https://doi.org/10.1115/OMAE2017-61446

Borg, M., & Collu, M. (2014). A Comparison on the Dynamics of a Floating Vertical Axis Wind Turbine on Three Different Floating Support Structures. *Energy Procedia*, *53*, 268–279. https://doi.org/10.1016/j.egypro.2014.07.236

Borg, M., Manuel, L., Collu, M., & Liu, J. (2015). Long-Term Global Performance Analysis of a Vertical-Axis Wind Turbine Supported on a Semi-Submersible Floating Platform. *Volume 9: Ocean Renewable Energy*, V009T09A066. https://doi.org/10.1115/OMAE2015-41734

British Oceanographic Data Centre,. (2003). *Centenary Edition ofthe GEBCO Digital Atlas [CD-ROM]* (Published on Behalf of the Intergovernmental Oceano-Graphic Commission and the International HydrographicOrganization).

Butterfield, S., Musial, W., Jonkman, J., & Sclavounos, P. (2005). *Engineering Challenges for Floating Offshore Wind Turbines*. 13.

Caceoğlu, E., Yildiz, H. K., Oğuz, E., Huvaj, N., & Guerrero, J. M. (2022). Offshore wind power plant site selection using Analytical Hierarchy Process for Northwest Turkey. *Ocean Engineering*, *252*, 111178. https://doi.org/10.1016/j.oceaneng.2022.111178

Chakrabarti. (2005). *Handbook of Offshore Engineering*.

Chen, P., Chen, J., & Hu, Z. (2020). Review of Experimental-Numerical Methodologies and Challenges for Floating Offshore Wind Turbines. *Journal of Marine Science and Application*, *19*(3), 339–361. https://doi.org/10.1007/s11804-020-00165-z

Climate Action Tracker. (2022). *Global reaction to energy crisis risks zero carbon transition*.

Coulling, A. J., Goupee, A. J., Jonkman, J. M., & Robertson, A. N. (2013). *Importance of Second-Order Difference-Frequency Wave-Diffraction*

Forces in the Validation of a FAST Semi-Submersible Floating Wind Turbine Model. 10.

Day, A. H., Clelland, D., Oguz, E., Dai, S., Armendáriz, J. A., Sarriguren, C., Bouchotrouch, F., Sarriguren, C., Lopez, J. A., Sánchez, G., & Almeria, G. G. (2017). *REALISTIC SIMULATION OF AERODYNAMIC LOADING FOR MODEL TESTING OF FLOATING WIND TURBINES*. 14.

Det Norske Veritas. (2010). *Recommended Practice DNV-RP-C203 Fatigue design of offshore steel structures*.

DNV GL. (2014). *DNV-RP-C205 Environmental Conditions and Environmental Loads* (p. 182). Det Norske Veritas.

DNV GL. (2018). *DNVGL-ST-0119: Floating wind turbine structures*.

Dr.techn. Olav Olsen AS. (2018). https://www.olavolsen.no/en/

EMODnet. (2022). *Seabed Habitats—Launch map viewer*. https://www.emodnet-seabedhabitats.eu/access-data/launch-map-viewer/

EMODnet Bathymetry Consortium. (2020). *EMODnet Digital Bathymetry (DTM)*. https://doi.org/10.12770/bb6a87dd-e579-4036-abe1-e649cea9881a

ESMAP. (2019). *Going Global: Expanding Offshore Wind to Emerging Markets*. World Bank.

Etemaddar, M., Vahidian, E., & Skjåstad, O. (2014). Fatigue Damage to the Spar-Type Offshore Floating Wind Turbine Under Blade Pitch Controller Faults. *Volume 9A: Ocean Renewable Energy*, V09AT09A015. https://doi.org/10.1115/OMAE2014-23235

Fevåg, L. S. (2012). *Influence of marine growth on support structure design for offshore wind turbines*. NTNU.

Freedman, J. M., Filippelli, M. V., & Bailey, B. H. (2010, October). *Comparison of Environmental Conditions Between Offshore Sites in Europe and the United States*. AWEA Offshore Wind Power Conference, Atlantic City, NJ.

Galván, J., Sánchez-Lara, M. J., Mendikoa, I., Pérez-Morán, G., Nava, V., & Rodríguez-Arias, R. (2018). NAUTILUS-DTU10 MW Floating Offshore Wind Turbine at Gulf of Maine: Public numerical models of an actively ballasted semisubmersible. *Journal of Physics: Conference Series*, *1102*, 012015. https://doi.org/10.1088/1742-6596/1102/1/012015

Galván, J., Sanchez-Lara, M., Mendikoa, I., Nava, V., Boscolo-Papo, F., Garrido-Mendoza, C., Berque, J., Perez-Moran, G., & Rodriguez-Arias, R. (2018). *Definition and analysis of NAUTILUS - DTU10 MW floating offshore wind turbine at Gulf of Maine, experiments at Sintef Ocean and Polimi*. Tecnalia R&I.

Global Wind Atlas. (2022). https://globalwindatlas.info

Goda, Y. (2008). *Random seas and design of maritime structures* (2. ed., Reprint). World Scientific.

Gueydon, S., Duarte, T., & Jonkman, J. (2014). Comparison of Second-Order Loads on a Semisubmersible Floating Wind Turbine. *Volume 9A: Ocean Renewable Energy*, V09AT09A024. https://doi.org/10.1115/OMAE2014-23398

Gueydon, S., & Weller, S. (2013). Study of a Floating Foundation for Wind Turbines. *Journal of Offshore Mechanics and Arctic Engineering*, *135*(3), 031903. https://doi.org/10.1115/1.4024271

H2OCEAN. (2014). *Final Report Summary—H2OCEAN Development of a wind-wave power open-sea platform equipped for hydrogen generation with support for multiple users of energy*. https://cordis.europa.eu/project/id/288145/reporting/fr

Hansen, M. H., & Henriksen, L. C. (2013). *Basic DTU Wind Energy Controller* (E-0028). DTU, Department of Wind Energy.

Hasselmann, K., Barnett, T. P., Bouws, E., Carlson, H., Cartwright, D. E., Enke, K., Ewing, J. A., Gienapp, H., Hasselmann, D. E., Kruseman, P., Meerburg, A., Müller, P., Olbers, D. J., Richter, K., Sell, W., & Walden, H. (1973). *Measurements of Wind-Wave Growth and Swell Decay during the Joint North Sea Wave Project (JONSWAP)*.

Hersbach, H., Bell, B., Berrisford, P., Biavati, G., Horányi, A., Muñoz Sabater, J., Nicolas, J., Peubey, C., Radu, R., Rozum, I., Schepers, D., Simmons, A., Soci, C., Dee, D., & Thépaut, J. N. (2018). *ERA5 hourly data on single levels from 1959 to present*. Copernicus Climate Change Service (C3S) Climate Data Store (CDS). 10.24381/cds.adbb2d47

Holthuijsen, L. H. (2007). *Waves in Oceanic and Coastal Waters*. 405.

Hopstad, A. L., & Pollicino, F. (2020). *Overview of offshore wind standards and certification requirements in selected countries* (No. 2020–1194, Rev. 01). DNV GL.

International Electrotechnical Commision. (2019). *IEC TS 61400-3-2:2019 Wind energy generation systems—Part 3-2: Design requirements for floating offshore wind turbines*.

ITTC Proceedings. (2021a). *Floating Offshore Platform Experiments—Recommended Procedures and Guidelines, Section 7.5-02-07-03.1*.

ITTC Proceedings. (2021b). *Model Tests for Offshore Wind Turbines—Recommended Procedures and Guidelines, Section 7.5-02-07-03.8*. 19.

Jonkman, J. (2009). *Dynamics of offshore floating wind turbines-model development and verification*. 34.

Jonkman, J. (2010). *Definition of the Floating System for Phase IV of OC3* (NREL/TP-500-47535, 979456; p. NREL/TP-500-47535, 979456). https://doi.org/10.2172/979456

Jonkman, J. (2013, January 7). The New Modularization Framework for the FAST Wind Turbine CAE Tool. *51st AIAA Aerospace Sciences Meeting Including the New Horizons Forum and Aerospace Exposition*. 51st AIAA Aerospace Sciences Meeting including the New Horizons Forum and Aerospace Exposition, Grapevine (Dallas/Ft. Worth Region), Texas. https://doi.org/10.2514/6.2013-202

Jonkman, J. M., Robertson, A. N., & Hayman, G. J. (2016). *HydroDyn User's Guide and Theory Manual*. National Renewable Energy Laboratory (NREL).

Jose, A., Falzarano, J., & Wang, H. (2020). Development of Coupled Program fast-simdyn and Study of Non-Linear Hydrodynamics, Coupled With Negative

Damping and Aerodynamics of Floating Offshore Wind Turbines. *Journal of Offshore Mechanics and Arctic Engineering*, *142*(2), 021904. https://doi.org/10.1115/1.4045188

Kamphuis, J. W. (2000). *Introduction to coastal engineering and management*. World Scientific.

Karimirad, M. (2013). Modeling aspects of a floating wind turbine for coupled wave–wind-induced dynamic analyses. *Renewable Energy*, *53*, 299–305. https://doi.org/10.1016/j.renene.2012.12.006

Karimirad, M., & Moan, T. (2011). Extreme Dynamic Structural Response Analysis of Catenary Moored Spar Wind Turbine in Harsh Environmental Conditions. *Journal of Offshore Mechanics and Arctic Engineering*, *133*(4), 041103. https://doi.org/10.1115/1.4003393

Karimirad, M., & Moan, T. (2012a). Feasibility of the Application of a Spar-type Wind Turbine at a Moderate Water Depth. *Energy Procedia*, *24*, 340–350. https://doi.org/10.1016/j.egypro.2012.06.117

Karimirad, M., & Moan, T. (2012b). A simplified method for coupled analysis of floating offshore wind turbines. *Marine Structures*, *27*(1), 45–63. https://doi.org/10.1016/j.marstruc.2012.03.003

Kaya, M. N., Uzol, O., Ingham, D., Köse, F., & Buyukzeren, R. (2022). The aerodynamic effects of blade pitch angle on small horizontal axis wind turbines. *International Journal of Numerical Methods for Heat & Fluid Flow*. https://doi.org/10.1108/HFF-02-2022-0128

Koo, B. J., Goupee, A. J., Kimball, R. W., & Lambrakos, K. F. (2014). Model Tests for a Floating Wind Turbine on Three Different Floaters. *Journal of Offshore Mechanics and Arctic Engineering*, *136*(2), 020907. https://doi.org/10.1115/1.4024711

Krieger, A., Ramachandran, G. K. V., Vita, L., Alonso, P. G., Berque, J., & Aguirre, G. (2015). *D7.2 Design Basis*.

Kyokai, N. (2012). *ClassNK Guidelines for Offshore Floating Wind Turbine Structures*.

Larsen, T. J., & Hansen, A. M. (2007). *How 2 HAWC2, the Users Manual* (Risoe-R-1597). Forskningscenter Risoe.

Lee, C. H. (1995). *WAMIT Theory Manual* (Technical Report No. 95–2). Massachusetts Institute of Technology (MIT).

Lee, J., & Zhao, F. (2022). *Global Wind Report*. GWEC.

Liu, Y. (2019). HAMS: A Frequency-Domain Preprocessor for Wave-Structure Interactions—Theory, Development, and Application. *Journal of Marine Science and Engineering*, *7*(3), 81. https://doi.org/10.3390/jmse7030081

Liu, Y. (2021). Introduction of the Open-Source Boundary Element Method Solver HAMS to the Ocean Renewable Energy Community. *Proceedings of the European Wave and Tidal Energy Conference: EWTEC 2021*, 6.

Liu, Y., Xiao, Q., Incecik, A., Peyrard, C., & Wan, D. (2017). *Establishing a fully coupled CFD analysis tool for floating offshore wind turbines*. http://dx.doi.org/10.1016/j.renene.2017.04.052

Madsen, F. J., Pegalajar-Jurado, A., Bredmose, H., Faerron-Guzmán, R., Müller, K., & Lemmer, F. (2018). *D4.6 Model validation against experiments and map of model accuracy across load cases* (p. 67).

MARINA Platform. (2014). *D1.12 Final Summary Report*.

Mas-Soler, J., Uzunoglu, E., Bulian, G., Soares, C. G., & Souto-Iglesias, A. (2021). An experimental study on transporting a free-float capable tension leg platform for a 10 MW wind turbine in waves. *Renewable Energy*, 16.

Matha, D. (2010). *Model Development and Loads Analysis of an Offshore Wind Turbine on a Tension Leg Platform with a Comparison to Other Floating Turbine Concepts: April 2009* (NREL/SR-500-45891, 973961; p. NREL/SR-500-45891, 973961). https://doi.org/10.2172/973961

Medvedev, I. P., Rabinovich, A. B., & Kulikov, E. A. (2016). Tides in Three Enclosed Basins: The Baltic, Black, and Caspian Seas. *Frontiers in Marine Science*, *3*. https://doi.org/10.3389/fmars.2016.00046

MERMAID. (2015). *Final Report Summary—MERMAID (Innovative Multi-purpose off-shore platforms: Planning, Design and operation)*. https://cordis.europa.eu/project/id/288710/reporting

Moriarty, P. J., & Hansen, A. C. (2005). *AeroDyn Theory Manual* (NREL/TP-500-36881, 15014831; p. NREL/TP-500-36881, 15014831). https://doi.org/10.2172/15014831

Muliawan, M. J., Karimirad, M., Gao, Z., & Moan, T. (2013). Extreme responses of a combined spar-type floating wind turbine and floating wave energy

converter (STC) system with survival modes. *Ocean Engineering*, *65*, 71–82. https://doi.org/10.1016/j.oceaneng.2013.03.002

Müller, K., Faerron-Guzmán, R., Manjock, A., & Borg, M. (2018). *D7.7 Identification of Critical Environmental Conditions and Design Load Cases* (p. 129).

Myhr, A., Maus, K. J., & Nygaard, T. A. (2011). *Experimental and Computational Comparisons of the OC3-HYWIND and Tension-Leg-Buoy (TLB) Floating Wind Turbine Conceptual Designs*. 8.

Myhr, A., & Nygaard, T. A. (2014). Experimental Results for Tension-Leg-Buoy Offshore Wind Turbine Platforms. *Journal of Ocean and Wind Energy*, *1*(4), 8.

Myhr, A., & Nygaard, T. A. (2015). Comparison of Experimental Results and Computations for Tension-Leg-Buoy Offshore Wind Turbines. *Journal of Ocean and Wind Energy*, *2*(1), 9.

Naqvi, S. K. (2012). *Scale model experiments on floating offshore wind turbines*. 108.

Nielsen, F. G., Hanson, T. D., & Skaare, B. (2006). Integrated Dynamic Analysis of Floating Offshore Wind Turbines. *Volume 1: Offshore Technology; Offshore Wind Energy; Ocean Research Technology; LNG Specialty Symposium*, 671–679. https://doi.org/10.1115/OMAE2006-92291

Nihei, Y., & Fujioka, H. (2010). Motion Characteristics of TLP Type Offshore Wind Turbine in Waves and Wind. *29th International Conference on*

Ocean, Offshore and Arctic Engineering: Volume 3, 283–292. https://doi.org/10.1115/OMAE2010-21126

Oguz, E., Clelland, D., Day, A. H., Incecik, A., López, J. A., Sánchez, G., & Almeria, G. G. (2018). Experimental and numerical analysis of a TLP floating offshore wind turbine. *Ocean Engineering*, *147*, 591–605. https://doi.org/10.1016/j.oceaneng.2017.10.052

O'Neill, A. (2012). Open Source Software. In *Encyclopedia of Applied Ethics* (pp. 281–287). Elsevier. https://doi.org/10.1016/B978-0-12-373932-2.00063-6

OpenFAST Documentation—OpenFAST v3.3.0 documentation. (2022). https://openfast.readthedocs.io/en/dev/index.html

ORECCA. (2011). *European Offshore Renewable Energy Roadmap*.

Pegalajar-Jurado, A., Bredmose, H., Borg, M., Straume, J. G., Landbø, T., Andersen, H. S., Yu, W., Müller, K., & Lemmer, F. (2018). State-of-the-art model for the LIFES50+ OO-Star Wind Floater Semi 10MW floating wind turbine. *Journal of Physics: Conference Series*, *1104*, 012024. https://doi.org/10.1088/1742-6596/1104/1/012024

Pegalajar-Jurado, A., Madsen, F. J., Borg, M., & Bredmose, H. (2018). *D4.5 State-of-the-art models for the two LIFES50+ 10MW floater concepts*. 42.

Penalba, M., Kelly, T., & Ringwood, J. V. (2017). *Using NEMOH for Modelling Wave Energy Converters: A Comparative Study with WAMIT*. 11.

Perez-Collazo, C. (2018). Hydrodynamic response of the WEC sub-system of a novel hybrid wind-wave energy converter. *Energy Conversion and Management*, 19.

Pérez-Collazo, C., Jakobsen, M. M., Buckland, H., & Fernández-Chozas, J. (2013). *SYNERGIES FOR A WAVE-WIND ENERGY CONCEPT*. https://doi.org/10.13140/2.1.5155.1523

Philippe, M., Babarit, A., & Ferrant, P. (2014). Aero-Hydro-Elastic Simulation of a Semi-Submersible Floating Wind Turbine. *Journal of Offshore Mechanics and Arctic Engineering*, *136*(2), 020908. https://doi.org/10.1115/1.4025031

Pierson, W. J., & Moskowitz, L. (1964). *A proposed spectral form for fully developed wind seas based on the similarity theory of S. A. Kitaigorodskii*. 10.

Republic of Turkey Ministry of Energy and Natural Resources. (2022). *Energy*. https://enerji.gov.tr/bilgi-merkezi-enerji-elektrik

Roald, L. (2013). The Effect of Second-order Hydrodynamics on Floating Offshore Wind Turbines. *Energy Procedia*, 12.

Robertson, A. N., Gueydon, S., Bachynski, E., Wang, L., Jonkman, J., Alarcón, D., Amet, E., Beardsell, A., Bonnet, P., Boudet, B., Brun, C., Chen, Z., Féron, M., Forbush, D., Galinos, C., Galvan, J., Gilbert, P., Gómez, J., Harnois, V., … Wohlfahrt-Laymann, S. (2020). OC6 Phase I: Investigating the underprediction of low-frequency hydrodynamic loads and responses of a floating wind turbine. *Journal of Physics: Conference Series*, *1618*(3), 032033. https://doi.org/10.1088/1742-6596/1618/3/032033

Roddier, D., Cermelli, C., Aubault, A., & Weinstein, A. (2010). WindFloat: A floating foundation for offshore wind turbines. *Journal of Renewable and Sustainable Energy*, *2*(3), 033104. https://doi.org/10.1063/1.3435339

Simos, A. N., Ruggeri, F., Watai, R. A., Souto-Iglesias, A., & Lopez-Pavon, C. (2018). Slow-drift of a floating wind turbine: An assessment of frequency-domain methods based on model tests. *Renewable Energy*, *116*, 133–154. https://doi.org/10.1016/j.renene.2017.09.059

Sirnivas, S., Musial, W., Bailey, B., & Filippelli, M. (2014). *Assessment of Offshore Wind System Design, Safety, and Operation Standards* (NREL/TP--5000-60573, 1122306; p. NREL/TP--5000-60573, 1122306). https://doi.org/10.2172/1122306

Skaare, B., Hanson, T. D., & Nielsen, F. G. (2007). Importance of Control Strategies on Fatigue Life of Floating Wind Turbines. *Volume 5: Ocean Space Utilization; Polar and Arctic Sciences and Technology; The Robert Dean Symposium on Coastal and Ocean Engineering; Special Symposium on Offshore Renewable Energy*, 493–500. https://doi.org/10.1115/OMAE2007-29277

Standards Norway. (2007). *NORSOK Standard N-003 Action and action effects* (N-003).

Staneva, J., Behrens, A., Ricker, M., & Gayer, G. (2020). *Black Sea Waves Reanalysis (CMEMS BS-Waves) (Version 2) set*. Copernicus Monitoring Environment Marine Service (CMEMS). https://doi.org/10.25423/CMCC/BLKSEA_MULTIYEAR_WAV_007_006

Stewart, G., & Muskulus, M. (2016). A Review and Comparison of Floating Offshore Wind Turbine Model Experiments. *Energy Procedia*, *94*, 227–231. https://doi.org/10.1016/j.egypro.2016.09.228

Sumer, B. M., & Fredsøe, J. (2006). *Hydrodynamics around cylindrical strucures* (Revised ed). World Scientific Publishing.

Svendsen, I. A. (2006). *Introduction to nearshore hydrodynamics*. World Scientific.

The International Organization for Standarization. (2007). *ISO 19902 Petroleum and natural gas industries – Fixed steel offshore structures*.

Thys, M., Chabaud, V., Eliassen, L., Sauder, T., & Berthelsen, P. A. (2018). *DOCUMENTATION VERIFICATION AND VALIDATION OF REAL-TIME HYBRID MODEL TESTS WITH THE 10MW OO-STAR WIND FLOATER*. 20.

TROPOS. (2015). *Final Report*. http://www.troposplatform.eu/

Tzinis, I. (2015, May 6). *Technology Readiness Level*. NASA; Brian Dunbar. http://www.nasa.gov/directorates/heo/scan/engineering/technology/technology_readiness_level

United Nations (UN). (2015). *Adoption of the Paris Agreement*. 21st Conference of the Parties, Paris.

Utsunomiya, T., Sato, T., Matsukuma, H., & Yago, K. (2009). Experimental Validation for Motion of a SPAR-Type Floating Offshore Wind Turbine Using 1/22.5 Scale Model. *Volume 4: Ocean Engineering; Ocean Renewable Energy; Ocean Space Utilization, Parts A and B*, 951–959. https://doi.org/10.1115/OMAE2009-79695

Uzunoglu, C. E. (2019). *A System for the Hydrodynamic Design of Floating Wind Turbine Platforms*. CENTEC.

Uzunoglu, E., & Guedes Soares, C. (2020). Hydrodynamic design of a free-float capable tension leg platform for a 10 MW wind turbine. *Ocean Engineering*, *197*, 106888. https://doi.org/10.1016/j.oceaneng.2019.106888

Veritas, B. (2015). *Classification and certification of floating offshore wind turbines* (Guidance Note NI No. 572).

Vita, L., Paulsen, U. S., Madsen, H. A., Nielsen, P. H., Berthelsen, P. A., & Carstensen, S. (2012). Design and Aero-Elastic Simulation of a 5MW Floating Vertical Axis Wind Turbine. *Volume 7: Ocean Space Utilization; Ocean Renewable Energy*, 383–392. https://doi.org/10.1115/OMAE2012-83470

Vittori, F., Azcona, J., Eguinoa, I., Pires, O., Rodríguez, A., Morató, Á., Garrido, C., & Desmond, C. (2021). *Model tests of a 10 MW semi-submersible floating wind turbine under waves and wind using hybrid method to integrate the rotor thrust and moments* [Preprint]. Offshore technology. https://doi.org/10.5194/wes-2021-148

Voltá, L., Roqueta, I., Thomas, S., & Schmidt Paulsen, U. (2020). Modelling of a wind-wave floating and semi-submersible power plant. *Journal of Physics: Conference Series*, *1618*(5), 052032. https://doi.org/10.1088/1742-6596/1618/5/052032

Wind Europe. (2021, September 9). *Turkey reaches 10 GW wind energy milestone*. WindEurope. https://windeurope.org/newsroom/news/turkey-reaches-10-gw-wind-energy-milestone/

Withee, J. E. (2004). *Fully coupled dynamic analysis of a floating wind turbine system* [Doctoral Thesis]. Massachusetts Institute of Technology.

Xu, K., Shao, Y., Gao, Z., & Moan, T. (2019). A study on fully nonlinear wave load effects on floating wind turbine. *Journal of Fluids and Structures*, *88*, 216–240. https://doi.org/10.1016/j.jfluidstructs.2019.05.008

Yu, W. (2018). *D4.2 Public Definition of the Two LIFES50+ 10MW Floater Concepts*. 32.

Zhang, M. H. (2015). *WIND RESOURCE ASSESSMENT AND MICRO-SITING*.

APPENDICES

A. Mesh Sensitivity Analysis for the HAMS (OO-Star Platform)

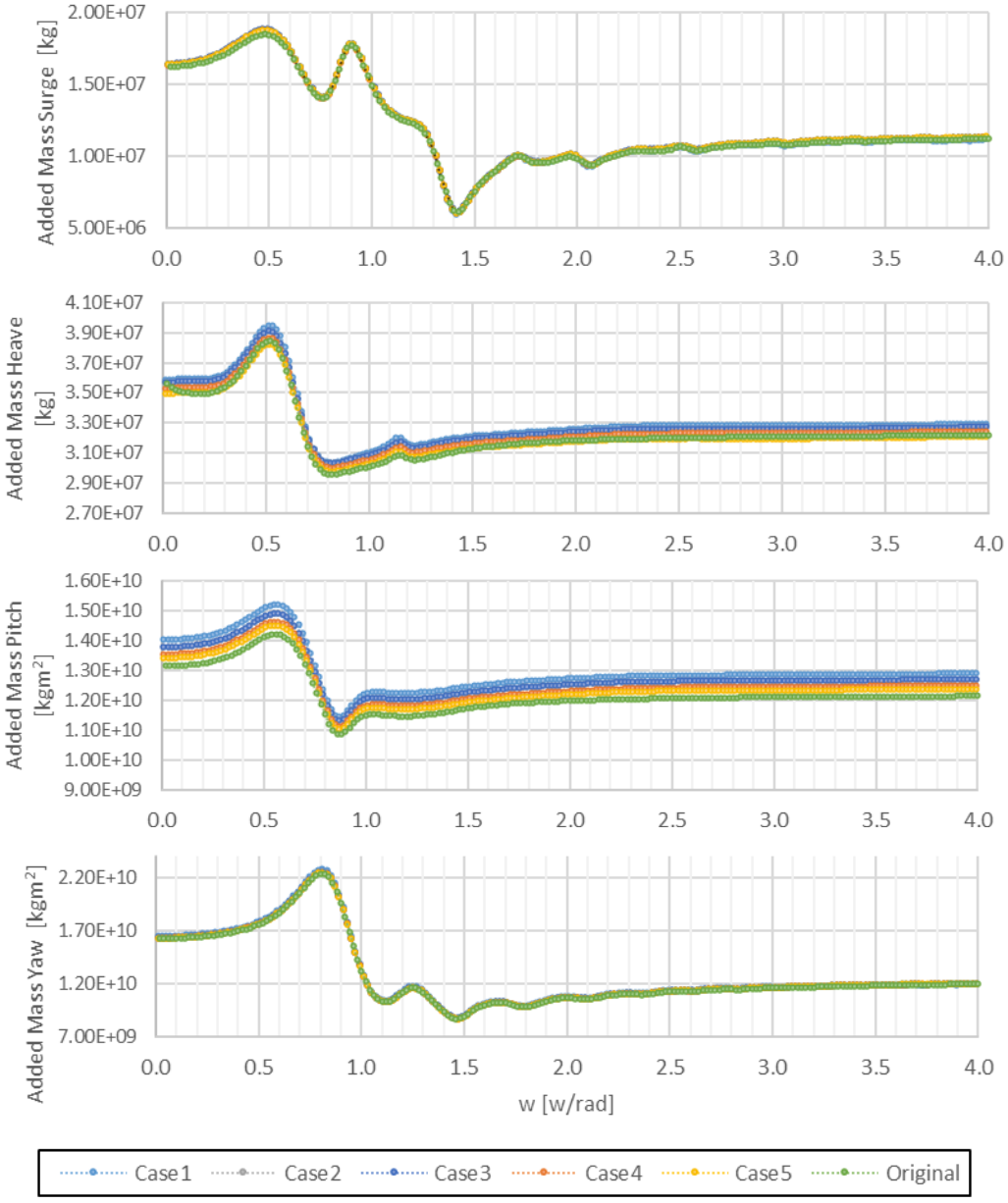


Figure 54 Added Mass for the OO-Star computed using HAMS

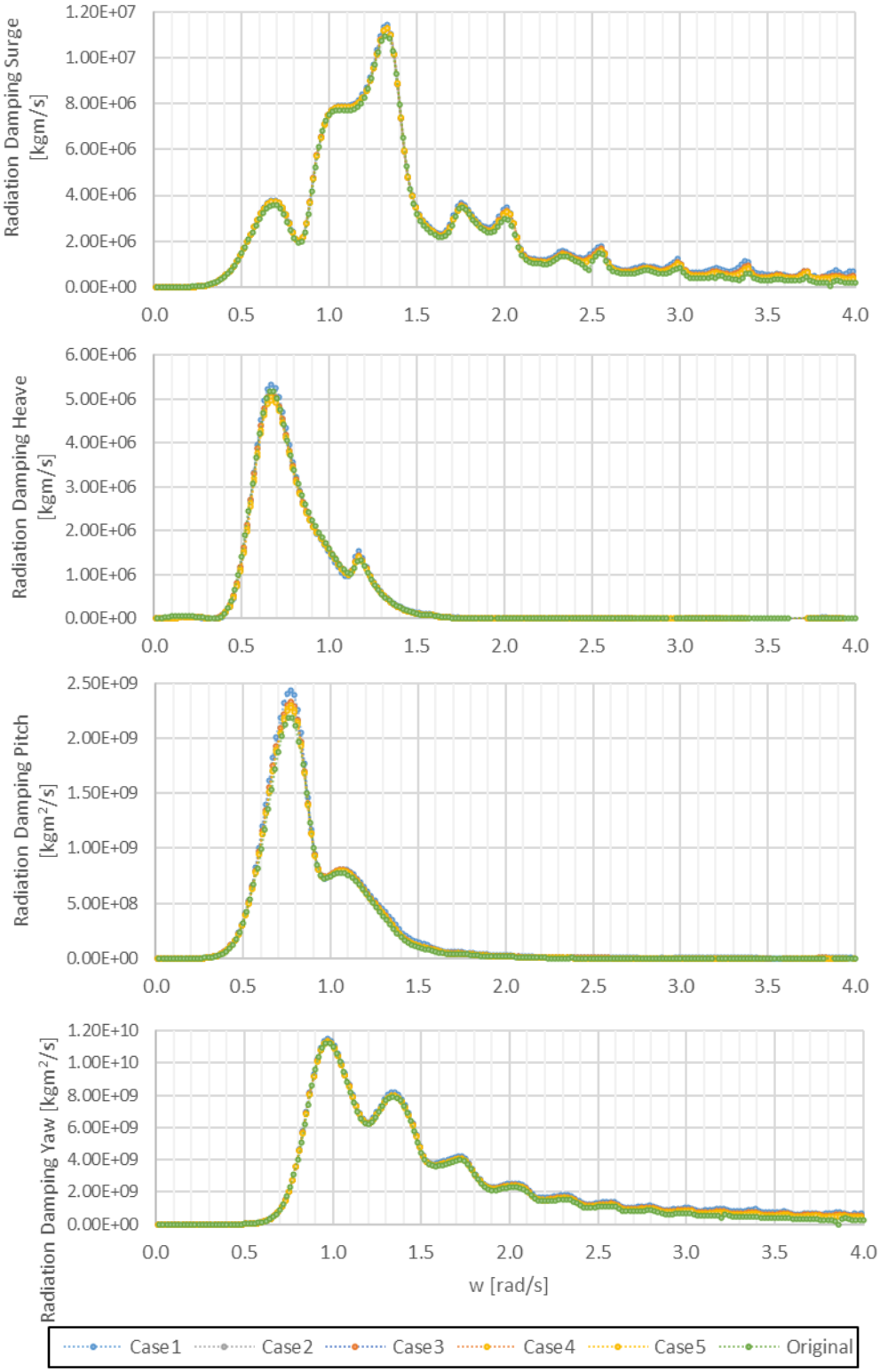


Figure 55 Radiation damping for the OO-Star computed using HAMS

A comparison of the hydrodynamic coefficients for each mesh case shows that in the OO-Star platform, the volumetric convergence is high, even in the coarsest mesh. As can be seen from Appendix, the change in the added mass is more evident in heave and pitch DOFs from the coarsest (Case 1) case and the finest (Case 5) case. For the surge and yaw of added mass, the convergence interval from Case 1 to Case 5 is not large as heave and pitch added mass. The results mostly match the benchmark case, which is the WAMIT output from the Lifes50+ project (Pegalajar-Jurado et al., 2018).

B. Input File for CENTEC TLP

As mentioned in Chapter 4, OpenFAST is a comprehensive engineering tool where one can model the aerodynamics, hydrodynamics, structural dynamics, control, and moorings of a FOWT system. The code requires multiple input files for the simulation where the system properties can be identified. OpenFAST, named as the glue code, is the driver code that consists of submodules. The input files should be prepared for AeroDYN, ServoDYN, HydroDYN, and Moorings. Wind input files areprepared using TurbSIM. For more information, see (*OpenFAST v3.3.0 Documentation*, 2022). The simplified inputs for the rated operational condition of CENTEC TLP can be seen below in Table 30. For the full simulations, detailed inputs must be considered.

Table 30 Input files for the CENTEC TLP rated operational condition

Wind Inputs	
Wind Type	Wind time series created (Turbsim)
Wind Grid Size	Created considering the turbine size
Turbulence Model	Kaimal
Wind Seed	Random Wind Seeds are used
IEC	Related IEC parameters can be defined
Wind Speed	11.4 m/s

Table 30 (Continued)

Height of reference wind speed / Hub Height	119 m
Power Law Exponent	0.14
Air Density	1.225 kg/m^3
Hydrodynamics Input	
Water Density	1025 kg/m^3
Water Depth	150 m
Wave Mode	Irregular Waves (JONSWAP Spectrum)
Wave Hs	8 m
Wave Period	11.5
Wave Direction	0
Potentiaf Flow	frequency-to-time-domain transforms based on WAMIT output
Platform Volume	7927.3549 m^3
Number of Joints	14
Number of Members	9
Member Based Drag Coefficients	Drag Coefficients are defined from the literature considering their hydrodynamic behavior (See Sumer, 2006)
Structural Inputs (ElastoDYN)	
DOFs	all DOFs except YAW DOF and teetDOF
Blade Pitch Angle	20.927 degrees
Rotor Speed	9.6 rpm
İnitial Heave	-0.2 m
Platform Center of Mass	(0, 0, -11.64) m
Platform Mass	2208600 kg

Table 30 (Continued)

Platform Roll Inertia	6.90E+08 kgm^2
Platform Pitch Inertia	6.90E+08 kgm^2
Platform Yaw Inertia	1.04E+09 kgm^2
Moorings	
Diameter	0.14 m
EA	1.17E09 N
Number of Mooring Lines	12